Ing. Manuel Natali, BSc

Development of a Semiautomatic Cleaning System for Optics of Biomedical Assemblies

MASTERS'S THESIS

to achieve the university degree of

Diplom-Ingenieur

Master's degree programme: Biomedical Engineering

submitted to

Graz University of Technology

Supervisor:

Ao.Univ.-Prof. Dipl.-Ing. Dr.techn. Hermann Scharfetter

Institute of Biomedical Imaging

Head: Univ.-Prof. Dipl.-Phys. Dr.rer.nat. Martin Uecker

Klagenfurt, January 2023

AFFIDAVIT

I declare that I have authored this thesis independently, that I have not used other than the declared sources/resources, and that I have explicitly indicated all material which has been quoted either literally or by content from the sources used. The text document uploaded to TUGRAZonline is identical to the present master's thesis.

<table>
<tr><td>. . . . .</td><td>. . . . .</td></tr>
<tr><td align="center">Date</td><td align="center">Signature</td></tr>
</table>

Abstract

In many cases, optics are a central component of biomedical assemblies and often have an influence on measurement results or the function of the end device. In this context, the cleanliness of these also plays an essential role. The aim of this work was to develop a cleaning system for the company *WILD GmbH* and to investigate whether the previously manual cleaning of round optics can be partially automated with it. The robot developed allows optical surfaces with different curvatures to be cleaned uniformly from the inside to the outside under rotational movement. An integrated force sensor also ensures that the pressure of the cleaning rod (polyester pad) on the surface of the optics is always kept constant. The results of the series of tests subsequently performed show that, from a functional point of view, the prototype is capable of automating manual cleaning and in combination with suitable solvents, removes soiling such as dust or greasy fingerprints almost without leaving any residue.

keywords: *optics, cleaning, automation, Python, CNC*

Kurzfassung

Optiken stellen in vielen Fällen einen zentralen Bestandteil biomedizinischer Baugruppen dar und haben auch nicht selten Einfluss auf Messergebnisse oder die Funktion des Endgerätes. In diesem Zusammenhang spielt auch die Sauberkeit dieser eine wesentliche Rolle. Ziel dieser Arbeit war es, ein Reinigungssystem für das Unternehmen *WILD GmbH* zu entwickeln und zu untersuchen, ob sich die bis dato manuell durchgeführte Reinigung runder Optiken damit teilautomatisieren lässt. Der entwickelte Roboter erlaubt es, unterschiedlich gekrümmte optische Oberflächen unter rotatorischer Bewegung gleichmäßig von innen nach außen zu reinigen. Ein integrierter Kraftsensor sorgt zudem dafür, dass der Druck des Reinigungsstäbchens (Polyester-Pad) auf die Oberfläche der Optik stets konstant gehalten wird. Die Ergebnisse der im Anschluss durchgeführten Versuchsreihen zeigen, dass der Prototyp aus funktionaler Sicht in der Lage ist, die manuelle Reinigung zu automatisieren und in Kombination mit geeigneten Lösungsmitteln Verschmutzungen wie Staub oder fettige Fingerabdrücke nahezu rückstandsfrei entfernt.

Schlüsselwörter: *Optik, Reinigung, Automatisierung, Python, CNC*

Contents

Symbols and Abbreviations

PCR	Polymerase Chain Reaction
PTFE	Polytetrafluoroethylene
PET-G	Glycol-modified Polyethylenterephthalat
PP	Polypropylene
HCl	Hydrochloric Acid
HFl	Hydrofluoric Acid
MEK	Methyl Ethyl Ketone
MEC	Ethyl Methyl Cellulose
TCE	Trichloroethylene
CaF$_2$	Calcium Fluoride
MgF$_2$	Magnesium Fluoride
SF11	Heavy Flint Glass
SCP	Surface Cleanliness by Particle Concentration
NVR	Non Volatile Residue
CNC	Computerized Numerical Control
DIY	Do It Youself
CAD	Computer Aided Design
STL	Standard Triangulation Language
FDM	Fused Deposition Modeling
PLA	Polylactid Acid
ABS	Acrylonitrile-Butadiene-Styrene-Copolymer
IC	Integrated Circuit
GPIO	General Purpose Input/Output

RPI4	Raspberry Pi 4th Generation
UART	Universal Asynchronous Receiver/Transmitter
PWM	Pulse-width Modulation
SPI	Serial Peripheral Interface
I²C	Inter-Integrated Circuit
GPU	Graphics Processing Unit
USB	Universal Serial Bus
HDMI	High Definition Multimedia Interface
TCP/IP	Transmission Control Protocol/Internet Protocol
LAN	Local Area Network
GTK+	GIMP Toolkit +
GUI	Graphical User Interface
NEMA	National Electrical Manufacturers Association
DC	Direct Current
CR	Carriage Return
LF	Line Feet
EEPROM	Electrically Erasable Programmable Read-Only Memory
POM	Polyoxymethylen
DMS	Strain Gauges
SPS	Samples Per Second
V$_{CC}$	Voltage At The Common Collector
NO	Normally Open
DIP	Dual In-Line Package
PEP 8	Python Enhancement Proposal 8

IP	Internet Protocol
PIP	Packet Installer for Python
APT	Advanced Packaging Tool
PyPI	Python Package Index
IDE	Integrated Development Environment
SSH	Secure Socket Shell
XML	Extensible Markup Language
X11	X-Window System
DI-Wasser	Deionized Water
HTML	Hypertext Markup Language
PDF	Portable Document Format

1 Introduction

1.1 Motivation

Optical components have become essential parts of many medical devices and instruments. The resulting optical systems help in the prevention and diagnosis of diseases, analyze samples at the molecular level and are also often used for therapeutic purposes. Modern medicine is thus supported in many ways and could not do what it is capable of today without optics. [1]

As a contract manufacturer of medical devices and instruments, the company WILD (Völkermarkt, Austria) incorporates a wide range of optics into a wide variety of medical systems. One of its specialties is *Medical Laser Technology*. The special properties of a laser make laser technology an indispensable component in fields such as dermatology or ophthalmology [2]. To ensure the long-term stability of these laser components, all optics involved must be free of particles and filmic contaminants [3].

Another focus of the company lies in the field of in-vitro diagnostics and analytics. WILD manufactures optomechatronic assemblies which are used, among other things, in measuring chambers of PCR analyzers [4]. In this case, cleanliness also plays an essential role in ensuring that terminal equipment operates with repeated accuracy and reliability.

The most typical types of contamination include small particles, which are in the ambient air and sooner or later inevitably find their way onto the optical surface. A high risk also emanates from humans, who represent the largest source of contamination with their existence and activities [5]. Incorrect handling of optical components often leads to fingerprints, which may have to be removed again at great expense. However, contamination can occur during the entire processing of an optical component. It starts with incorrect storage and ends with unsuitable working environments. For the production of an optically flawless device, many points must be taken into account, which is discussed in more detail in Chapter 1.2.

In contrast to manufacturing-related defects, such as air inclusions in the glass body or defective surface coatings, the impurities can be completely removed again in most cases. Over the course of time, various manual cleaning techniques have become established for this purpose [6].

The present work deals with the possibility of automating the cleaning process, which has been carried out manually up to now. The focus is placed on the automation of the so-called *Brush Technique*. For this purpose, a CNC-based cleaning robot was designed, developed, built and then subjected to various test series.

1.2 Correct Handling of Optical Components

Before considering how to clean optical surfaces best, it should be investigated what circumstances lead to soiling in the first place. From the knowledge gained, useful actions for dirt prevention can be derived so that cleaning is not necessary after all. It is also important to prevent recontamination of optics that are already clean. With each cleaning cycle, the risk of accidentally damaging the usually very sensitive surfaces increases [6].

1.2.1 Types of Contamination

Contamination of optical surfaces can be roughly divided into two categories. On the one hand, they occur in the form of discrete particles and, on the other, as a continuous film of dirt covering the surface. It is also possible that a mixture of both types exists. While particles cause the incident light to be scattered, dirt films cause unwanted absorption bands. [7] These effects have a negative impact on the optical performance of the components; depending on the application, there is a loss of image quality or transmission losses, for example [5].

When one speaks of „particles" one generally means dust and this in turn, is a collective term for different types of solid particles in gases, which can be either organic or also inorganic in nature [8]. Dust can also be categorized based on size. Particles with a diameter $> 10\mu m$ belong to the class of *Coarse Dust*, everything below that is called *Particulate Matter* [9]. When dust is referred to in the following chapters, it always refers to *Coarse Dust*.

A practical example of inorganic dust would be fluff that comes off textiles or abrasions of different materials such as glass or metals. Organic dust, on the other hand, includes e.g. skin flakes, hair or pollen, which are increasingly found in the air, especially during the flowering season. [10]

Contamination without defined dimensions, such as fingerprints, evaporation residues of various liquids or outgassing of other components, is deposited as a layer on the surface and thus falls into the category of molecular contamination (dirt films) [5].

1.2.2 Sources of Contamination

Pollution Due to Production

Production steps such as drilling, turning, milling or grinding optical glass generate particles which, especially in combination with cutting oils, can lead to stubborn contamination. Therefore, care should be taken beforehand to use oils that can be easily removed after processing. [5]

Contamination During Assembly

Another source of contamination that should not be underestimated arises during the mounting of optics. For example, it is a common method to fix round optics in their mounts by means of *Retaining Rings*. If the external thread of the *Retaining Ring* or the internal thread of the optics mount is not perfectly clean, it is possible that abrasion will occur during gripping, which will then be deposited on the optics in the form of small metal chips or anodized residues and contaminate them again. A further risk of contamination arises when optics are fixed using various bonding techniques. Resins, cements and special adhesives are used here, which contaminate optically relevant surfaces if the work is not carried out properly. In this case, it is necessary to react quickly, as these are very difficult to remove once cured and there is a risk that the optics will be damaged as a result [11].

Contamination by Humans

The greatest risk of contamination for optics is posed by people. Apart from the fact that people themselves release a lot of organic particles during the course of the day, you also pick them up continuously by moving around. [5] During the handling of optics, they can become detached again and contaminate optical surfaces.

However, people do not contaminate optics exclusively by particles. Coughing or sneezing releases small aerosol particles into the ambient air. These settle on the surface of the optics and leave behind small films of dirt.

Unlike dust, this type of contamination cannot be easily removed with compressed air. In this case, the contamination can only be „rubbed off" the surface with the aid of a solvent and a suitable cleaning medium. There are different methods for this, which are described in more detail in Chapter 1.3 on page 7.

Continuous training in the proper handling of optics and appropriate work equipment help to keep human-caused contamination low [5].

1.2.3   The Right Working Environment

Once optics have been joined together with mechanical or electrical components to form a functional assembly, cleaning is no longer possible in many cases. This means that the final cleaning must take place before assembly or integration. From this point on, it is important to keep the assembly clean and this requires a defined working environment. [5]

To avoid recontamination of already clean optics, it is important that certain points are noticed when designing the workplace. Table 1 gives a brief overview of what to pay special attention to in optics workstations.

Table 1: Tips for the design of an optics workstation

Equipment	The workstation is spatially delimited (e.g. in the form of a cabin) and the interior walls are lined with a matte black cover. The work mat should also be dark, this allows better control of the optics and prevents stray light. [12]
Lighting	The interior lighting is flexible and the illuminance is about 500 to 600 lx. As light color a neutral white is suitable. [12]
Tools	Tools must be stored outside the work area to keep the work surface as clear as possible. [12]
Packaging material	Cardboard, paper or similar fibrous packaging material must be kept away from the workplace as they contaminate it. Span-generating work steps must not be performed on optical workstations. [12]

The optimal workplace for this purpose is represented by so-called *Flow Boxes*. A *Flow Box* is a special cabinet that takes in ordinary ambient air contaminated with particles and forces it through particulate filters of varying fineness. The resulting low-particle air, flows streamlined from the top of the cabinet to the bottom, creating a local clean room by moving the particles inside the cabinet to the outside. [13]

If very sensitive optics are involved, *Flow Boxes* alone are often no longer sufficient. In this case, a full-fledged clean room can be used. In addition to the laminar air flow already explained, there is also a continuous overpressure in cleanrooms, which ensures that particles cannot enter from the outside [13]. This means that even higher cleanliness classes can be achieved. Another advantage is that temperature and humidity can be kept at a constant level. A defined room climate is important, as optical glass is often very sensitive to temperature fluctuations [6]. For the best possible working environment, *Flow Boxes* and cleanroom can also be combined.

Working in clean rooms requires that certain rules of conduct are followed. These include, for example, the wearing of special work clothing which, with a few exceptions, covers all parts of the body. In addition, care must be taken to ensure that no contaminated tools or components are introduced. A violation of the rules can quickly lead to the particle count (locally) increasing to a multiple of the permitted value, and the actual advantage of a cleanroom is no longer given.

1.2.4 Personal Work Equipment and Tools

In addition to the requirements for the working environment, it is equally important that the personal work equipment is suitable for handling optics.

Particular attention must be paid to the cleanliness of the hands, especially that they are free of grease and silicone [12], because fingerprints are often difficult to remove again. As a general rule, touching optically effective surfaces with bare skin should be avoided in any case. This can be easily prevented by wearing disposable finger covers or disposable gloves made of cotton, nitrile or powder-free latex. [6, 12] When handling particularly small optics, the use of optics tweezers can be advantageous. These are typically made of plastic or bamboo wood to prevent accidental damage to the optics. Alternatively, the market also offers air-assisted pick-up tools called *Vacuum Tweezers*. [14]

To better detect contamination, it can be useful to use aids such as magnifying glasses or microscopes. On the one hand, these help to better detect dust or fingerprints, and on the other hand, they can also be used to check the cleaning success. They also help to distinguish dirt from damage, because wiping over a scratch is of course pointless and only increases the risk of further damaging the surface. [15]

Other accessories that no optics workstation should be without are various light sources. Depending on the type of visual inspection you are performing, you will need either a transmitted light with a diffuser, a reflected light, or a flexible fiber optic light guide, also known as a *Gooseneck Light* [12]. Ideally, the light intensity of the light source is adjustable.

1.2.5 Storage and Transport

Other essential points concern correct storage and transport. Optics should be transported in airtight containers and stored there until further use.

For less demanding components, simple, sealable plastic blisters can be used. For components with sensitive surfaces, it is recommended to additionally pack them individually for protection. Bags made of *Pergamin Paper* or special „lint-free" optical wipes [6] are suitable for this purpose. Semi-finished or fully assembled assemblies

are best stored in plastic boxes made of Polycarbonate, PTFE (Polytetrafluoroethylene) or PET-G (Glycol-modified Polyethylene Terephthalate). Boxes made of PP (Polypropylene), on the other hand, should not be used because they outgas and thus affect the coated optics by contaminating the surface with deposits. [16] Minor impurities are already sufficient to cause laser-induced damage to the surface coating, which can become a problem, especially in the area of high-power lasers [17]. The optimum storage conditions are achieved at a temperature between 15 and 25 °C and a relative humidity < 30 % [16].

1.3 Manual Cleaning Methods

In the context of this master's thesis, research was also performed to determine which cleaning methods correspond to the current state of the art. It was found that the procedures and recommendations for care and cleaning have not changed significantly over the last 400 years. [18] Nevertheless, an optics-specific standard has not been established, neither for cleaning nor for assessing the cleanliness of optical surfaces [19].

„If it's not dirty, don't clean it!"

Cited from [20]

At the outset, it should be mentioned that optics should only be cleaned if they are actually dirty because every cleaning process also involves the risk of accidentally damaging the surface [20].

Over the course of time, different methods have become established, whereby not every method of cleaning is suitable for every optic. This means that it must be estimated in advance which method is best suited based on the type of contamination, the degree of contamination, the number of optics to be cleaned, and the respective coating [6].

1.3.1 Detergents

In addition to the right cleaning method, it is also important to use the right detergents. While distilled water is sufficient for water-soluble soiling, greasy soiling, such as fingerprints, can only be removed with the help of solvents [10].

The most commonly used solvents include *Acetone* and *Isopropyl Alcohol*, also known as *Isopropanol*. Pure *Acetone* has the disadvantage that it evaporates very quickly and therefore sometimes does not dissolve all impurities. The problem can be circumvented by diluting it with *Methanol*. [21]

Isopropanol, on the other hand, is suitable for almost all optics except those with aluminum coatings (e.g. mirrors). The reason is that the alcohol reacts with the aluminum. [19] Other incompatible optics-cleaning agent combinations are listed in Table 2 on page 8.

Table 2: Combinations to avoid when cleaning optical components [19]

Cleaning agent or method	Coating
Alcohol	Aluminium coating or substrate
Acids like HF oder HCl	Coated optics, Zinc sulfide, Zinc selenide, VIS and UV optical glasses
MEC, MEK, TCE	Coated optics
All	Bare metal coating like gold, copper or aluminium
Ultrasonic cleaning	Metal coatings, soft optical glasses (e.g. CaF_2, MgF_2, $SF11$)

1.3.2 Compressed Air Cleaning

Particles have the potential to scratch the surface during cleaning. Before falling back to various wiping or brushing techniques, it is advisable to blow the poorly adhering dirt from the surface without touching it. For this purpose, the generation of air blasts utilizing so-called *Blower* or compressed air from a can is suitable. [6, 20]

The company *Carl Zeiss*, points out in the online article „*Microscope Cleaning and Maintenance*" that with compressed air sprays there is a risk of extremely cold air or freezing liquids hitting the surface and damaging it permanently [22]. Ordinary compressed air generated by a compressor usually contains a lot of moisture and oily residues. It is only suitable if the air has previously been cleaned and dried by special compressed air filters. [11]

In any case, „blowing off" the particles using breathing air is unsuitable and are more likely to result in the surface being further contaminated by fine saliva droplets. If blowing off using compressed air remains unsuccessful, one of the following methods can be resorted to.

1.3.3 Mechanical Scrubbing Methods

There is broad agreement in the literature regarding the scrubbing methods. Basically, a distinction is made between the *Drop and Drag*, the *Brush Technique* and the *Wipe Technique*. [6, 20, 21]. Which method to use depends largely on how stubbornly the dirt adheres to the surface. Basically, however, you should always start with the method that is gentlest for the surface.

Drag and Drop

This method allows to remove minor impurities and is only applicable for unmounted lenses and mirrors [6].

The optics to be cleaned are first placed on a clean, non-abrasive cloth. Special cleanroom cleaning cloths are particularly suitable for this purpose, as no tissue fibers come loose from them. A second, unfolded cloth is then wetted with *Acetone*, *Isopropyl Alcohol* or another suitable cleaning solution. The soaked cloth is now slowly and carefully pulled over the surface of the optics until the solvent has evaporated. [6, 14, 20]

When selecting the solvent, make sure that it is suitable for the optics present. Acetone, for example, is an aggressive solvent and must therefore never be used on plastic optics [14]. For minor soiling, it is often sufficient to use distilled water [23].

Brush Technique

This cleaning technique requires an additional aid in the form of a „brush". This can be made from simple materials.

One possible variation is to wind absorbent cotton (100 % cotton) onto a wooden handle until an elliptical cotton ball is formed. Ordinary commercially available cotton swabs are not recommended, because they often contain a certain amount of synthetic fibers, which can damage the surface. [22]

Furthermore, the cleanroom wipes already mentioned can also be converted into brushes. To do this, they are folded several times so that the length of the folded edge roughly spans the optics surface. Tweezers, for example, can be used to hold the folded cloth. [6]
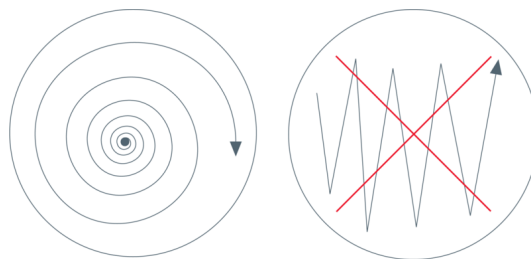

Figure 1: Correct cleaning using the spiral pattern (left), and incorrect cleaning using zig-zag movements (right). Image source: [24]

Cleaning is done by moistening the cotton swab or lens tissue brush with solvent and wiping in a spiral motion starting from the center and working outward, see Figure 1.

The spiral movement is essential, because it collects the impurities and wipes them to the edge of the optics. A zig-zag movement, in contrast, only causes the dirt to be distributed. [22] It is also important to ensure that the movement is carried out continuously to avoid drying traces of the solvent [20]. For smaller optics, special swabs out off *Polyester* with long handles can be used as an alternative to the self-made brushes.

Wipe Technique

This technique is used for particularly stubborn dirt. Basically, it corresponds to the brush method, with the difference that the folded cloth is clamped between the fingers. When wiping the surface, care should be taken to apply adequate, even pressure. The method is not suitable for cleaning metal-coated surfaces. [20, 6]

1.3.4   Cleaning With Liquid Polymers

Another approach to cleaning optics is the use of a *Liquid Polymere*, which, unlike the cleaning methods already described, requires neither compressed air nor solvents. The technology behind it was developed back in the 1980s. The driving force behind it was the problem that mirrors that had already been mounted and adjusted had to be removed for cleaning. The invention of the *Liquid Polymer* made it possible for the first time to clean optics in place without having to readjust already adjusted optics. [18]

For cleaning, the polymer is applied directly to the dirty optical surface, either by brushing or spraying. After a few minutes, the layer hardens into a thin plastic film, which binds the dirt to itself. The polymer can then be easily removed. [18]

In principle, this technique is suitable for most optical surfaces; however, it is not recommended for poorly adhering coatings [25].

Due to its tough and flexible properties, polymer films can also be used to protect already cleaned optics until they are installed. Scratches and contact can thus be effectively prevented during transport. When dry, the film also protects against moisture and sulfide contamination. [18, 25]

The cleaning success of this method is also supported by studies. In the paper *„Increased Laser Damage Threshold by Protecting and Cleaning Optics Using First Contact Polymer Stripcoatings: Preliminary Data"* published by Eric S. Bailey et al. it is confirmed that the laser-induced damage threshold is increased by up to 10 % by cleaning using polymer films [26].

1.4 Mechanical Cleaning Methods

1.4.1 Ultrasonic Cleaning

Ultrasonic cleaning is a cleaning technique in which the *Cavitation* of solvents is used to clean surfaces [27]. The cleaning equipment essentially consists of an oscillating tank and ultrasonic generators, which are usually located at the bottom of the tank. The generators produce oscillations in the ultrasonic range (20 kHz to 500 kHz), which are transmitted through the tub into the cleaning liquid. This causes negative as well as positive pressure waves to be generated in the cleaning liquid. The constant alternation between negative and positive pressure generates small cavitation bubbles, which grow until they implode. The water pressure created by the implosion dissolves the impurities from the cleaning material. [28]

The frequency and power of the ultrasound are variable and can be adapted to the material to be cleaned and the degree of contamination. The size of the cavitation bubbles is inversely proportional to the ultrasonic frequency, while the cavitation intensity increases proportionally to the ultrasonic power [27].

The cleaning result also depends to a considerable extent on the choice of the right cleaning liquid. It is important to know what type of soiling is involved in order to use a suitable solvent on the basis of this. It should also be noted that the cleaning solution should be replaced at regular intervals, as the level of contamination in the solution increases with each pass. Ultrasound removes particles larger than 25 μm in diameter quite effectively, making it well suited for cleaning during the production of optics. For high-precision optical elements, however, the cleaning technique should be considered at best for removing coarse contaminants and not as a final cleaning method. [7]

1.4.2 Further Machine-Assisted Cleaning Methods

In addition to the cleaning methods just described, there are other approaches to cleaning optical surfaces, see Table 3. These techniques are not widely used, because their field of application is either very limited or the implementation is very complex.

Table 3: Brief description of other common cleaning methods

Method	Operating principle
CO_2-cleaning	In this method, snow generated from CO_2 is thrown onto the optics surface at high speed. The impact of the snow causes contaminants to be kicked off the surface. This method is suitable for both intermediate and final cleaning and is usually used for surfaces that are difficult to access. [11]
Steam cleaning	Steam cleaning is suitable for particularly sensitive surfaces for which a mechanical cleaning method is not applicable. Solvents such as *Alcohol* or *Acetone* are first heated to boiling point in a bath. The surface to be cleaned is then held slightly tilted over the bath for a short time. The vapor produced by the heating condenses on the significantly colder optical surface. Condensate droplets form, which rinses the dirt from the surface. This technique requires increased safety measures, as the solvent vapor generated can quickly reach a highly flammable level. [29]
Micro-vacuum cleaning	This technique is based on the generally known vacuum cleaner principle. A micro vacuum probe is placed close to the contaminated surface. The air sucked in through the nozzle generates such high shear forces that dust can be detached from the surface and sucked in. The principle is only suitable for particle sizes $> 50 \mu m$ and is very time-consuming. [7]

1.5 Verification of Cleanliness

1.5.1 Quantitative Determination of Contamination

Irving F. Stowers and Howard G. Patton write in their paper „*Cleaning Optical Surfaces*" that the quantitative determination of the cleanliness of a surface proves to be difficult [7]. However, there are three approaches that should help to determine the degree of cleanliness, see Table 4.

Table 4: Comparison of cleanliness based on thickness, weight and number of particles, in reference to [7]

Monolayer	A monolayer, also called an atomic layer corresponds roughly to 10^{14} - 10^{15} Atoms per cm^2
Weight	One $\mu g/cm^2$ corresponds to five carbon monolayers
Particle count	One particle (Ø=10 μm) per cm^2 is equivalent to $\frac{1}{20}$ of a monolayer

Theoretically, surfaces are considered „extremely clean" if their purity level is less than one-tenth of a monolayer. From a practical point of view, purities of up to 10 particles per cm^2, with a particle diameter $> 10\mu m$, can be achieved in production environments. [7]

There are basically two methods to quantify the degree of contamination of a general surface: Particulate contamination, such as dust, can be easily quantified using the counting method. In contrast, dirt films are not so easy to determine. In this case, one relies on a NVR analysis (Non-volatile Residue) [30]. Its concept is based on *Gravimetric Determination* and basically corresponds to a high-precision weight measurement [31].

1.5.2 Classification of Surface Cleanliness

The purity of a surface can be classified according to different norms and standards. For example, Part 9 of *ISO 14644* deals with the classification of *Particulate Surface Cleanliness*. The scope of application spans all cleanroom solid surfaces and their associated cleanroom areas. This includes tools, equipment and *products*. It is divided into eight SCP (Surface Cleanliness by Paricle Concentration) classes and is based on the maximum permissible particle concentration per square meter, with particle size also included in the classification. [32] The impurities described in the

standard refer to particles only; dirt films are not covered.

The U.S. counterpart to *ISO 14644-9:2022* is the industry standard *IEST STD-CC1246E*, which governs product surface cleanliness levels for commercial and non-commercial purposes. Unlike the ISO standard, the *IEST STD-CC1246E* specifies not only particulate surface cleanliness, but also non-volatile residues. The particle-based cleanliness level is defined by the maximum number of particles per 0.1 m^2 and also takes particle size into account. For non-volatile residues, a maximum allowed mass per 0.1 m^2 is specified for each level. [30]

By definition, the degree of purity of optical surfaces could be defined using both standards. The units „per m^2" resp. „per 0.1 m^2", however, suggest that an application to the usually much smaller optical surfaces is not considered.

Up to now, there has been no standard regulating surface cleanliness for explicitly optical components. This is also confirmed by the well-known optics manufacturer *asphericon* (Jena, Germany), see electronic request in Appendix D.

1.5.3 Visual Inspection Before Mounting

Robert Schlack writes in his book „*The Proper Care Of Optics*" that the human eye is able to detect the position and height of objects through its stereo-visual system. It is therefore well suited to identify defects and contaminants on optical surfaces. This ability can be further improved by training the eye to compare clean, defect-free optical surfaces with dirty or defective ones. A trained eye can detect even minor deviations in contrast, color and texture. [11]

To provide the best possible support for the eye during visual inspection, an inspection environment is required as described in Chapter 1.2.3, page 3. The systematic use of different light sources helps to detect impurities more easily. In this way, the eye can resolve particles as small as 10 μm [7]. Over time, different methods of visual inspection have become established. These differ mainly in the type of illumination. It must be remembered that the results of visual inspections are always linked to the subjective perception of the inspector, regardless of which method is used [12].

Transmitted Light Control

In transmitted light inspection, the optics to be inspected are placed between a light source and the eye. The typical inspection distance between the eye and the lens is between 25 and 40 cm. An LED light source with a diffuser plate is suitable for transmitted light illumination, as can be seen in Figure 2. [12]

Eye

Optic to be checked

Light source with diffusor
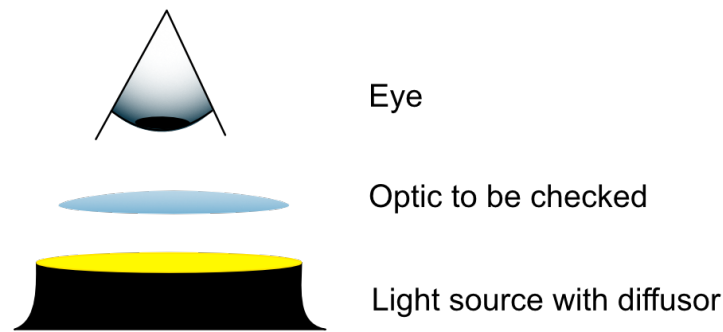
Figure 2: Principle of transmitted light control, based on [12]

Stray Light Control

The stray light control is performed against a black background. The light source must be positioned so that the light from the opposite side hits the optics at an angle of at least 45 °. [11] By slightly tilting the optics, the incident light is scattered differently, so dirt and defects can be easily detected.

Light Source   Optic to be   Eye
                   checked

Reflected
light
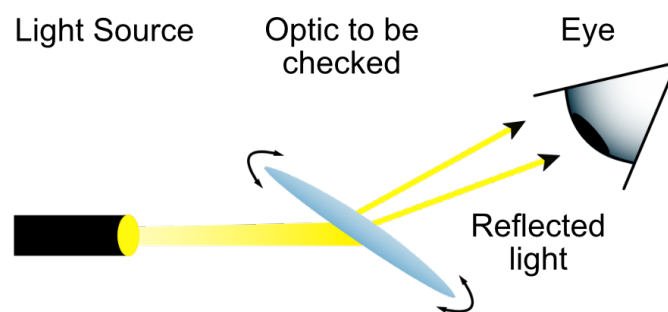
Figure 3: Schematic representation of scattered light control, based on [12]

The most suitable light for this type of test is highly focused light in the form of a cold light source with a flexible light guide, also called *Gooseneck* [12]. The principle is illustrated in Figure 3.

Incident Light Control

This method is particularly suitable for identifying inhomogeneities of the coating and cementation. Either a flexible light bar, or a large area diffuse light source (see Figure 4) can be used as the light source. Also with this technique, the optical surface specified in the drawing is inspected for cleanliness and damage such as scratches, pressure marks, or decorative abnormalities. [12]
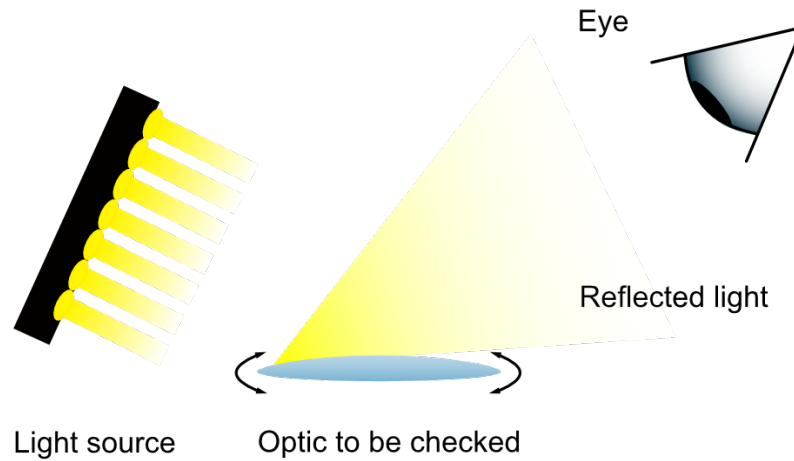
Figure 4: Illustration of a surface inspection using incident light, following [12]

1.6 Influence of Contamination

Contaminated surfaces affect the optical performance of a component in different ways. The form in which they have an effect essentially depends on whether the contamination is present as particulate dirt, or as film-like impurities.

1.6.1 Obscuration and Scattering

When light falls on an optical surface contaminated by particles, scattering effects occur on the one hand and shadowing or transmission losses on the other. While the size and number of particles in the optical path are decisive for shadowing, scattering depends on the ratio between particle size and the wavelength of the incident light. [5]

a   b
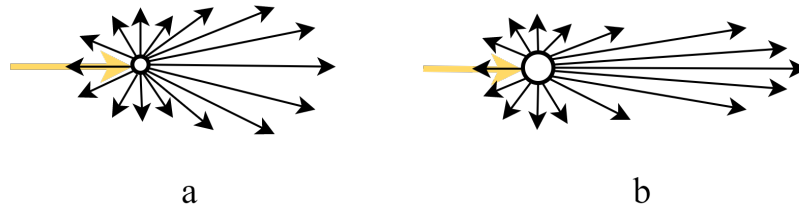
Figure 5: Typical patterns produced by *Mie Scattering* on a) smaller and b) slightly larger particle illuminated from the left, in the style of [33]

Assuming a particle diameter $>10~\mu m$, the wavelength of visible light is much smaller in comparison. In this case, the resulting scattering can be calculated using *Mie Theory* [33]. It is to be noted that the function behind this theory only holds for scattering caused by one particle [5]. Figure 5 shows the pattern of *Mie Scattering* from particles of different sizes.

It also should be mentioned that the phenomenon of scattering affects the optical path not only within an optical system. The generated scattered light can also affect other parts of the optical system outside the affected component. [5]

In spectroscopy, for example, stray light can cause problems because the underlying principle is based on measuring light intensities. A too high degree of stray light influences the measurement. [34]

In microscopy, dirty optics express themselves in the form of reduced image sharpness and contrast. Not all contamination has the same effect on the image. The crucial factor is which optical component is affected. As a general rule, the influence of a contaminant on the image increases the closer it is to the object to be examined [10] or to an itermediate „image" in the optical path.

Therefore, sufficient cleanliness must be ensured, especially for the front lenses of the objectives. In the case of digital microscopes, the surface of the sensor and its protective glass also have a strong influence on the imaging. [10]

1.6.2 Absorbance Bands

Impurities in the form of a dirt film lead to undesirable absorption bands and can cause problems, especially with laser systems [7]. The incident light is absorbed to a greater or lesser extent by the dirt film, depending on the wavelength, and generates local heating there. If the energy absorption of the dirt film is high enough, thermal-related damage to the optics can occur. [5, 35]

Mathematically, the absorption of light can be estimated with the help of *Lambert-Beer's law* (1). Nonlinearities and scattering effects are not considered. The linear absorption coefficient α depends on the wavelength of the laser and the concentration of the absorbing layer. The light intensity supplied by the laser corresponds to I_0. That part of the light that passes through the dirt film of thickness d exits as light intensity $I(d)$ and hits the surface of the optics. The higher the difference $I_0 - I(d)$, the higher the risk of irreversible damage to the optics. [35]

$$I(d) = I_0 \cdot e^{-\alpha \cdot d} \tag{1}$$

A term often mentioned in this context is the so-called *Laser Damage Threshold*. It is an important parameter in the field of laser optics and indicates the maximum laser power per area to which an optical component can be exposed without being destroyed [36]. The higher the degree of contamination, the lower the laser damage threshold.

If the dirt film is in the form of a droplet, it can additionally be seen as a particulate contaminant, which leads to scattering effects as mentioned above [5].

1.7 Aim and Requirements

The aim of this master thesis is the development of a cleaning system to be used in the assembly process of optical assemblies at WILD GmbH.

Until now, the cleaning of optics has been performed exclusively manually, using the *Brush Technique* described in Chapter 1.3.3. If too much force is applied, the surface coating may be damaged, which subsequently impairs the optical performance of the component.

The cleaning system to be developed should ensure that the inserted optics are cleaned with a constant pressure over its entire surface. The main focus lies on the cleaning of exclusively round optics (mainly lenses) of different size and curvature. The cleaning process should be automated to such an extent that the contaminated optics only have to be inserted into the robot.

1.7.1 Mechanical Requirements

The basic cleaning principle of the *Brush Technique*, should be maintained but automated. Excluded from automation are the insertion, turning and removal of the optics to be cleaned.

Mounting Unit

The mounting unit must be designed in such a way that a wide range of different round optics can be clamped. The following conditions must be met with regard to the shape and diameter of the material to be cleaned:

Table 5: Requirements to the mounting unit

Dimension \ Value	Min. in mm	Max. in mm
Optics diameter	15	60
Radius of curvature	23	305

Solvent Unit

The solvent should also be supplied by the cleaning robot. Since *Acetone* is largely used as a solvent during cleaning, it is important to ensure that only resistant materials are used.

Cleaning Swab Pickup

Special *Polyester Swabs* from Texwipe (Kernersville, USA) are to be used as „Brushes“. Since these have to be changed from time to time, it is important to ensure that the brush holder is designed in such a way that replacement is straightforward and does not take much time.

Energy Efficiency and Sustainability

In the context of the current energy crisis, the system must be designed to be as energy-efficient as possible. Furthermore, the current high consumption of solvents is to be reduced.

1.7.2 Functional Requirements

Surface Profiles

The cleaning system should be flexible enough to allow cleaning of stepped profiles or flat surfaces in addition to ordinary convex- or concave-curved optical surfaces. The pressure of the cleaning rod on the optical surface must not change significantly as a result.

Mode of Operation

In general, the cleaning system is to be operated as a standalone device. As an option, however, it should also be possible to operate the robot via network-compatible devices such as a PC, notebook or tablet, for example, to change basic settings.

It should also be possible to adapt the cleaning settings to the respective lens. The cleaning profile of a lens includes at least the following adjustable parameters:

- Rotation speed of optics pickup (mounting unit)

- Amount of solvent dispensed

- Force with which the cleaning rod pushes on the surface of the optics

- Number of cleaning cycles

It must be possible to save the parameters just listed in the form of a cleaning profile. Users should be able to create, delete and change profiles.

2 Methods and Materials

2.1 Concept Development

2.1.1 Approach

The basic role of the robot is to imitate the manual cleaning process and, in a broader sense, the movements of the employees. In order to develop a concept, it was first necessary to examine the process, so the project was started by examining the manual cleaning process on-site (WILD). For this purpose, the individual work steps of the employees during cleaning were closely observed and analyzed. The information gained from this was used to specify the task and to work out various possible solutions.

2.1.2 Basic Mechanical System

The analysis of the cleaning process showed that at least a two-axis system is required to imitate the *Brush Technique* described in the Chapter 1.3.3 on page 8. As a basis for this, a CNC-based (Computerized Numerical Control) positioning system was considered, which can be used flexibly and is moreover available as a DIY (Do It Yourself) kit.

The positioning accuracy of such DIY kits is not comparable with that of professional systems, but it is sufficient for the planned use and especially for the construction of a prototype.

2.1.3 CAD Construction

For better illustration, a three-dimensional model of the cleaning robot was created from the project idea, see Figure 6 on page 22. A digital version of the project idea offers several advantages. For example, the spatial representation helps in design discussions. In addition, 2D drawings for the subsequent manufacture of the production parts can be derived from the 3D models, without much effort. With almost all common CAD applications (Computer Aided Design), it is also possible to export the component models for 3D printing in the form of STL files (Standard Triangulation Language).
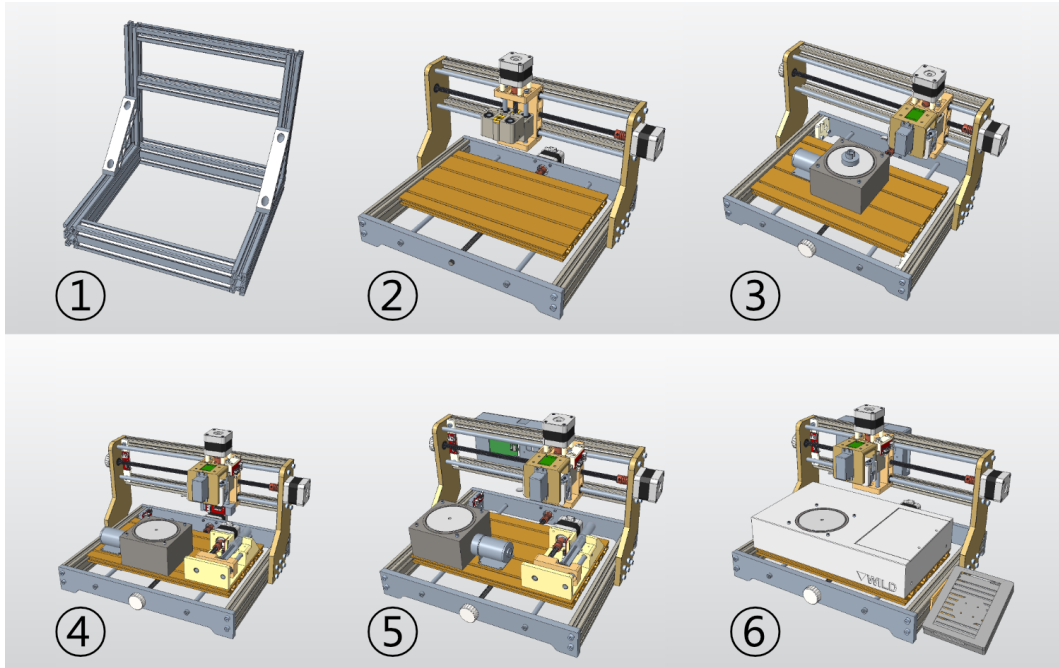
Figure 6: Different phases during concept development
(1) First attempt of the basic construction
(2) Fully functional 3-axis positioning system
(3) Extension of the base with cleaning head and turntable unit
(4) Extension by a solvent transport unit
(5) Extension by the central control including its housing
(6) Final device including all covers (without touch display)

The CAD software *Creo* (PTC Inc., Boston, USA) was used to develop the concept. A helpful feature of *Creo* is that movements can also be simulated. This allowed problems such as collisions of components to be detected and corrected before manufacturing or printing.

For standard parts such as screws, nuts, pins, etc., freely accessible libraries of the company Trace Parts GmbH (Amberg, Germany) were used. *Creo* allows, in addition to its own file formats, models from other CAD software manufacturers to be imported and incorporated into the existing project.

2.2 Materials and Manufacturing Technologies

2.2.1 Mechanische Komponenten

The production of the manufacturing parts was largely based on *Rapid Prototyping* in the form of 3D printing. The great advantage of 3D printing is that components can be manufactured quickly and inexpensively, which is especially interesting for prototyping.

Printing was mainly done with the material *Onyx* (Markforged, Watertown, USA). The chemical composition of *Onyx* allows the printed parts to be resistant even to strong solvents such as acetone [37]. For the less demanding parts, filaments made of *Polylactide Acid* (PLA) and *Acrylonitrile-Butadiene-Styrene-Copolymer* (ABS) were used. In order to keep the print quality constant, three different printers were used, each of which was previously optimized for one filament, see Table 6.

Table 6: Listing of all 3D printers, which were used for the construction of the cleaning robot. The *Mark Two* and the *EL-102* are professional industrial printers, unlike the *Ender3 S1*.

Printer	Manufacturer	Filament	Printing space in mm
Mark Two	Markforged	Onyx	320 x 132 x 154
Ender 3 S1	Creality	PLA	220 x 220 x 270
EL-102	EVO-TECH	ABS	500 x 400 x 510

Despite the well-developed 3D printing technology and the sometimes excellent material properties of the filaments, *Rapid Prototyping* is not suitable for every component. In such cases, classical manufacturing processes in combination with higher-quality materials (metals) were used.

2.2.2 Electronic Components

Breakout Boards

In addition to the mechanical components, the cleaning system also requires some electronic components. For example, modules such as stepper motor drivers, ADC (analog to digital converter) or DC-DC converters in the form of a *Breakout Board* are used.

On *Breakout Boards*, the *ICs* (Integrated Circuits), on which the function is based, are already soldered on small PCBs and all important connections are brought out as plug-in connections. This simplifies the development of the overall system and makes the modules easy to replace in the case of a defect. In addition, the cleaning system can also be more easily duplicated in the future by using *Breakout Boards*. However, one disadvantage of *Breakout Boards* is that they are not particularly flexible. The external circuitry is often crucial for the configuration of an IC, and with *Breakout Boards* this can only be changed to a very limited extent, if at all. Chapter 2.5.4 on page 43 describes a concrete case where it was necessary to manipulate the board.

Logic Levels

When selecting the electronic modules, in addition to the functional requirements, it was important to ensure that they were compatible with the logic technology of the control board. The single-board computer used for the system control *Raspberry Pi* (Raspberry Pi Ltd., Cambridge, England), is based on a 3.3 V logic and not tolerant to a 5 V logic [38]. This means that any directly connected peripherals must also be based on 3.3 V logic. If the GPIO (General Purpose Input/Output) pins of the Raspberry Pi are connected with more than 3.3 V, there is a risk of irreversible damage.

Cable Connectors

The cabling of the robot is mostly based on clamp and plug connections, which eases any changes or repairs of the system. Since both, the controller board and the *Breakout Boards*, have pin headers soldered, flat ribbon cables were used in combination with the widely popular *Dupont Connectors*. Plugs and sockets of the JST-RE series were used for the connections of stepper motors and limit switches.

2.2.3 Standard Parts

For all mechanical components not addressed so far, such as screws, nuts, dowel pins, plain bearings, etc., standard parts from different manufacturers were used.

2.3 Preliminary Tests

Before the cleaning robot was actually built, the sensors and actuators under consideration were tested for their suitability. The aim was to find out if the components were suitable for implementation in the cleaning system. It was also determined how the electronic components could be controlled or read out by software. The following tests were performed:

- Establishing a serial communication between PC and CNC controller via UART (Universal Asynchronous Receiver / Transmitter).

- Reading of limit switch states via *Polling-* and *Interrupts*

- Indirect and direct control of a servo motor via pulse width modulation (PWM)

- Control and readout of a PWM-based leveling sensor

- Force measurement by load cell in combination with an ADC-*Breakout Board*

The widely used microcontroller development board *Arduino UNO R3* (Arduino S.r.l., Monza, Italy) was used as the controller. A detailed description of the test series carried out can be read in the seminar paper named „*Ansteuerung unterschiedlicher Sensoren und Aktoren über einen Microcontroller*" [39].

2.4   System Overview

The cleaning system can basically be divided into a CNC positioning system, a central control system, a display unit, a rotary table with optics pick-up, a solvent transport unit and the cleaning head with scanning function. Table 7 contains a brief functional description of all the units mentioned. Details will be covered in more detail in the following chapters.

Table 7: Brief description of the six units of the cleaning robot

Unit	Description
CNC-Positioning System	The positioning system forms the basis of the cleaning robot. All further units are based on it. The main function is to position the cleaning head in three-dimensional space and thus to imitate the movements of the *Brush Method* described in Chapter 1.3.3. The positioning is performed by three stepper motor-driven trapezoidal spindles.
Central Control	As the name indicates, this unit coordinates the entire cleaning process by controlling the various actuators and reading out sensors.
Operation and Display Unit	The unit enables interaction with the user in the form of a touch-capable LCD monitor.
Rotary Table Unit	The rotary table unit rotates the optics to be cleaned via a DC gear motor. The speed is variable and is controlled via the CNC positioning system.
Solvent Transport Unit	It consists of a syringe pump and a tubing system through which the solvent is transported to the cleaning rod.
Cleaning Head	This multifunctional unit has several tasks: On the one hand, it serves as a holder for the cleaning rod. On the other hand, the force (or pressure) with which the rod presses on the optics is measured by its integrated load cell. With the built-in leveling sensor *BLTouch*, it is possible to scan the surface profile of the optics.

All units of the cleaning robot are shown in Figure 7. Normally, the pump unit of the solvent transport system (5) is covered by a flap; for better clarity, this has been hidden in the CAD model.
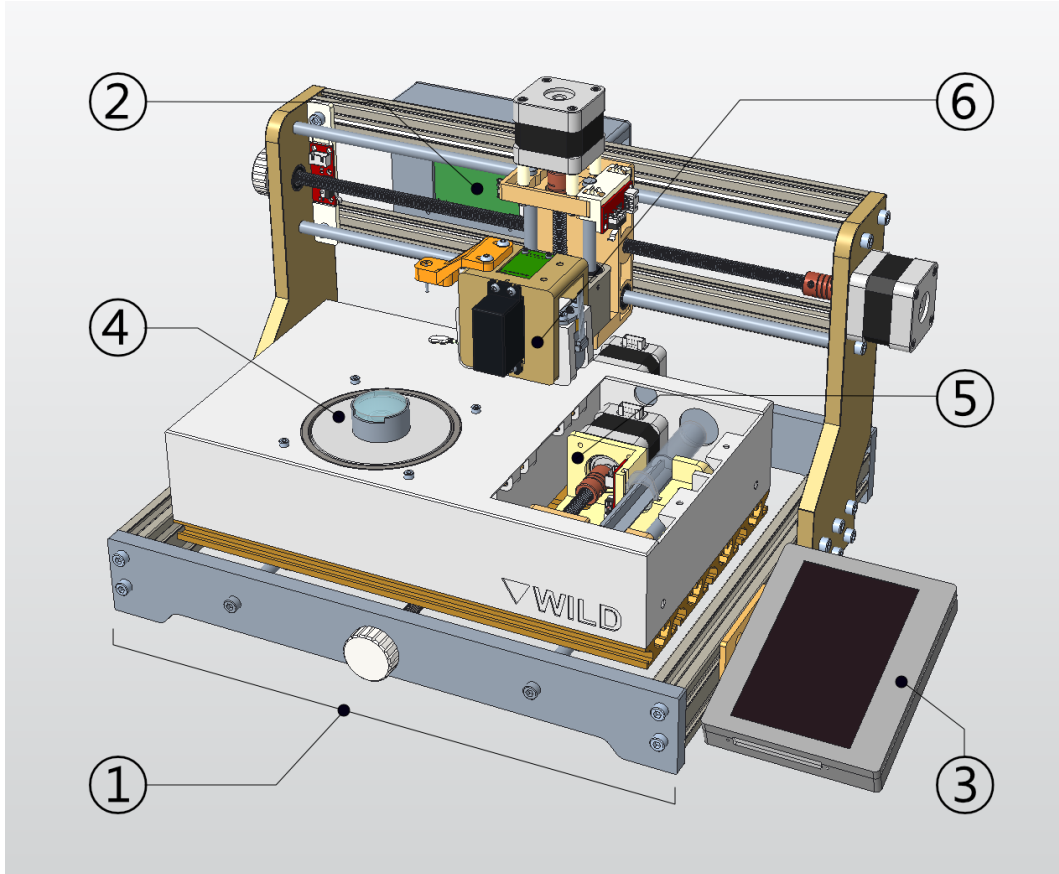
Figure 7: CAD model of the cleaning robot in its most current version, as of January 2023.
(1) CNC-Positioning System (basic structure)
(2) Central Control Unit
(3) Operating and Display Unit
(4) Rotary Table Unit
(5) Solvent Transport Unit
(6) Cleaning Head

Figure 8, page 28 illustrates how the individual system units are linked to each other. The direction and content of the information flow are visualized in the form of arrows. The two dashed lines between the controller and the PC indicate that this is an optional connection.

Figure 8: Block diagram of the cleaning system with visualization of the information flow

2.5 Hardware

2.5.1 Central Control Unit

As already mentioned, the central control of the cleaning robot is based on a fourth-generation *Raspberry Pi*, or RPI4 for short. The great advantage of this single-board computer is that it combines the ease of use of a desktop PC with the hardware proximity of microcontrollers. This combination makes the RPI4 a predestined controller for the current project.
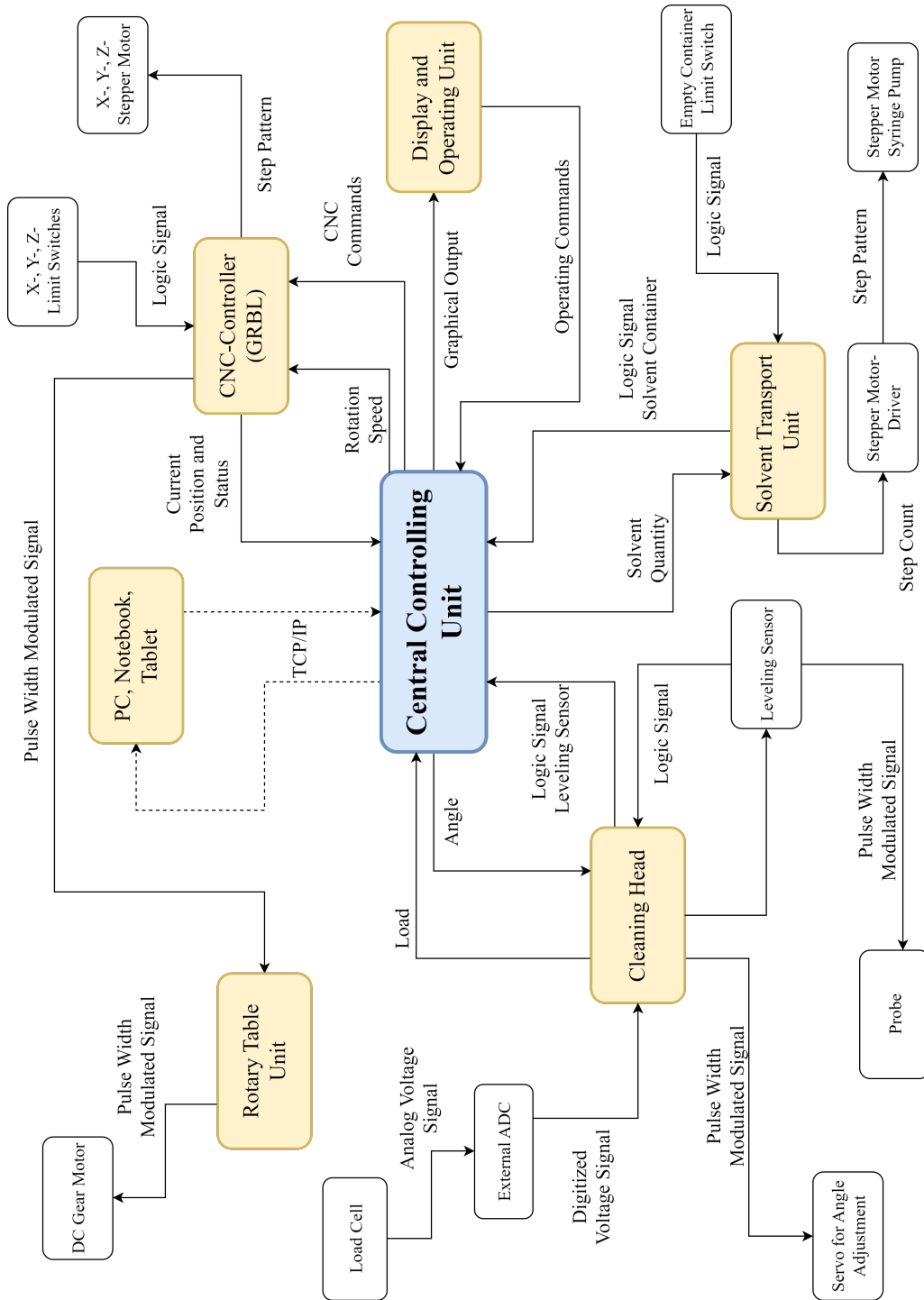
I/O Pins

Based on an ARM architecture, the RPI4 offers 40 GPIO pins (not all of them are freely configurable) [38], enough inputs and outputs to operate all sensors and actuators used in the system.

Table 8: Configuration of the 40-pin RPI4 pin header. Colored pins are used for power supply or are reserved for other functions (green).

Actuator/Sensor	Function	Pin		Function	Actuator/Sensor
	3.3V	1	2	5V	BLTouch Supply
	GPIO 2	3	4	5V	
	GPIO 3	5	6	GND	Ground Connection
	GPIO 4	7	8	GPIO 14	
	GND	9	10	GPIO 15	
Steppermotor Step	GPIO 17	11	12	GPIO 18	
Steppermotor Enable	GPIO 27	13	14	GND	BLTouch Ground
Steppermotor Direction	GPIO 22	15	16	GPIO 23	Servo PWM
	3.3V	17	18	GPIO 24	BLTouch PWM
	GPIO 10	19	20	GND	
	GPIO 9	21	22	GPIO 25	
	GPIO 11	23	24	GPIO 28	
BLTouch Endstop	GND	25	26	GPIO 7	
BLTouch Endstop	GPIO 0	27	28	GPIO 1	
	GPIO 5	29	30	GND	
	GPIO 6	31	32	GPIO 12	
	GPIO 13	33	34	GND	HX711 Ground
	GPIO 19	35	36	GPIO 16	HX711 Clock
Steppermotor Endstop	GPIO 26	37	38	GPIO 20	HX711 Data
Steppermotor Endstop	GND	39	40	GPIO 21	

The pins are multifunctional, i.e. they can also be used as SPI (Serial Peripheral Interface), I^{2}C (Inter-Integrated Circuit) or UART interface, if required, to address additional hardware [38].

One disadvantage of the RPI4 is that, unlike most microcontrollers, it has no analog inputs. This means that an external ADC is required to capture analog signals. In the specific application, this was done using an HX711 (AVIA Semiconductor Ltd., Xiamen, China), which sends the digitized sensor signal to the RPI4 via a serial two-wire protocol.

Among other things, the control system must also be able to generate a PWM signal. This is required to control the servo motor, which is used to adjust the angle of the cleaning head. With the RPI4, PWM signals can be generated both by software and hardware and emitted at the corresponding pins. [38].

USB Interfaces

Two USB 3.0 and two USB 2.0 interfaces are available to the RPI4 for operating *Plug and Play* devices [38]. They are used, for example, to communicate with the CNC controller of the positioning system. The USB interfaces are also utilized to supply the display and to capture the inputs of the touch display.

Graphics

Unlike microcontrollers, a *Raspberry Pi* has a GPU (Graphics Processing Unit) [38]. The GUI (Graphical User Interface) of the robot can thus be easily displayed on an external display via HDMI (High Definition Multimedia Interface).

Connectivity

For the connection to TCP/IP networks, the RPI4 has both a wired 1GbE Ethernet interface and a wireless LAN (Local Area Network) network card according to the IEEE 802.11ac standard [38]. The network connection of the device allows users to operate the robot via an external device such as notebooks or PCs. This functionality will mainly be used to change basic settings of the cleaning robot.

Operating System

Different Linux distributions can be installed on a *Raspberry Pi*. Since the cleaning system is to be operated via a user interface in combination with a touch display, it was necessary to ensure that the operating system also provides a desktop environment. The Linux *Debian* based operating system *Raspberry Pi OS* version 11 and the GUI Tookit *GTK+3* were installed.

2.5.2 3-Axis Positioning System

The realization of the 3-axis positioning system is based on an open-source hardware kit. The kit actually corresponds to an engraving machine, whose positioning system was repurposed for this project. The kit used is *Genmitsu 3018 Pro* (SaintSmart, Las Vegas, USA), which includes all necessary mechanical components, as well as CNC control and stepper motors.

Since this type of kit is intended for DIY, accuracy and precision are not comparable with professional positioning systems. The mechanical resolution is not specified by the manufacturer, but based on own calculations it is theoretically 0.0025 mm, see calculation (2) on page 35. A resolution in the range $\frac{1}{10}$ mm is sufficient for the planned application, so the system is more than adequate for positioning the cleaning head.

Basic Mechanical Structure

The rigid basic structure is formed by 20x20 mm wide double aluminum profiles which are screwed together with synthetic resin plates. This combination provides sufficient stability, which is necessary for the further construction of the robot. The aluminum profiles also have the advantage that they are very flexible with regard to the mounting of other components. For example, the limit switches can be mounted anywhere along the profile groove. The base of the Y-carrier is implemented as an aluminum profile plate (300x180 mm) and offers sufficient space to accommodate both the turntable and the solvent transport unit.

Linear Guides

The movements along the three axes are carried out via the linearly guided X-, Y- and Z-carriers. Trapezoidal lead screws with a pitch of 2 mm are used for positioning the carriers. These are driven by stepper motors. So-called *Anti-Backlash* nuts are used for movements that are as backlash-free as possible.

This refers to a two-piece spindle nut that is preloaded with the aid of a compression spring in order to suppress the slackness between the threaded spindle and the nut, see Figure 9, page 32.
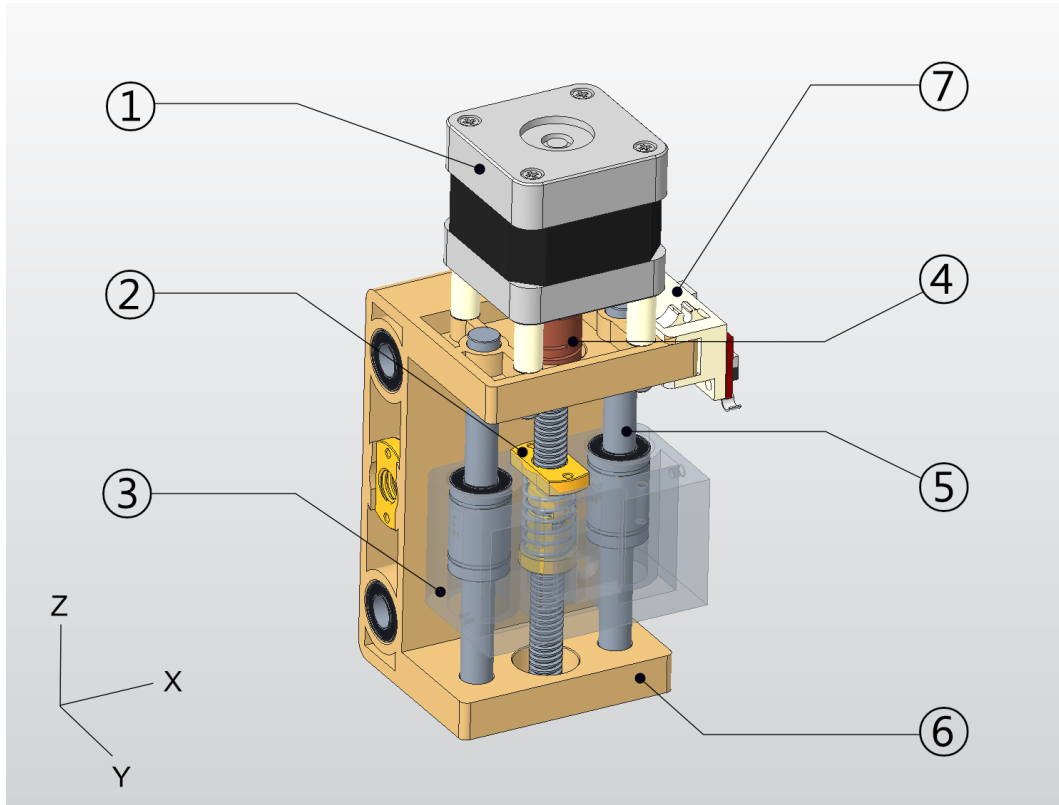

Figure 9: Illustration of the linear guide technology and the *Anti-Backlash* system using the XZ-carrier. The spring force eliminates the axial slackness between the spindle and the nut.
(1) Stepper motor
(2) Anti-backlash system consisting of two nuts and a compression spring
(3) Z-carrier with dovetail mounting
(4) Flexible coupling
(5) Guide rods with linear ball bearings
(6) Original X-carrier
(7) Adapter for Z limit switch board

The connection between the drive shaft of the stepper motor and the trapezoidal lead screw is realized with a flexible coupling. This allows any axial offset between the spindle and motor shaft to be compensated slightly, which would not be possible with a rigid coupling.

CNC-Controller Hardware

The task of the CNC controller is to receive the GCODE commands from the central control unit and to convert them into movements. This concerns both the positioning of the cleaning head via the three stepper motors and the rotation of the turntable via the DC gearmotor.

The CNC controller is based on a *ATmega328P* (Microchip, Chandler, USA) [40] microcontroller. The required driver components are soldered on the controller board and the maximum coil currents are already adjusted to the stepper motors. This means that the motors can be operated without an additional output stage, i.e. directly via the CNC controller. It is also possible to connect up to six limit switches (two per axis) to the controller.
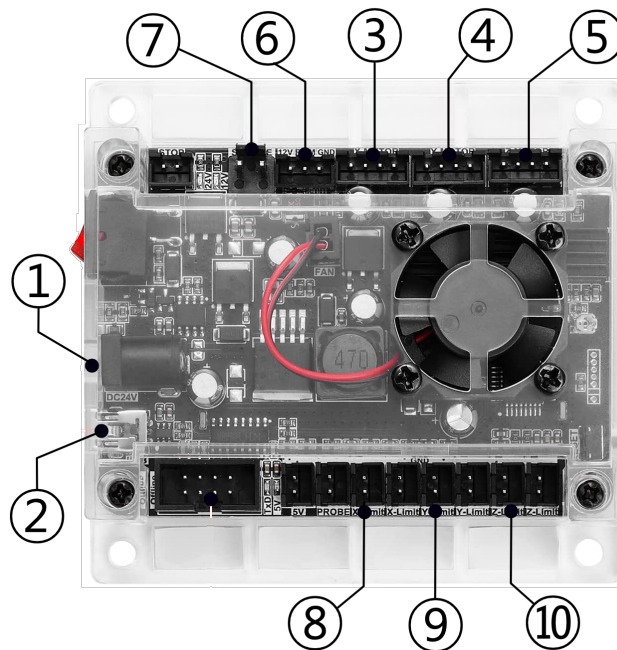

Figure 10: Connection diagram of the CNC controller board, based on [41]
(1) Supply connection for a 24 V power supply
(2) USB port for communication with the central control
(3) Stepper motor X-axis
(4) Y-axis stepper motor
(5) Z-axis stepper motor
(6) Connection for step-down converter
(7) PWM output for DC gear motor
(8) Limit switch X-axis
(9) Limit switch Y-axis
(10) Limit switch Z-axis

The controller board also has a three-pin supply connection (6) which is originally intended to operate an engraving laser via PWM. In this case, the 12 V output voltage of the connection is used to supply other peripherals of the cleaning robot. Details on this are explained in Chapter 2.5.3.

Limit Switches

The limit switches are mounted just before the mechanical stop of the respective axis and have two tasks: On the one hand, they prevent the mechanical stop from being reached and, on the other hand, they are used as a reference.
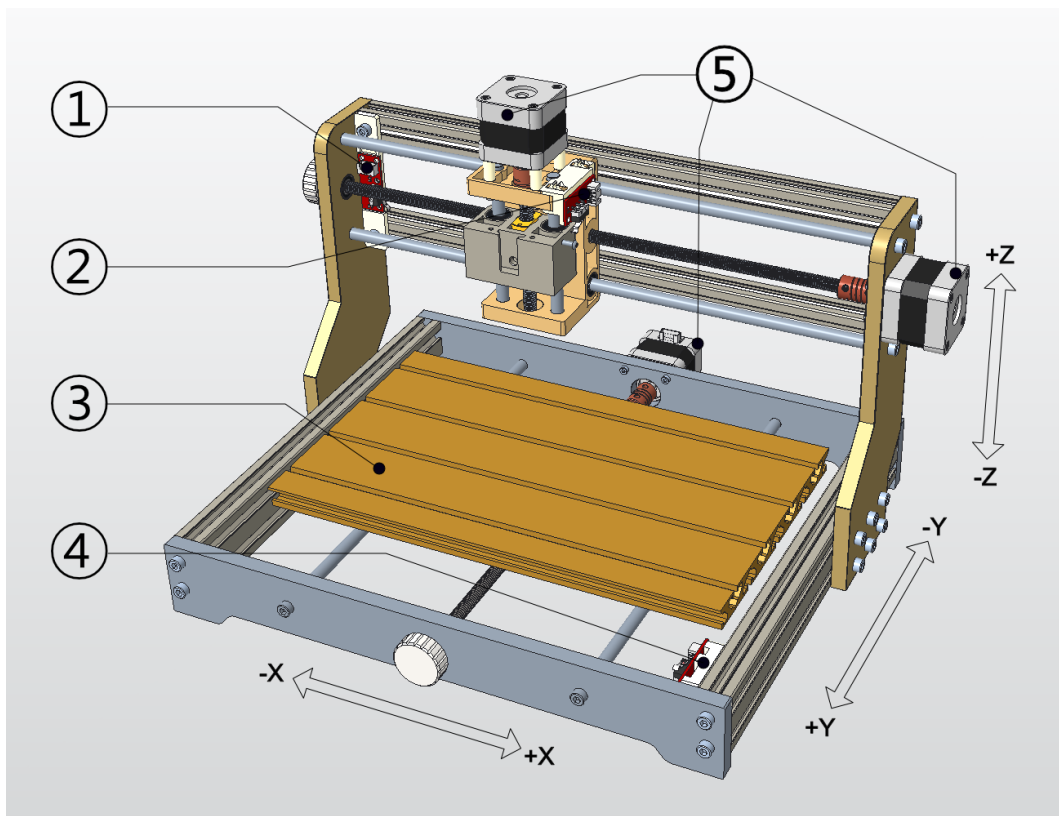

Figure 11: Positioning system modified with limit switch
(1) Limit switch of the X-axis
(2) Limit switch of Z-axis
(3) Aluminum profile plate (Y-carrier)
(4) Y-axis limit switch
(5) X-, Y- and Z-stepper motor

A reference is important because the stepper motor control is an open control loop. This means that the CNC controller does not receive feedback on the absolute position of the carriers. The position is determined exclusively on the basis of the steps traveled. For an absolute positioning of the carriers, the definition of the machine origin is therefore necessary. This requires at least one limit switch per axis. The second extreme position of each axis can be defined via the maximum travel of the respective axis, see Table 10, page 36.

Mechanical Resolution

The driving motors of the axes are ordinary NEMA17 (National Electrical Manufacturers Association) bipolar stepper motors. The standard step size of the motors is $1.8\,^{\circ}$. Thus, 200 steps are required for one full revolution [42]. To increase positional accuracy, the motors are operated in *Quarter-Step Mode*. This means that the original 200 steps/revolution are „inflated" to 800 steps/revolution.

$$d_{mech} = \frac{spindle\ pitch}{steps\ per\ revolution} = \frac{2\,\frac{mm}{revolution}}{800\,\frac{steps}{revolution}} = 0.0025\frac{mm}{step} \tag{2}$$

If the spindle pitch of 2 mm per revolution is taken into account, the calculation (2) yields a theoretical mechanical resolution of d_{mech}=0.0025 mm. However, this value is practically unattainable due to the manufacturing tolerances of other mechanical components.

CNC-Controller Firmware

The firmware of the CNC controller is an open source software project *GRBL* in version 1.1f. It accepts instructions in the form of a character string via the UART interface and processes them further. The parameters shown in Table 9 are required to establish the connection.

Table 9: Parameters for establishing a connection with the GRBL-based CNC controller [43]

Parameter	Value
Baudrate	115200 baud
Databits	8
Stopbits	1
Parity	none

To make sure that the string can be interpreted by the CNC controller, it must correspond to a certain format. Each string sent by the RPI4 must therefore be terminated with the two control characters *CR* (Carriage Return or `'\r'`) and *LF* (Linefeed or `'\n'`):

<command string>\r\n

If an applicable command is recognized in the string, the controller responds with a „ok" or the requested data. Unrecognized commands are discarded without feedback.

The command format just described can be used not only to execute instructions in the form of GCODEs, but also to read out information about the device status and modify basic settings.

Adjustment of the Default Settings

The latter must be carried out before initial startup, as some settings must be adapted to the requirements of the cleaning robot. In addition to the activation of the homing cycle and the software limit switches, this also includes the inversion of the X-axis and the storage of the maximum travels and speeds of all axes. The currently stored basic settings can be read out via the command `'$$'` [43]. The controller responds with a list of parameters and the related values.

Table 10: Excerpt of all changed basic settings of the GRBL firmware. For all parameters not listed, the default value was retained.

Parameter	Value	Description
$20	1	Activates the software limit switches
$22	1	Activates the homing cycle
$23	1	Inverts the direction of the X-axis
$100	800	Sets the steps/mm for the X-axis
$101	800	Sets the steps/mm for the Y-axis
$102	800	Set the steps/mm for the Z-axis
$110	1500	Max. feed rate of the X-axis in mm/min
$111	1500	Max. feed rate of Y-axis in mm/min
$112	600	Max. feed rate of the Z-axis in mm/min
$130	200	Max. travel of the X-carrier in mm
$131	75	Max. travel of the Y-carrier in mm
$132	36	Max. travel of the Z-carrier in mm

The maximum travel of the Y-slide can be overwritten, for example, by sending the command '`$131=<value>`' to the controller. All changes to the basic settings are written to the non-volatile *EEPROM* (Electrically Erasable Programmable Read-Only Memory) of the controller and must therefore only be performed once.

GCODE Instructions

For a movement of the carriers, instructions must be sent to the controller in the form of GCODEs. For example, instructions looks like this:

```
1: G91
2: G01 X10 Y-7.5 Z-1.73 F500
3: G90
4: G00 X1 Y1 Z1
5: M03 S100
6: M05
```

In the above example, '`G91`' first sets the positioning mode to *relative* [43]. The following line makes the carriers move 10 mm in the X-direction, -7.5 mm in the Y-direction and -1.73 mm in the Z-direction, regardless of which position they are currently in. The parameter '`F`' allows defining the feed rate [43], in the current example it is set to 500 mm/min. G parameters indicate the motion mode. '`G01`' corresponds to a linear movement, while '`G00`' is used to move between two points in *Rapid Traverse* mode [43]. Line 3 and line 4 switches the controller to *absolute* positioning and moves to the point (1/1/1) mm.

Absolute positioning requires that a *Homing Cycle* has been performed previously. The *Homing Cycle* is a reference run in which the limit switches of all axes are moved. The *Homing Cycle* must be executed every time the CNC controller is restarted.

In lines 5 and 6, parameter '`M`' is used to activate or deactivate the drive motor of the turntable. '`S100`' stands for the speed of the motor in $\min^{-1}$.

The instruction format is very flexible. The controller does not distinguish between upper and lower case and the order of the coordinates can be chosen arbitrarily. If no F-parameter is passed, the last value is used. For negative values, the minus can also be placed before the axis designation.

Real-Time Commands

Other essential commands for the cleaning robot are the characters `'?'`, `'!'`, `'~'` and `'\030'`. These are real-time commands that cause the CNC controller to respond immediately [43].

For example, if you send a `'?'`, the CNC controller responds with its current status (`Idle, Run, Alarm,`...) and its current machine position in the form of XYZ coordinates [43]. The central controller polls status and coordinates every 20 ms. The short interval is necessary because the controller must know at any time where the carriers are or if there is a problem with the positioning system. This is especially important when probing the optics surfaces.

A `'!'` pauses the current positioning operation [43] by stopping all stepper motors. During this operation the current position of the carriers isn't lost. It should be noted that the command has no effect on the movement of the turntable - it will keep rotating regardless. The command `'~'` resumes the positioning operation [43]. It may be necessary to perform a *Softreset* of the CNC controller. To do so, the control character `'CTRL+X'` must be sent to the controller [43]. This is necessary e.g. if the controller loses the position of one of the carriers.

Fixed Positions

Basically, the carriers are moved by using relative positioning. This requires fixed machine points to which the relative movements refer. Three fixed positions in the form of absolute coordinates were stored in the basic settings of the robot software.

Table 11: Coordinates of the fixed positions

Axis / Position	X in mm	Y in mm	Z in mm
Loading position	152	0	0
Start position	152	-69	0
Probing position	62	-67	0

Loading position: This position is approached when an optic is to be inserted into or removed from the cleaning robot. The Y-carrier positions itself in the `Y=0` position, in which the optics holder is most accessible, see Figure 12.

Start position: In this position, the head of the cleaning rod (polyester pad) is located centered above the optics. The position serves as a reference point for the relative movements of the X- and Z-carriers during cleaning.

Probing position: The probing position serves as the starting point of the profile recording, the sensor probe and the optical axis coincide in this position.
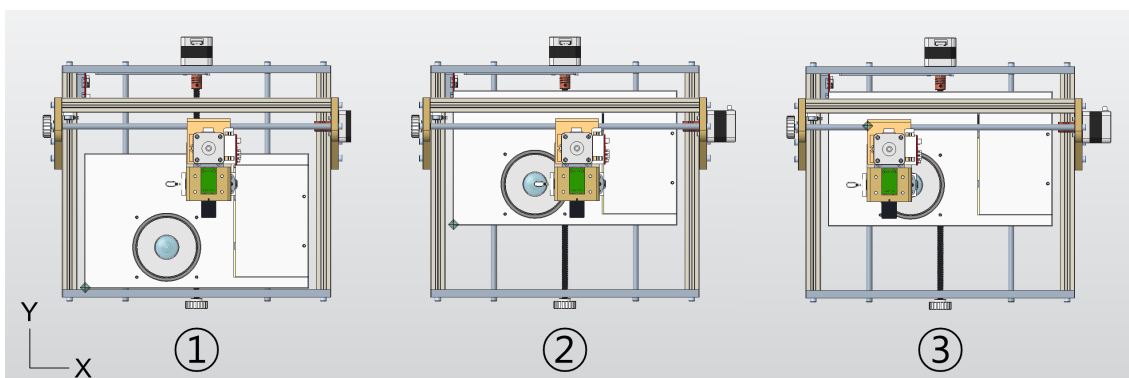

Figure 12: Illustration of loading (1), start (2) and probing position (3)

2.5.3 Rotary Table Unit

From a mechanical point of view, the design of the turntable unit presented the greatest challenges of the project. On the one hand, the development had to take into account that the Y-carrier, on which the turntable is mounted, only offers a limited surface area. On the other hand, it had to be ensured that the noise generated by the rotating parts was kept within limits.

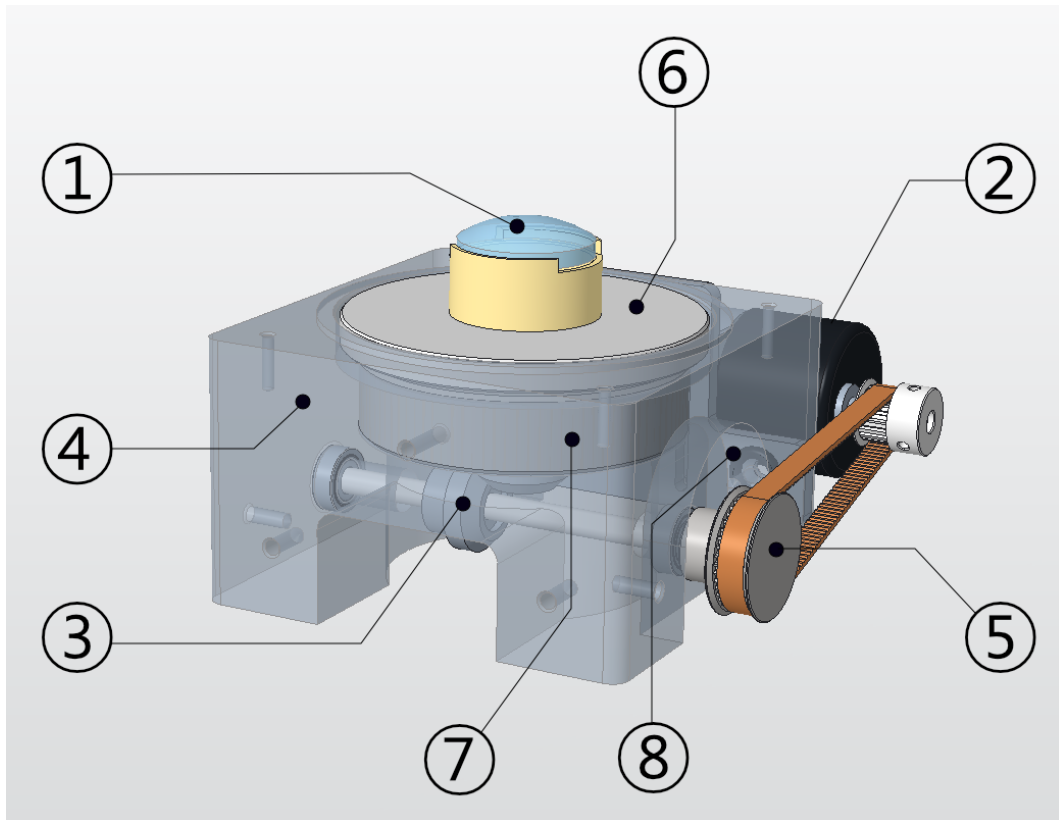Figure 13: Mechanical system of the rotary disk unit. For better illustration of the 90° bevel gearbox, the gearbox block is shown slightly transparent.
(1) Optics holder with inserted lens
(2) DC gear motor with synchronous pulley GT2-16T
(3) Gear shaft with clamped bevel gear
(4) Gear block
(5) Synchronizer pulley GT2-40T
(6) Turntable with bolted bevel gear
(7) Main bearing
(8) Elastic buffer

Mechanics

The gear block forms the basis of the turntable unit. It contains the radial main bearing, which supports the turntable. The difference between the outer diameter of the main bearing and the outer diameter of the turntable was deliberately chosen to be small, as this allows the turntable to rotate more smoothly. The solid deep-groove ball bearing also provides more weight, which stabilizes the relatively lightweight gear block printed from *Onyx*. As can be seen in Figure 13, page 40, the drive is stepped down twice. The reason is, on the one hand, to reduce the speed of rotation slightly and thus increase the torque at the same time. On the other hand, the assembly is kept small and compact.

The purpose of the bevel gear is to achieve a $90\,°$ conversion of the rotary motion. In this case, neither step-up nor step-down is performed. The two bevel gears are made of POM (Polyoxymethylene). This material was chosen to reduce running noise a little, especially at speeds $> 200\ min^{-1}$. Synchronous pulleys and belts of the GT2 standard are used for the toothed belt drive between the motor shaft and the shaft of the bevel gearbox. The reduction is from 16 to 40 teeth.

In addition to the implemented concept, a direct drive of the turntable or a direct coupling of the drive shaft of the motor with the gear shaft was also considered. However, neither of these options was effective due to the high noise level and lack of space on the Y-carrier.

Optics Mount

Due to the variety of optics surfaces and diameters, a universal mount is not practical. The better solution in this case are adapters which are customized to the optics and which can be attached to the turntable via a screw connection. The adapters are designed in such a way that the optics are clamped in the holder by means of a press connection. This makes it easier to switch between optics of the same type.

Speed Control

The turntable is driven by a DC gearmotor, which can be supplied with a voltage of up to 15 V and can convert a power of max. 19.8 W [44].

The speed is controlled by the CNC controller, which generates a pulse-width modulated square-wave voltage and outputs it at connection (7) (see Figure 10, page 33). Varying the ratio between on-time and off-time of the voltage results in different mean voltage values [45] at the motor terminals. The speed of the motor in turn behaves proportionally to the applied voltage mean value [46].
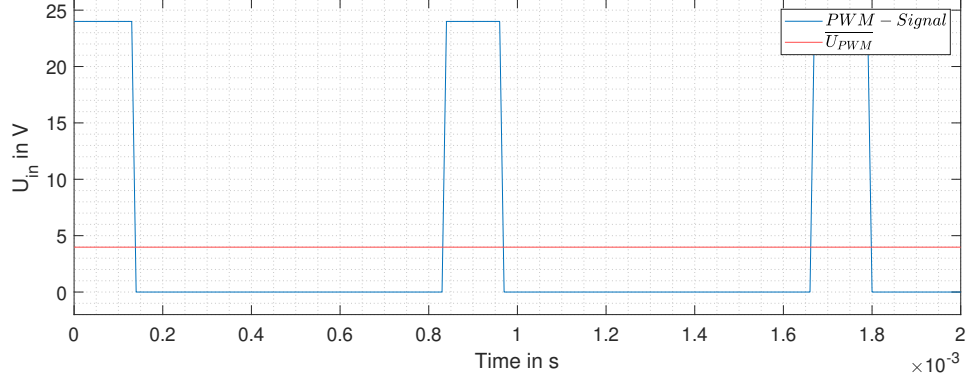
Figure 14: Example of a PWM signal generated by the CNC controller used. The values are based on measurements.

The following calculation example refers to the signal from Figure 14 and explains the relationship between pulse width and speed of the motor at a supply voltage of U_{in}=24 V, a PWM frequency of 1204 $\frac{1}{s}$ and an on-time of t_{on}=137.6 μs:

$$\overline{U_{PWM}} = U_{in} \cdot \frac{t_{on}}{t_{on} + t_{off}} = U_{in} \cdot t_{on} \cdot f_{PWM} = \tag{3}$$

$$= 24V \cdot 137.6 \cdot 10^{-6}s \cdot 1204\frac{1}{s} = 3.98V$$

According to the data sheet [44], the gear motor achieves a speed of 1648 $\frac{1}{min}$ at a supply voltage of 15 V. The specification refers to the already reduced speed of the planetary gear in a ratio of 1:10. Using this relation k, the theoretical speed at the gear shaft n_{GW} can be calculated as follows:

$$n_{GW} = k \cdot \overline{U_{PWM}} = \frac{1648\frac{1}{min}}{15V} \cdot 3.98V = 437.27\frac{1}{min} \tag{4}$$

To determine the turntable speed, the reduction of the toothed belt drive from z_{GW}=16 to z_{DT}=40 teeth has to be taken into account using the following ratio:

$$\frac{z_{GW}}{z_{DT}} = \frac{n_{DT}}{n_{GW}} \tag{5}$$

$$n_{DT} = n_{GW} \cdot \frac{z_{GW}}{z_{DT}} = 437.27\frac{1}{min} \cdot \frac{16}{40} = 174.91\frac{1}{min}$$

The result from (3) to (5) showing that for a pulse width of 137.6 μs, a theoretical rotation speed of 174.91 min^{-1} can be expected.

2.5.4 Cleaning Head

This unit represents the most complex assembly of the cleaning system, as it combines various functions. The built-in load cell measures the pressure applied to the optics surface. A servo motor makes it possible to adjust the angle of the cleaning head to the curvature of the optics, and an integrated leveling sensor probes the surface of the inserted optics and creates a surface profile.

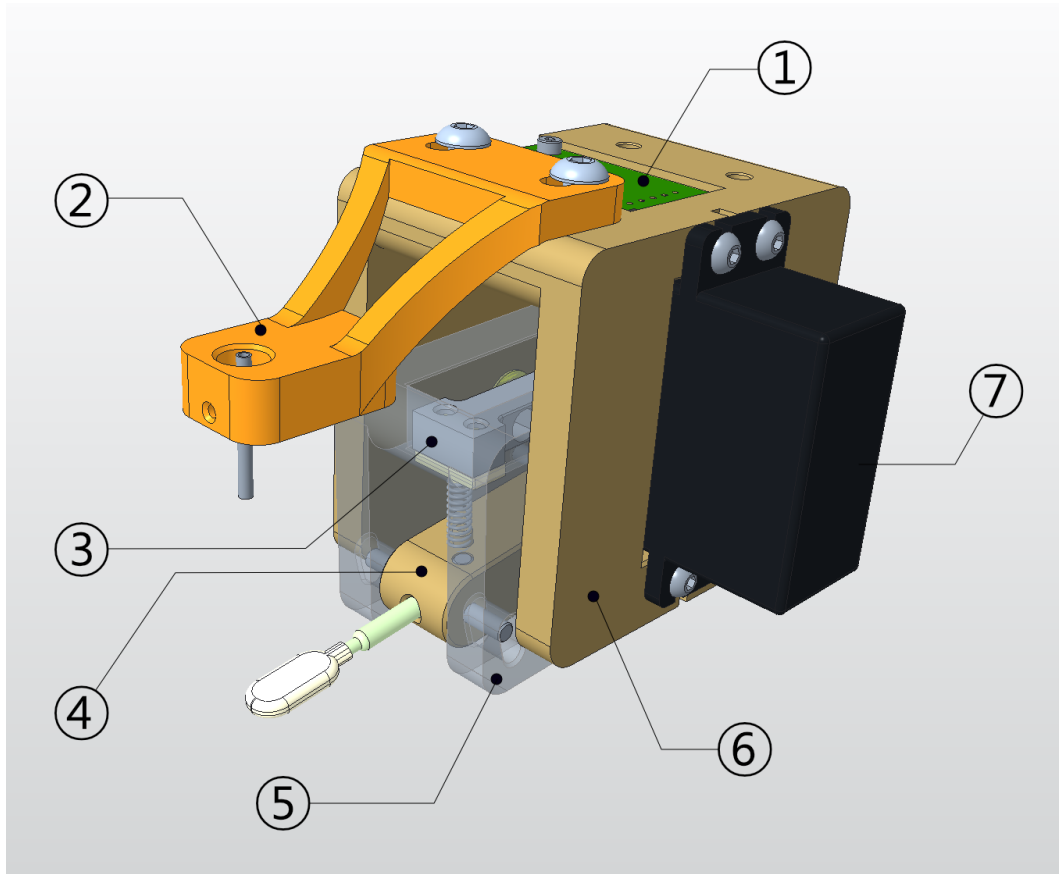Figure 15: Mechanical design of the cleaning head. The leveling sensor, invisible in this view, is mounted on the right side of the sensor holder.
(1) HX711 breakout board
(2) Bracket with solvent nozzle
(3) Compression spring buffered load cell
(4) Beared holder with inserted cleaning rod
(5) Sensor holder with upper and lower limit stop
(6) Head base with dovetail mount (not visible)
(7) Servo motor

Force Measurement

The force is measured with the aid of a compression spring-buffered load cell, which is designed for a maximum load of 200 g. Thanks to the continuous recording of the measured values, the contact pressure previously set in the GUI can be kept constant. On the one hand, this is intended to ensure consistent cleaning quality and, on the other, to prevent damage to sensitive coatings.

The load cell used consists of in total four strain gauges, which are interconnected to form a *Wheatstone's Bridge Circuit*. The analog output signal of the measuring bridge is amplified and digitized via an external 24-bit ADC (HX711). The subsequent evaluation of the digital voltage signal is performed by the central control unit. Figure 16 shows the relationship of the components just mentioned.
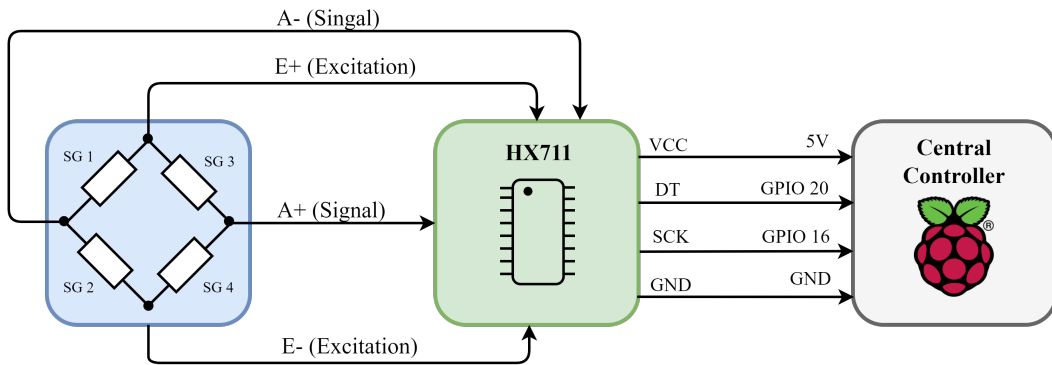

Figure 16: Block diagram of the force measurement by load cell. The excitation wires of the bridge are marked E+ and E-. An analog voltage signal in the millivolt range is taken from the terminals A+ and A-. The digitized signal is transmitted via a two-wire bus (DT and SCK).

The HX711 supports two different sampling rates. If the application requires accurate measurement results, the IC provides max. 10 SPS (Samples Per Second). For a higher sampling rate, the external circuitry must be changed. Concretely, the logic level of Pin 15 (RATE) has to be changed from `'LOW'` to `'HIGH'`. Under the loss of accuracy, this configuration allows a sampling frequency of up to 80 SPS. [47]

In the present application, the priority lies in a faster sampling rate. Since the type of HX711 *Breakout Board* used is set to 10 SPS by default, a modification of the hardware was necessary. For this purpose the existing Pin 15 $\leftrightarrow$ GND trace on the PCB was cut and a connection between Pin 15 and the supply Pin V_{CC} (Voltage at the Common Collector) was placed.

Calculation of Maximum Pressure

As shown in Figure 15, page 43, the adjustment of the mounting is limited by a lower, as well as an upper mechanical stop. This feature serves to protect the load cell, as it would be irreversibly overstretched if the maximum load capacity is exceeded.

When the load cell is at the upper stop, the force acting on the sensor corresponds to a load of m_{max}=140.5 g. This is the maximum load that can act on the sensor. This mass also represents the maximum load that can be applied on the surface of an optic. Due to the compression spring, a mass of 32.69 g acts permanently on the load cell even in the unloaded state of the cleaning head. If the area of the polyester pad of 14x6.8 mm (cleaning rod) is taken into account, the maximum pressure that can act on the optics surface can be calculated as follows:

$$p_{max} = \frac{F}{A} = \frac{m_{max} \cdot G}{l_{Pad} \cdot w_{pad}} = \frac{140.5 \cdot 10^{-3} kg \cdot 9.81 \frac{m}{s^2}}{14 \cdot 10^{-3} m \cdot 6.8 \cdot 10^{-3} m} = \tag{6}$$

$$= 14.478 \cdot 10^3 \frac{N}{m^2} = 1.4478 \frac{N}{cm^2}$$

Pressure Cleaning Process

The ideal cleaning pressure basically depends on the degree of soiling and the surface coating. To take these two factors into account, the cleaning pressure can be set individually for each optic. The challenge here is that the set pressure must also be kept constant for non-planar surfaces. Thus, a regulation of the pressure is required. The pressure is built up by the robot lowering the complete cleaning head via displacement of the Z-carrier. The polyester pad is thus pressed more and more onto the rotating optic. When a previously defined pressure threshold is reached, the Z displacement stops. The robot then moves the cleaning head in +0.05 mm steps along the X axis. If the inserted optic has a convex surface, after every X movement a check is made to see whether the pressure has fallen below the set threshold.

If this is the case, the head is additionally lowered by -0.05 mm to build up the pressure again. This procedure is repeated until the robot has traversed the entire optical radius.

In contrast, for concave-curved optics, the robot constantly determines whether the current pressure is below the set threshold and re-adjusts it if necessary by raising the cleaning head by +0.05 mm.
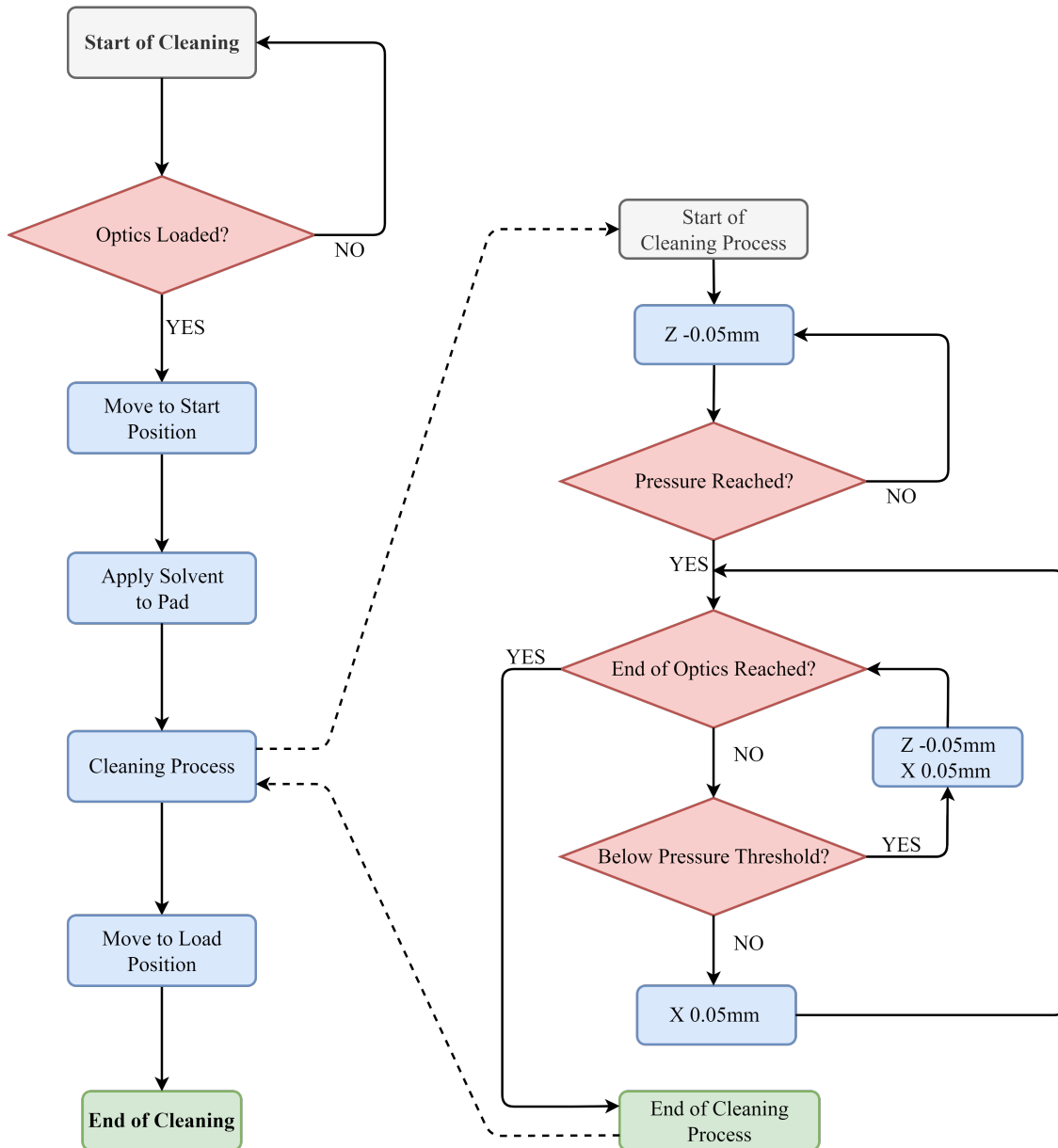

Figure 17: The flow chart on the left shows the rough program sequence during a cleaning procedure. On the right, the detailed cleaning process, furthermore the pressure control at a convex optics is shown.

Head Positioning

The differently curved optical surfaces require that the cleaning head can be adapted to them. The sensor holder is therefore rotatably mounted and can be positioned in an angle range from -20° to 30°. The adjustment of the angle is done by an ordinary model servo motor. To ensure that the angle does not change even under load, the holding torque of the servo must be greater than the torque applied via the cleaning rod.

The installed servo motor *SPT4412LV* (SPT-Servo, Shantou, China) achieves a maximum holding torque of 10 kgf·cm [48] with a 4.8 V supply. The lever applied to the motor shaft (axis of rotation to tip of polyester pad) has a length of 6.5 cm and the maximum mass that can be applied (limited by the upper stop on the sensor holder) is 140.5 g. This results in the following moment inequality if gravity is neglected:

$$M_{servo} > M_{sensor\ holder} \tag{7}$$

$$M_{servo} > m_{max} \cdot l_{lever}$$

$$10 kgf \cdot cm > 140.5 \cdot 10^{-3} kgf \cdot 6.5 cm$$

$$10 kgf \cdot cm > 0.913 kgf \cdot cm$$

Inequality (7) shows that the holding torque of the servo motor is about a factor of 10 higher than the maximum expected torque. It follows that, in terms of force, the selected servo motor is suitable for the intended application.

The electrical control is similar to the DC gearmotor via a PWM signal (see Chapter 2.5.3, Speed Control), with the difference that pulse width and period duration of the signal are specified by the manufacturer. The necessary PWM frequency is given as 50 Hz, which corresponds to a period duration of 20 ms [48]. By varying the pulse width, the position angle of the servo and thus the position of the sensor holder can be changed.

To avoid a mechanical collision between the sensor holder and the head base, an upper as well as a lower maximum position has been defined. All positions outside this range are ignored by the software to prevent damage to the cleaning robot.

Table 12: Relation between pulse width and angle of the sensor holder. The angles were determined using the 3D model of the robot.

Position	Pulswidth t_{on} in μs	Angle in $°$
Maximum position	1900	30
Wetting position	1880	28.8
Normal position	1540	0
Minimum position	1300	-20

As shown in Table 12, in addition to the minimum and maximum positions, there are two other important servo positions: the normal position and the wetting position. The normal position corresponds to the position in which the sensor holder is aligned parallel to the head base. It is always taken when a cleaning process is completed or the robot is initialized. In this position, the cleaning rod is at an angle of 15 $°$ to the horizontal plane.

Figure 18: Frontal section of the cleaning head in normal position (left) and during wetting of the polyester pad (right)
(1) Cleaning rod with polyester pad
(2) Sensor holder
(3) Nozzle
(4) Head base
(5) Leveling sensor
(6) Load cell

The wetting position is adopted to moisten the polyester pad of the cleaning rod with solvent. The distance between the nozzle and the polyester pad has been selected so that they just do not touch. This prevents a droplet from forming under

the nozzle, whose surface tension makes it difficult for the solvent to be drawn into the polyester pad.

XZ Correction of the Start Position

Any position of the cleaning head that deviates from the normal position also causes the absolute X and Z coordinates of the polyester pad to change. As a result, the pad does not touch down centrally on the surface of the optics during cleaning, so it is necessary to correct the start position.

Figure 19: Geometric representation of the correction. If the cleaning head is in the normal position, the position of the pad can be determined via the normal position vector V_0. The vector V_R describes the position of the pad with a changed cleaning angle. V_K corresponds to the correction vector with its projections X and Z.

The angle α=22.7° and the magnitudes of the two vectors ($|V_0| = |V_R| = 66\,\text{mm}$) are given by the mechanical design and can thus be determined via the 3D model. The angle β is variable and corresponds to the set cleaning angle.

In the following calculation example, an angle $\beta = 20°$ ($\widehat{=}$ minimal position) is assumed for the cleaning vector:

$$\vec{V_0} = |V_0| \cdot e^{j(180° + \alpha)} = 66mm \cdot e^{j(180° + 22.7°)} \tag{8}$$

$$= 66 \cdot [cos(202.7°) + j \cdot sin(202.7°)]$$

$$= -(60.888 + j25.470)mm$$

$$\vec{V_R} = |V_R| \cdot e^{j(180° + \alpha + \beta)} = 66mm \cdot e^{j(180° + 22.7° + 20°)}$$

$$= 66 \cdot [cos(222.7°) + j \cdot sin(222.7°)]$$

$$= -(48.504 + j44.759)mm$$

To obtain the X and Z correcting values, the difference vector V_K must be calculated and then separated into its components.

$$\vec{V_K} = \vec{V_0} - \vec{V_R} \tag{9}$$

$$= X + jZ$$

$$= -(60.888 + j25.470)mm - (-(48.504 + j44.759)mm)$$

$$= (-12.384 + j19.289)mm$$

The results in (8) and (9) show that when the cleaning angle is adjusted by $20°$, the start position of the cleaning head must be corrected by X=-12.384 mm and Z=19.289 mm. The corrections are made via the CNC system by adding the X and Z values as an offset to the start position which is stored in the basic settings.

Cleaning by Surface Profiles
In addition to the *Cleaning by Pressure* method just described, the cleaning system offers two alternative methods: *Cleaning by Profile* resp. *by Coordinates* and *Cleaning by Radius*.
The idea behind *Cleaning by Profile* is to „train" the robot to the surface of an optic by scanning it and storing the acquired coordinates in the form of a surface profile. During the subsequent cleaning process, the stored coordinates are traced. At the beginning of the cleaning process, *Cleaning by Profile* differs only slightly from *Cleaning by Pressure*. After reading in the surface profile, the head is also lowered

here until the set target pressure is reached. From this point on, in contrast to the *Cleaning by Pressure* process, permanent pressure monitoring is no longer required, because the surface is traced point by point on the basis of the stored coordinates. Figure 20 illustrates the *Cleaning by Profile* method in the form of a flow chart.
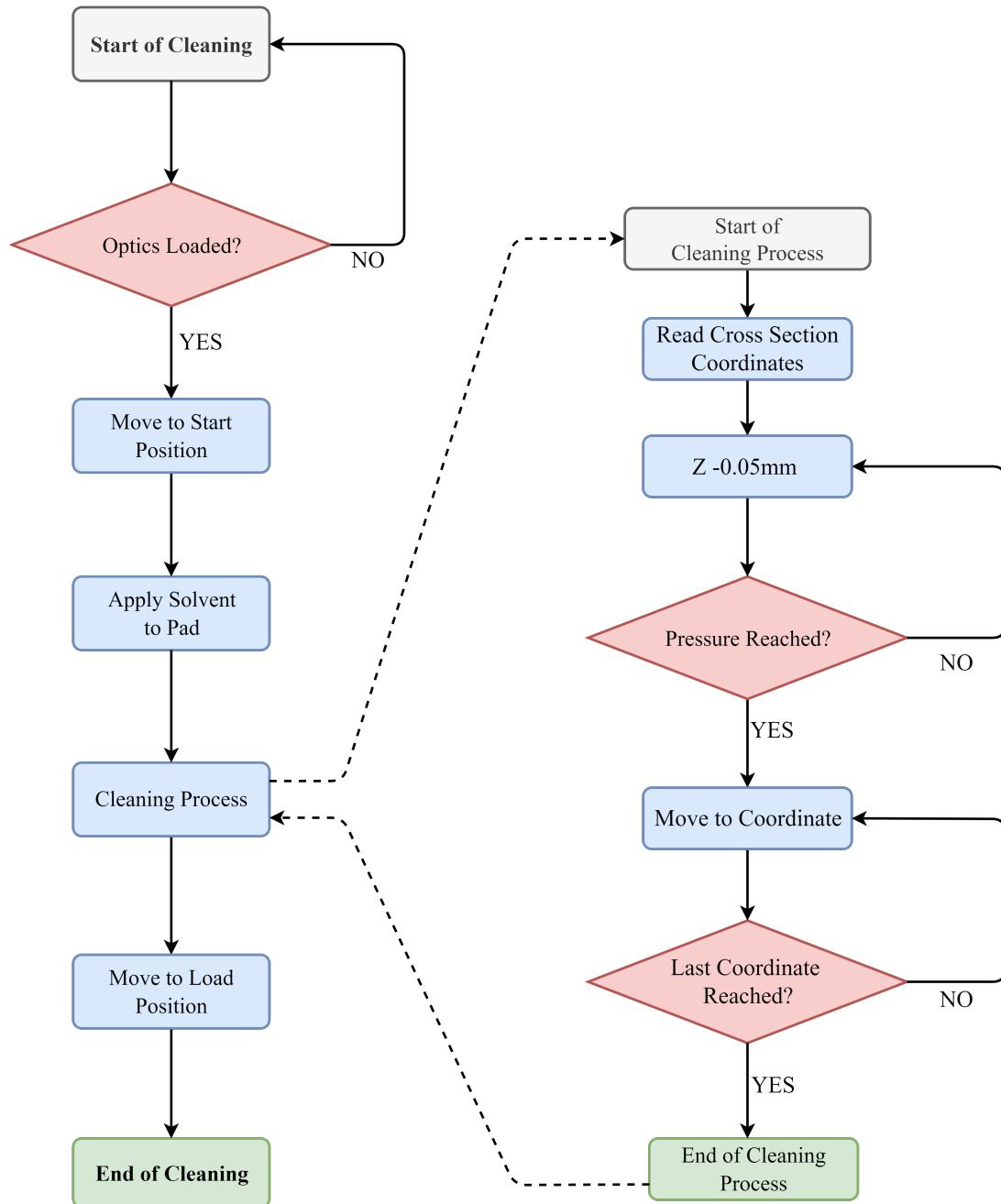

Figure 20: Left side of the flowchart shows the complete cleaning process. The right side shows the sequence of the cleaning process over the previously stored coordinate points.

Cleaning by Radius

Cleaning by Radius is a special form of the *Cleaning by Profile* method. The robot software calculates the radius of curvature of the optics surface based on the stored coordinates. This requires that at least three points have been probed beforehand. Ideally, the starting point, the end point and a point in between are selected for this, see Figure 21.
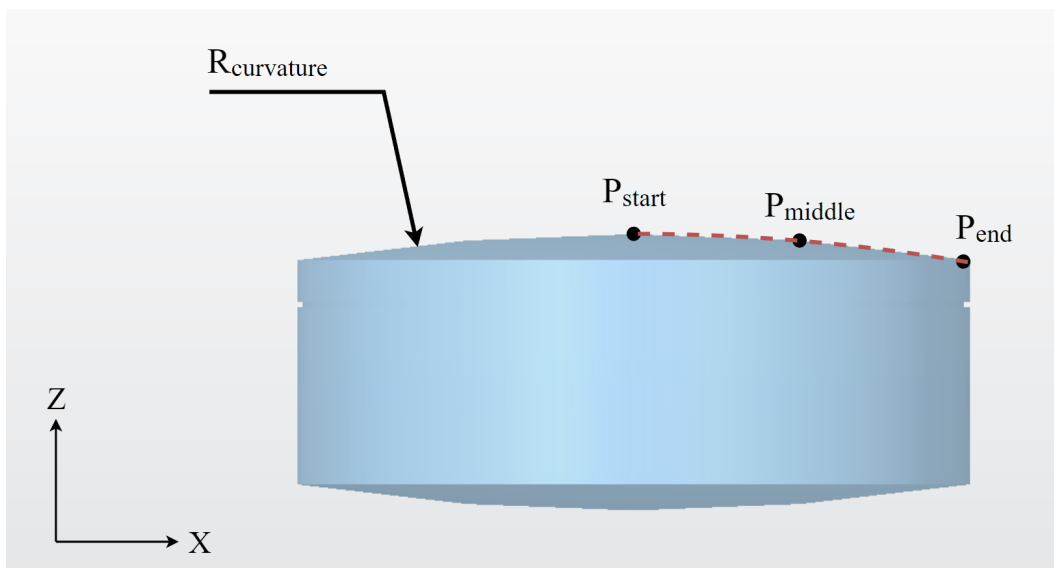

Figure 21: Achromat with drawn in probing points to calculate the radius of curvature. The red dashed line indicates the intended traverse path of the cleaning head.

During cleaning, the CNC positioning system, starting from the current position P_{start}, interpolates the traverse path specifying the radius of curvature $R_{curvature}$ and endpoint P_{end}. For this purpose, the central controller sends one of the following commands to the CNC controller:

```
1: G02 X(P_end) Z(P_end) R(curvature)
2: G03 X(P_end) Z(P_end) R(curvature)
```

The GCODE parameter `'G02'` in the first line causes a clockwise circular interpolation, while with `'G03'` an anticlockwise interpolation is achieved [49], which is necessary for example when cleaning concave lenses. The Z coordinate of the starting point is variable and, as with *Cleaning by Profile* and *Cleaning by Pressure*, results from reaching the previously set target pressure, which is slowly built up by lowering the Z carrier.

Determining the Surface Profile

Two different sensors were considered to detect the surface profile: a capacitive proximity switch and a leveling sensor. The main difference between these two sensors is that the proximity switch works without contact, while the leveling sensor only triggers as soon as the surface is touched. To ensure that optics with large radii of curvature are also reliably detected, the sensor used must have an accuracy of at least 0.1 mm.

Capacitive Proximity Switch

This type of sensor is based on the de-tuning of an RC oscillator. If an object (metallic or non-metallic) enters the active zone of the sensor, the capacitance of the RC oscillator circuit changes and thus its amplitude. When a certain threshold is reached, a post-connected *Schmitt trigger* changes the initial state of the sensor. The capacitance and thus the switching distance depends on the permittivity of the object to be detected. [49]

By stepwise lowering the cleaning head, the proximity switch approximates the optics and triggers as soon as a previously adjusted switching distance is reached. At the same time, the central control unit stops all movements and determines the current Z and X coordinates. This process is repeated at any number of points along the X axis. An XZ profile of the surface can be created from the stored coordinate points. For this approach, the *LJC18A3-B-Z/BX* proximity switch (Heschen Electric Co. Ltd, Foshan, China) was used.

Leveling Sensor

The primary purpose of leveling sensors is to probe the print bed of 3D printers. The resulting height map can be used to compensate for any surface unevenness of the bed via software.

However, the principle can also be used to create the aforementioned two-dimensional surface profile of an optical component. In this case the sensor *BLTouch Smart V3.0* (Antclabs Inc., Seoul, Korea) was used. Figure 22 on page 54 shows how the sensor must be connected to the central controller in order to use it to probe a profile.
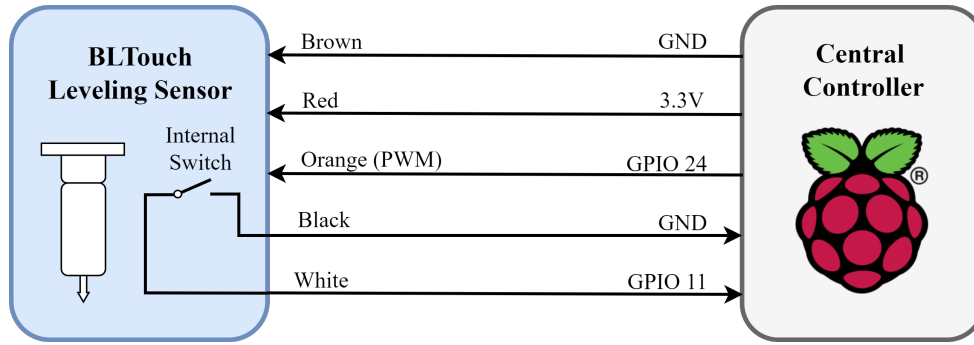
Figure 22: Connection diagram between the leveling sensor and the pin header of the *Raspberry Pi*. The illustrated limit switch (NO, Normally Open) closes as soon as the probe touches a surface.

The leveling sensor basically consists of a microcontroller, a *Hall Sensor*, a magnetic coil and a probe. The probe is also permanently magnetized on one side and can thus be raised and lowered via the magnetic coil, similar to a *Solenoid*. When the probe hits a surface, it is lifted slightly, triggering by the internal *Hall Sensor*. The microcontroller responds by powering the *Solenoid* and immediately raising the probe again. The probe is controlled by pulse width modulation. For this purpose, the microcontroller evaluates the PWM signal generated by the central controller, furthermore its pulse width, and reacts to it with different actions. [50]

Table 13: Excerpt of the PWM signals relevant for the cleaning system. The sensor-internal microcontroller tolerates deviations of $\pm$ 20 μs. [50]

Instruction	Pulswidth in μs
Selftest, probe will extend and retract 10x	1780
Retract probe	1475
Extend probe	650

Probing Process Using Leveling Sensor

For profile acquisition, the CNC positioning system first takes in the scanning position. In this position, the optical axis and probe axis match. By sending the corresponding PWM signal (see Table 13, page 54), the probe is extended. The CNC positioning system now lowers the cleaning head step by step until the probe hits the surface and is retracted again as already described. At the same time, the central control system is signaled that the surface has been reached. The current X and Z coordinates are saved and the CNC positioning system raises the cleaning head again. This process is repeated until the radius of the optics has been completely sampled.

Figure 23: Visualization of the probing process along the surface of a lens by means of the leveling sensor
(1) Sensor housing
(2) Plastic tip of the probe
(3) Convex lens

As the tip of the sensor's probe is made of plastic and hits the surface only very slowly, no damage to it is to be expected. In addition, the probe is retracted immediately after contact with an obstacle.

Since the optics rotate during cleaning, it is sufficient to probe only one half. The smaller the step size along the X axis, the longer the probing process, but the higher the resolution. A surface profile consists of at least three probing points and the number can be set via the robot's software.

2.5.5 Solvent Transport Unit

The following chapter explains the technology used to automatically integrate the solvent into the cleaning process. In principle, the unit can be divided into a pump with solvent tank and a tube system including a nozzle. For space reasons, the pump is located on the Y-carrier of the robot. As a consequence, the solvent must be transported to the cleaning head via a tube system. Through the nozzle attached there, it is dispensed in adjustable quantities onto the polyester pad of the cleaning rod.

Syringe Pump
The solvent is delivered with the aid of a syringe pump. The principle is simple and well suited for the in this case non-continuous pumping of liquids.
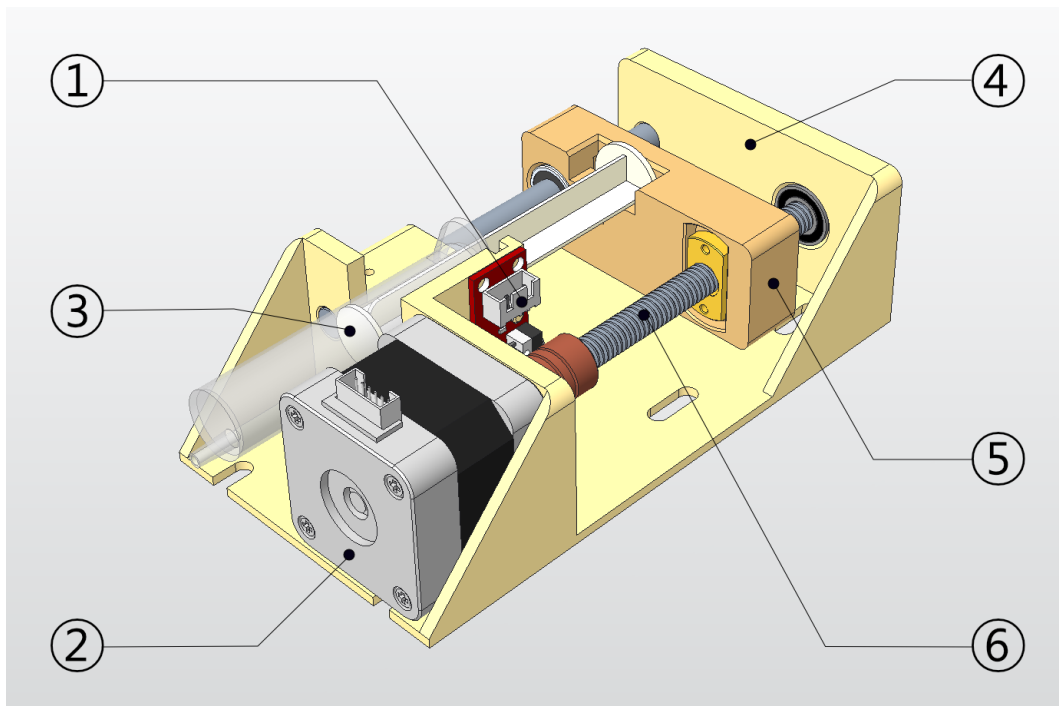

Figure 24: Stepper motor driven pump unit with a disposable syringe as solvent reservoir
(1) Limit switch board
(2) NEMA17 stepper motor
(3) One-way syringe
(4) Base
(5) Piston slider
(6) T8 trapezoidal lead screw with 2 mm pitch

For power transmission to the syringe piston, the concept of the CNC positioning system was retained: A trapezoidal threaded spindle converts the rotary motion of the drive motor into a translatory motion. The piston slider, which is connected to the syringe piston, can thus be moved along an axis and thus presses the solvent out of the syringe. The drive is provided by a bipolar stepper motor, which is operated in microstepping mode. This allows the dispensing quantity to be dosed even more finely. Ordinary disposable syringes with a capacity of 12 ml are used as solvent container.

The limit switch attached to the base prevents the piston slide from moving to the stop. If it is triggered, the user is informed that the syringe must be reloaded.

Stepper Motor Control

In contrast to the CNC positioning system, the stepper motor of the syringe pump is not controlled via the CNC controller, but via the central controller. For performance-related reasons, this cannot be operated directly via the RPI4. This means that an additional stepper motor driver is required. The driver module *DRV8825* (Texas Instruments, Dallas, USA) is used in combination with a *Breakout Board*.
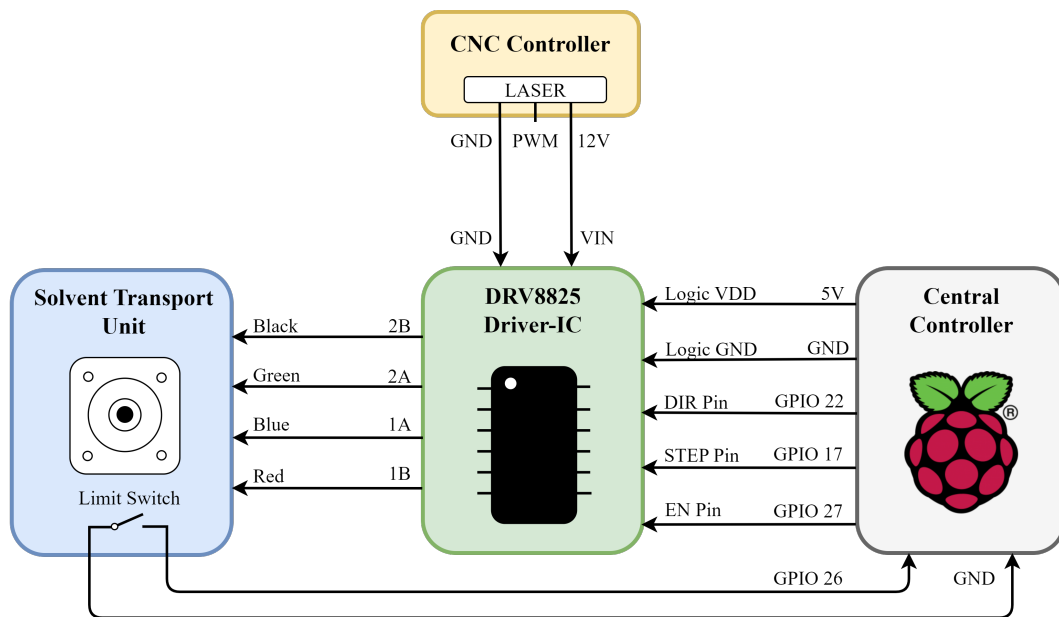

Figure 25: Block diagram of the stepper motor control. For the supply of the stepper motor, the 12V of the not needed laser output of the CNC controller was tapped.

The driver module used also allows the stepper motor to be operated in microstepping mode. The configuration is done in hardware via the DIP switches (Dual In-Line Package) located on the *Breakout Board*. The driver is configured in the finest step resolution. This means that one step is divided into another 32 steps.

Table 14: Required switch positions of the DIP switches to operate the stepper motor in 1/32 microstepping mode [51].

IC-Pin	DIP switch	Status
MODE0	MS1	ON
MODE1	MS2	ON
MODE2	MS3	ON

The bipolar stepper motor *17HS4401S* (Handson Technology) is used as the drive, which according to the data sheet [42] may be loaded with a maximum current of 1.7A per phase.

To avoid damage to the motor windings, the maximum current can be limited via the reference voltage of the driver IC. The relation between reference voltage $V_{(xREF)}$ and current limitation $V_{(xREF)}$ is defined as follows [51]:

$$I_{CHOP} = \frac{V_{(xREF)}}{5 \cdot R_{ISENSE}} \tag{10}$$

As shown in the calculation rule (10), the maximum current depends not only on the reference voltage, but also on the installed measuring resistor R_{ISENSE}. The measurement resistors soldered to the *Breakout Board* have a value of 0.1 Ω. This means that the reference voltage must be set to the following value:

$$V_{(xREF)} = I_{CHOP} \cdot 5 \cdot R_{ISENSE} = \tag{11}$$

$$= 1.7A \cdot 5 \cdot 0.1\Omega = 0.85V$$

The voltage can be both adjusted and measured via the trim potentiometer on the *Breakout Board*. All measurements necessary in this context were performed with a handheld multimeter.

Tubing System

The tubing system runs from the syringe tip to the nozzle on the cleaning head and is bent several times by up to 180 ° along the way. The material requirements for the hose are correspondingly high. On the one hand, it must be flexible enough to be able to be routed and, on the other, resistant enough to withstand the permanent movements of the carriages during cleaning.

Figure 26: Tubing system of the cleaning robot for transporting various solvents. For a better illustration, the hose is shown shortened. The symbolic markings M1 and M2 are used to determine the delivery rate.
(1) Tube
(2) Industrial cannula with *Luer-Lock* external thread
(3) Nozzle
(4) Disposable syringe

In addition, resistance to different solvents such as *Acetone* is necessary. On the pump side, the tube is connected to a dispensing needle (industrial cannula), which can be easily attached and detached from the syringe tip. On the cleaning head side, the tube ends directly at the nozzle. The nozzle is basically a dispensing needle with the threaded body *Luer-Lock* removed.

Calculation of the Dispensing Quantity per Step

The dispensing quantity per microstep was determined by the difference in the liquid level in the tube. Mark M1 indicates the liquid level before the pumping process and mark M2 afterwards. If the stepper motor is rotated by 400 micro steps, the difference in length between the two markings is $\Delta M = 51$ mm.

Since the inner diameter of the tube is also known to be d_i=1.6 mm, the delivered quantity V_{400} can be calculated using the cylinder volume formula:

$$V_{400} = \pi \cdot \left(\frac{d_i}{2}\right)^2 \cdot \Delta M = \pi \cdot \left(\frac{1.6mm}{2}\right)^2 \cdot 51mm \qquad (12)$$

$$= 102.54mm^3 = 102.54\mu l$$

From the result in (12), the flow rate per micro step (mstep) can then be determined.

$$\frac{V_{400}}{400\, msteps} = \frac{102.54\mu l}{400\, msteps} = 256.35\frac{nl}{mstep} \qquad (13)$$

Tube Capacity and Storage Volume

The total length of the laid tube is approximately l_{tube}=1000 mm, from which it follows that a filled tube contains about 2 ml of solvent.

$$V_{tube} = \pi \cdot \left(\frac{d_i}{2}\right)^2 \cdot l_{tube} = \pi \cdot \left(\frac{1.6mm}{2}\right)^2 \cdot 1000mm \qquad (14)$$

$$= 2010.62\mu l$$

The amount of solvent used to wet the polyester pad of the cleaning rod depends on the area of the optics to be cleaned. Assuming an average of 50 μl per cleaning, with a full 10 ml syringe 200 cleanings can be performed.

2.5.6 Operating and Display Unit

The operating and display unit is used for interaction with the user and essentially consists of a display, a ventilated housing and a mounting by which the unit is fixed to the robot.

Thanks to the touch function of the display, no further input devices such as a mouse or keyboard are required. If needed, however, these can still be plugged into the RPI4 and used. In addition to operation with the fingers, the robot can also be controlled via a capacitive input pen. The video signal is transmitted over HDMI and the supply voltage required for operation is provided by one of the USB interfaces of the central controller. The same USB connection is also used for data exchange between the touch matrix and the central controller.

Figure 27: Operating and display unit of the robot
(1) Display with integrated capacitive touch matrix
(2) Mounting bracket for attachment to the right aluminum profile rail
(3) Lower housing ventilated by slots
(4) Upper housing part

The installed touch display is the model *RC050* (Elecrow, Shenzhen, China). It measures 5 inches diagonally and manages a screen resolution of 800x480 px [52].

As can be seen in Figure 27, the display is installed vertically. The rotation by 90° has two reasons: On the one hand, it results in more compact dimensions of the overall system, and on the other hand, it would not be possible to connect the cables when the display is horizontally oriented.

2.5.7 Electrical Supply and Power Consumption

All electrical components connected to the system are supplied via the power supply unit of the CNC controller. Since these operate with different voltages, it is necessary to divide the output voltage of the power supply into further voltage levels. This is done primarily via the CNC controller board, which has a 24 V, a 12 V and a 5 V output as standard. To avoid overloading the 5 V output, the 12 V of the unused laser connection is converted to 5 V via a DC/DC converter in order to operate the central controller with it, see Figure 28.
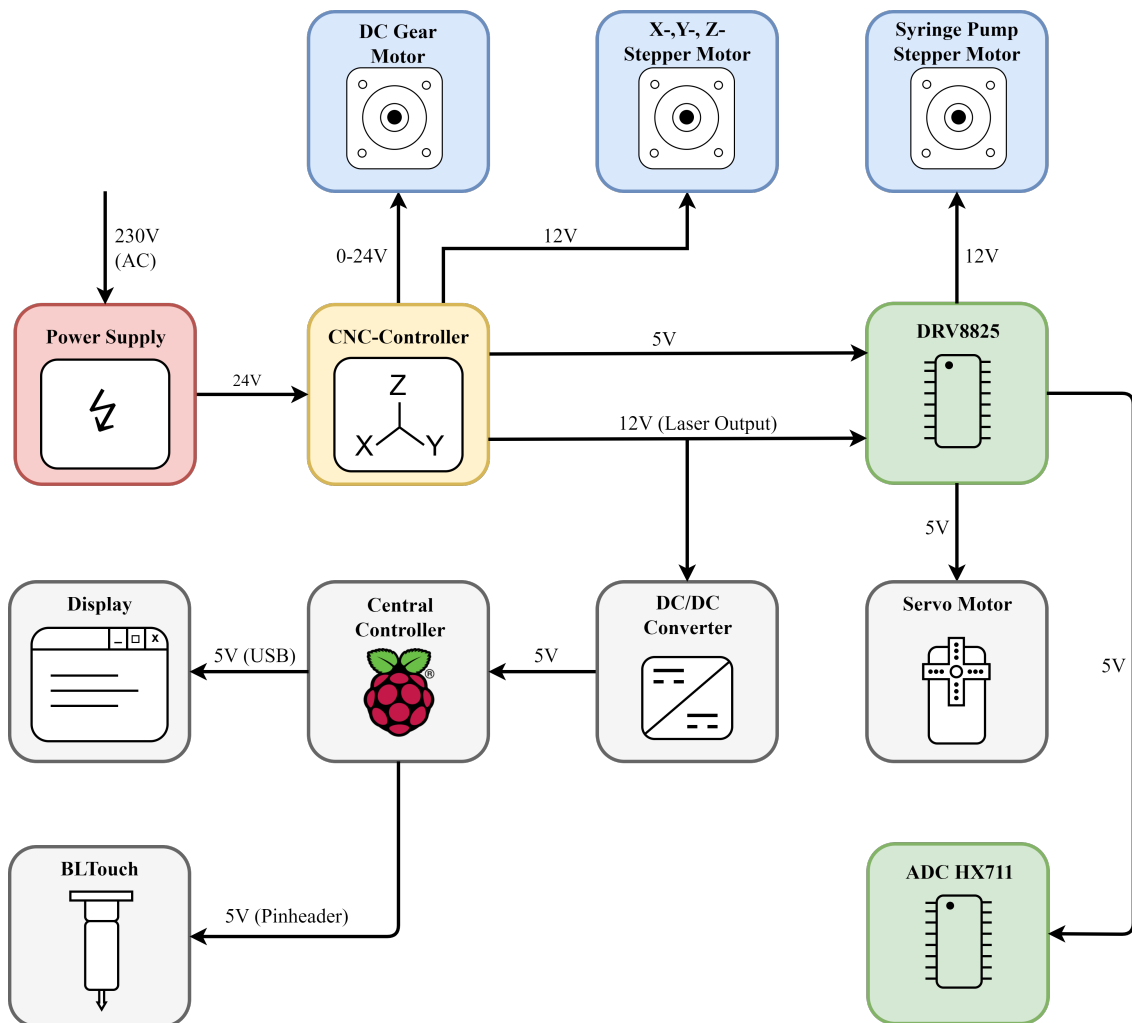

Figure 28: Structure of the electrical supply of the cleaning robot

The maximum possible output power of the power supply is 96 W according to the nameplate. In ordinary use, the robot requires an average power of about 12 W.

2.6   Software

The control software of the robot is developed in the programming language *Python*, since there are numerous open-source libraries for *Python* to control the hardware connected to the *Raspberry Pi 4*. The programming style used is based on the *PEP 8* (Python Enhancement Proposal 8) coding standard.

The operating system *Raspberry PI OS*, version 11, which is installed on the central controller, already includes the required *Python* interpreter. However, for the development and execution of the software, additional packages had to be installed and changes to the system settings had to be made, see Chapter 2.6.1.

2.6.1   Preliminary Work

Operating System Configuration

The basic configuration of the central controller can be changed via the console with the command `'$ sudo raspi-config'` [53]. For example, the SSH (Secure Socket Shell) interface, which is disabled by default, must be enabled here to allow remote access to the *Raspberry Pi*.

Since the robot is also planned to be operated via other devices such as PC, notebook or tablet, it is also necessary that an RDP tool (Remote Desktop Protocol) is installed. The required Linux package is called XRDP and can be retrofitted via `'$ sudo apt install xrdp'`.

Installing Additional Python Packages

Some of the *Python* packages included in the source code are pre-installed by default, others have to be installed via the package manager PIP (Packet Installer for Python) or APT (Advanced Packaging Tool).

In order to start the robot software in its final version, all packages listed in Table 15, page 64 are necessary. The installation is done via terminal of the RPI4 and can be achieved following the syntax below:

```
$ sudo pip3 install <package name>
```

An exception are the packages `HX711` and `PySide2`. These are not available via PyPI (Python Package Index), which is the source that PIP uses. In this case, the installation is done via APT.

```
$ sudo apt install <package name>
```

It should be noted that on Linux some commands require root privileges. Commands with the prefix `'sudo'` indicate that they are executed as *Superuser*, which means with the highest privilege level.

Table 15: Python packages used in the robot software, which are not installed by default

Package	Version	Description
pigpio	1.78	The package allows to generate PWM signals and output them to one of the GPIO Pins.
RPi.gpio	0.7.0	`'RPi.gpio'` allows to access the GPIO Pins. It is used to read the limit switch of the syringe pump and is also a prerequisite for the stepper motor module `'rpimotorlib'`.
pyserial	3.5b0	The package `'pyserial'` allows to access to the serial ports (USB) of the *Raspberry Pi* and is needed to establish a connection with the CNC controller.
rpimotorlib	3.1	`'pyserial'` is used to control the stepper motor of the solvent transfer unit.
matplotlib	3.5.2	The `'matplotlib'` package is used in combination with the graphical user interface. It can be used to create and animate diagrams in *Matlab* style. The software needs it to graphically display the pressure curve as well as the optics profile.
netifaces	0.11.0	Used to read the hostname and current IP (Internet Protocol) address of the network adapters for remote access.
HX711	1.0.0	This allows the external ADC, in a broader sense the force acting on the built-in load cell, to be read.
PySide2 (core)	5.15.2-1	`'PySide2'` allows to link the GUI design created with *Qt-Designer* (The Qt Company, Espoo, Finland) to the individual methods of the software and can thus be seen as an interface between the frontend and the backend of the software.

2.6.2 Development Tools

Programming Environment

Theoretically, the development of the robot software would also have been possible directly on the RPI4. However, the *Python* editor *Thonny* used at the beginning and already preinstalled in *Raspberry Pi OS* has only limited functionality and is therefore suitable at best for short scripts or small software projects. For software of larger scope, like that of the robot, it makes more sense to use a more comprehensive IDE (Integrated Development Environment).

Due to limited power, it is not possible to run performance-intensive IDEs on the RPI4. Therefore it was necessary to switch to remote development via SSH. In this case, the IDE installed on the development system (e.g. Windows PC) connects to the target system, in this case the RPI4, via the TCP/IP protocol. The source code is written on the remote PC, but execution and storage take place on the target system.

As IDE the software *Visual Studio Code* (Microsoft, Redmond, USA) was used. For this programming environment, there are several *Add-Ons*, which simplify the development and debugging of *Python* projects. In addition, *Visual Studio Code* supports the already mentioned remote development via SSH.

X-Window System

One fact that arises from remote development is that the graphical output takes place on the target system, in this case on the robot's display. This is basically desirable, since the robot is mainly operated as a standalone device, but especially in the development phase it is often helpful to output the GUI on the development PC. This can be realized by installing an X11 server (X-Window System). Figure 29 illustrates the principle graphically.
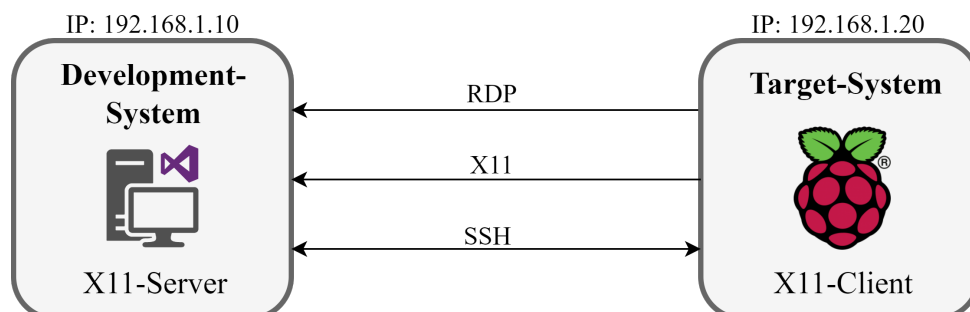

Figure 29: Representation of all protocols based on TCP/IP between development and target system

The development system thus becomes a „network monitor" on which X11 clients can forward their graphical output. The following commands can be used to switch between local and remote display:

```
$ sudo export DISPLAY=192.168.1.10:0.0   #Output on Dev-PC
$ sudo export DISPLAY=localhost:0.0      #Local Touch-Display
```

Qt-Designer

The graphical user interface of the robot software was created with the program *Qt-Designer*. Controls like buttons, text fields, checkboxes etc. are already predefined and can be placed in the window via *Drag & Drop*.

The program saves the designed window as a UI file, which can be read in directly via the *Python* code and then linked to the individual methods of the software via the `'PySide2'` package mentioned earlier. UI files are based on the language XML (Extensible Markup Language), minor adjustments of the design can therefore be done without the *Qt-Designer*.

2.6.3 Structure of the Robot Software

All files relevant for the software can be found in the `'\linsenfischer'` folder, which is located in the `'\home\wild\Python'` directory.

Table 16: Listing of the different file formats of the software project and their relative paths

Type	Extension	Description and Location
Config file	*.cfg	There is a configuration file which is stored in the `'./einstellungen'` folder. All basic settings are stored in it.
Profil files	*.profil	Profile files contain specific information about the optics to be cleaned and are stored by default in the `'./profile'` folder.
Modul files	*.py	They can be found in the root directory of the project folder and contain the source code of the software.
Design files	*.ui	Design files describe the structure of the GUI in XML format and are also stored in the root directory.
Image files	*.png	All logos and icons used in the GUI can be found in the `'./logos'` folder.

Basic Configuration

In the file `'einstellungen.cfg'` all essential basic settings of the software are stored. For example it contains the USB connection settings for the CNC controller, various constants and conversion factors, the GPIO Pin configurations, the fixed positions of the CNC positioning system and much more. The content is not coded and can be modified via any ordinary text editor. During program start the file is read and evaluated line by line. Each line corresponds to a setting and must have the following format:

```
attribute:value
```

Comments are marked with a `'#'` and are discarded, like blank lines. The basic configuration can be displayed via a separate menu in the software, but for security reasons changes can only be made in the file itself. For these to be adopted, a restart of the robot software is necessary.

Optics Profiles

The format of an optics profile is similar to that of the configuration file. The information is stored and read out according to the same principle. An optics profile essentially consists of three sections: the general data, the cleaning parameters and the XZ profile coordinates.

The general data consists of information such as part number, customer or curvature type. In the cleaning parameters section, the amount of solvent, maximum pressure, optics radius, rotation speed, etc. are defined. The XZ profile coordinates section is optional and is only present if the optics were probed before saving the profile.

Program Modules

For a better overview, the software is divided into nine individual modules. The methods are summarized in such a way that they can always be assigned to a hardware or a software unit. For example, the module `'bltouch.py'` contains all the necessary functions for controlling and reading out the leveling sensor.

The file `'main.py'` mentioned in Table 17 (page 68) represents the main module and is thus the file that must be passed to the *Python* interpreter to start the robot's software.

Table 17: Listing of all Python modules created for the robot software

Modul name	Brief description
bltouch.py	The module enables raising and lowering of the probe via PWM and processes the change of state of the limit switch, which triggers when a surface is touched. It also controls the entire probing operation during the recording of a surface profile.
controller.py	This module is used for serial communication with the CNC controller. In addition to setting up and initializing the interface, this also includes sending commands and receiving the device status.
hilfsfunktionen.py	This file contains a collection of small auxiliary functions. For example, the received device status is decomposed in order to extract the current coordinates and the state of the device. In addition, the module contains various functions that are used to perform conversions and corrections.
main.py	As a central module, it links the elements of the GUI to the individual methods and functions, captures user input, coordinates the cleaning processes and manages the display of the main window as well as the settings window.
profil.py	The module is called up when the profile of an optic is saved or read. An optics profile always consists of general data, specific cleaning parameters and optional profile coordinates. The implemented methods are mainly related to file manipulation.
schrittmotor.py	The `schrittmotor.py` is used to control the stepper motor of the syringe pump via the GPIO Pins of the RPI4.
sensor.py	The module is required to initialize and read out the force sensor (loading cell).
servo.py	The cleaning head is positioned through the `servo.py`. As in the module `bltouch.py`, a PWM signal is generated and emitted at one of the GPIO pins.

User Interface

The design of the user interface is defined by the two files `'hauptfenster.ui'` and `'einstellungen.ui'`. The file `'hauptfenster.ui'` is loaded when the program is started and creates the main window out of it.

The screen resolution of the touch display is limited to 800x480 px. In order to still find enough space for all necessary elements of control (buttons, text fields, diagrams, etc.), the contents are categorized and divided into the four tabs *Profile*, *Reinigung*, *Manuelle Kontrolle* and *Aufzeichnung*. Vertical, horizontal and grid layouts are used in combination with placeholders for uniform alignment of the different elements. The size of the main window is adapted to the display and cannot be changed. Dynamic resizing of the various controls is therefore not necessary.
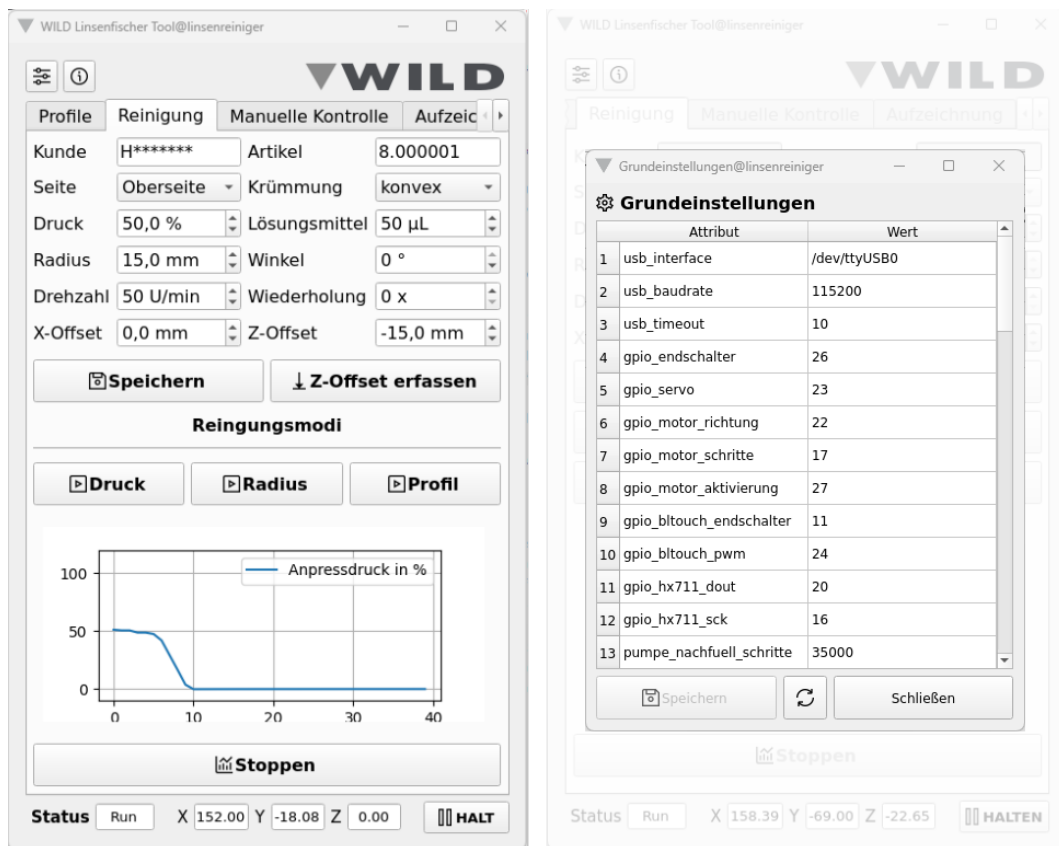

Figure 30: The left side shows the main window of the program. On the right side you can see the opened settings window.

The `'einstellungen.ui'` file is used to create the basic settings window. It displays the attributes and values read from `'settings.cfg'` in the form of a table.

For better clarification of the function, each button is additionally provided with an icon. All necessary image files are stored in the `'\logos'` folder and the link to the design file is made by specifying the relative storage path.

2.6.4 Executing the Software

To avoid starting the program via the console, the shortcut `'linsenfischer.dekstop'` is placed on the desktop of the *Raspberry Pi*. If this link is opened, the executable shell script `'run.sh'` starts in the background, in which the file `'main.py'` from the root directory of the software project is passed to the *Python* interpreter. For a manual start of the program, the working directory must be changed first.

```
$ cd ~/Python/linsenfischer     #Switches to software directory
$ python main.py                #Executes the software
```

2.6.5 Interrupts

When creating optical profiles, the reaction time of the central controller plays an essential role. For the acquisition of the Z-coordinate, the controller lowers the Z-carrier in 0.01 mm steps. If the probe of the sensor hits the surface, the logic level at GPIO Pin 11 changes from `HIGH` to `LOW` and thus stops the lowering. If the control reacts too slowly, the actual Z-coordinate will be falsified by 0.01 mm with each further loop pass.

For this reason the level change at the GPIO Pin is captured via *Interrupts*. With *Interrupts*, in contrast to *Polling*, a change is responded to immediately by interrupting the current program [54]. This saves time and thus prevents wrong results when probing the profile.

2.6.6 Multithreading

During cleaning, it is necessary for the central control system to perform certain tasks simultaneously. These include, for example, the permanent query of the current position, the reading of the force sensor or also the positioning of the carriers. In order to keep the time sequence of the cleaning process as unaffected as possible, *Threads* are used. *Python* provides its own threading module for this purpose, which allows tasks to be processed at least quasi-parallel.

In addition to the tasks just mentioned, the live visualization of the pressure curve is also handled by threads. A real-time view during cleaning would not be possible without *Threading*, since the permanent updating of the diagram takes a relatively long time. This would greatly slow down the already time-critical cleaning process

and lead to unpredictable time conflicts.

In the current software project, up to four additional *Worker Threads* are running simultaneously besides the *Main Thread*, which, among other things, manages the update of the user interface.

The principle of *Multithreading* solves any timing problems, but leads to new challenges, which are discussed in more detail in the chapters *Lock Objects* and *Signals* on page 72.

2.6.7 Lock Objects

When using *Multithreading* it can happen that under certain circumstances several threads access one and the same resource simultaneously. In the current case this concerns the serial interface (USB), which is used to communicate with the CNC controller, see Figure 31.
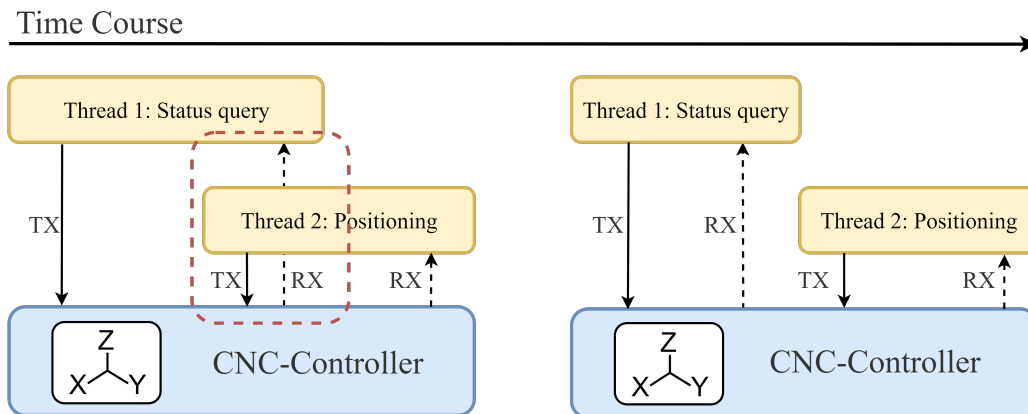

Figure 31: The left side visualizes the situation which can occur due to *Multithreading*. Thread 2 tries to send data to the CNC controller although the USB interface is still occupied by Thread 1. On the right side, the access is done one after the other and thus without overlaps.

To prevent multiple access, *Python* provides the possibility to lock critical program sections via a *Lock Object* [55]. In the concrete case, Thread 1 locks access to the serial port until the requested information of the status query is received. After that, the code section is released for Thread 2, which sends a positioning command to the controller.

2.6.8 Signals

Another property that must be taken into account when using *Multithreading* is that the direct manipulation of user interface objects (e.g. lables) is only possible through the generating *Thread*, in this case the *Main Thread*.

In a concrete use case (see Figure 32), the user is to be informed via a popup that the cleaning is complete and the optic can be removed. Since the cleaning process is also handled by a *Thread*, the popup cannot be generated via it, as mentioned above. If the popup window is created directly by the *Main Thread*, it will already appear at the start of the cleaning process due to the parallelization, and thus too early.
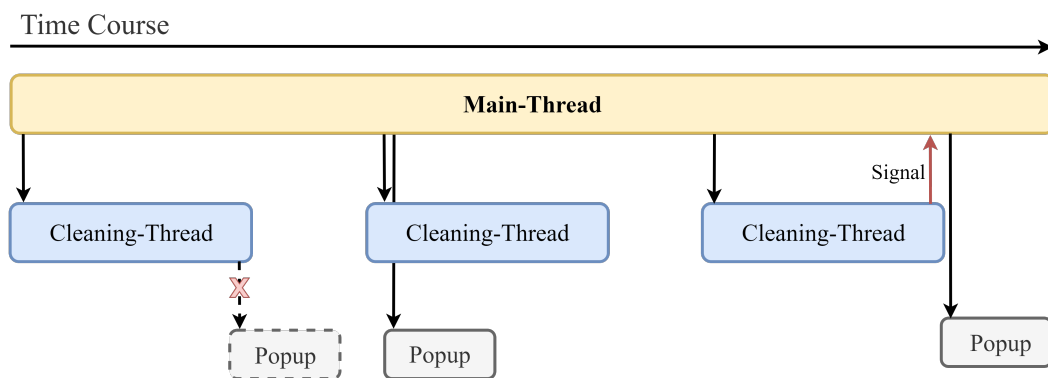
Time Course

Figure 32: Visualization of the situation using a block diagram
Left: Popup cannot be created
Middle: Popup is created at the wrong time
Right: Popup is created at the correct time

To make sure that the popup is opened at the right moment, *Signals* were used. Via *Signals* communication between the *Main Thread* and the *Cleaning Thread* can be established. The *Cleaning Thread* tells the *Main Thread* at which time changes to the user interface should be made. The principle is also used when probing a surface profile. In this case, the *Probing Thread* signals the *Main Thread* after each sampled point that the progress bar (tab *Aufzeichnung*) needs to be updated.

2.6.9 Overview of Software Features

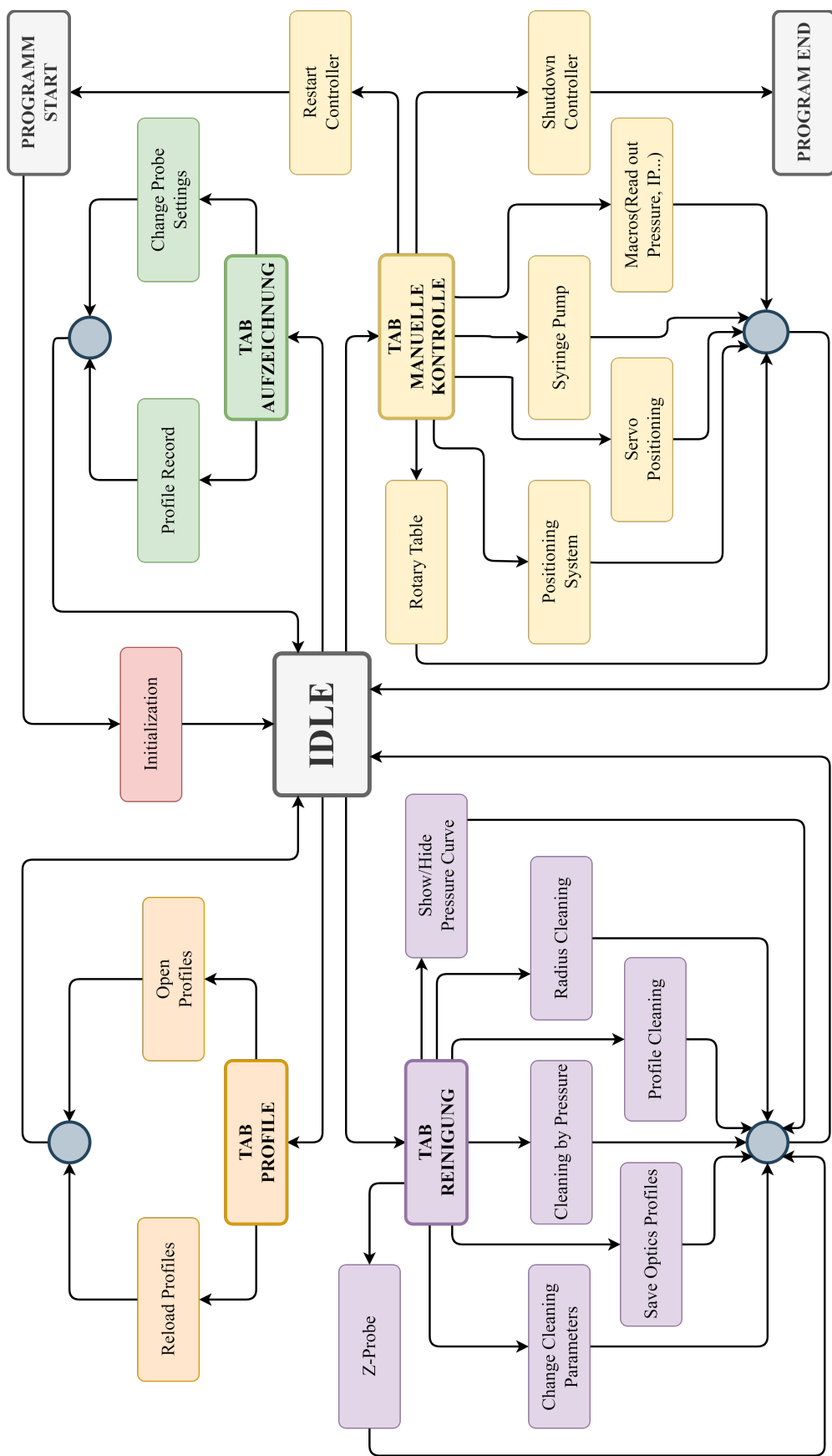Figure 33 on page 73 shows an overview of the different program features of the robot software.

Figure 33: Overview of individual robot software functions categorized by tab

2.6.10 Documentation

The documentation of the software is based on *DocStrings* and inline comments. *DocStrings* are comments which can span several lines starting and ending with three single (`'''`) or double (`"""`) quotes.

Unlike single-line comments, which in *Python* are initiated with a *Hashtag* (`'#'`), *DocStrings* can be read with suitable tools like *Sphinx* to automatically create a documentation of the software project. The precondition is that a certain format is adhered to. A typical *DocString* comment of a function looks like this:

```
"""Calculates the rotational speed to be sent to the CNC
    controller via linear regression.

Args:
    desired_speed (int): Rotational speed in 1/min.
    slope (float): Slope of linear equation.
    offset (float): Offset of linear equation.

Returns:
    float: Returns the corrected rotational speed
            in 1/min.
"""
```

The above example corresponds to Google's *DocString* style, recognizable by the keywords `'Args'` and `'Returns'`. Sphinx searches the entire source code for *DocStrings*, collects the information it contains, and generates the documentation out of it, which is then available in various formats such as *HTML* (Hypertext Markup Language) or *PDF* (Portable Document Format). [56]

2.7 Test Series

After initial commissioning, the robot was subjected to various test series. The results obtained from these tests are used on the one hand to specify the precision and linearity of the installed sensors and on the other hand to evaluate the cleaning success.

2.7.1 Probing Sensors

Precision of Single Point Probing

For profile probing, the point probing precision was first determined for both sensors (leveling and capacitive proximity sensor). For this purpose, three points along the surface of an achromat (Ø=30 mm) were sampled 200 times each in order to determine the measurement uncertainty and mean value. The Z-carrier was lowered with a resolution of 0.01 mm.
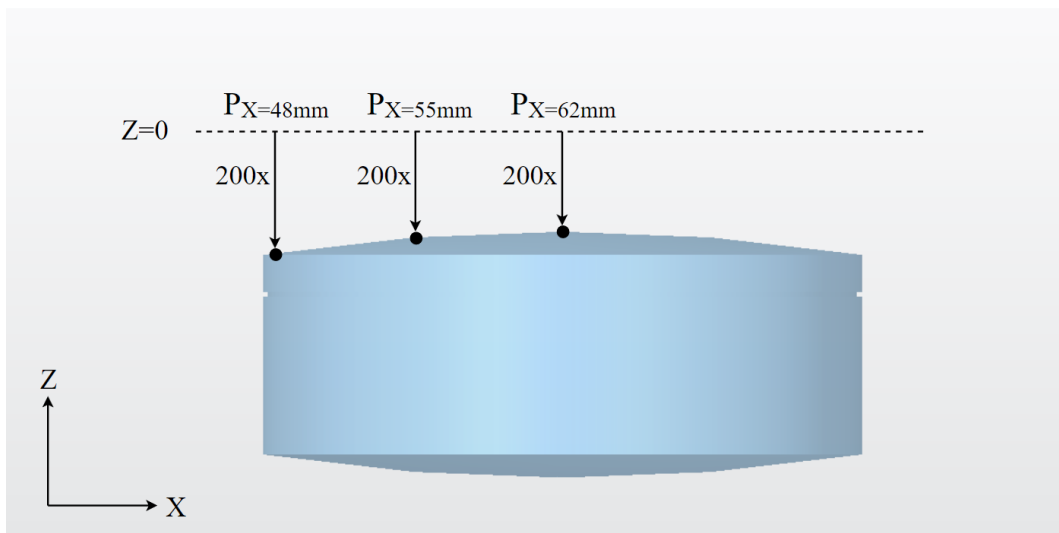
Figure 34: Achromat with drawn in sampling points

Precision of a Surface Profile

The two sensors were then subjected to a further series of tests to find out whether the measured values could be reproduced even after an intermediate shift in the X axis.

For this purpose, 10 measuring points (at a distance of d=1.61 mm) were recorded along the surface to create a profile. Each of the 10 measuring points corresponds to the median of five individual samples. The lowering of the Z-carrier was performed with a resolution of 0.01 mm, as was already the case with the single-point probing.

Figure 35 illustrates the procedure with the aid of a graphic. A total of three surface profiles were recorded and compared for each sensor.
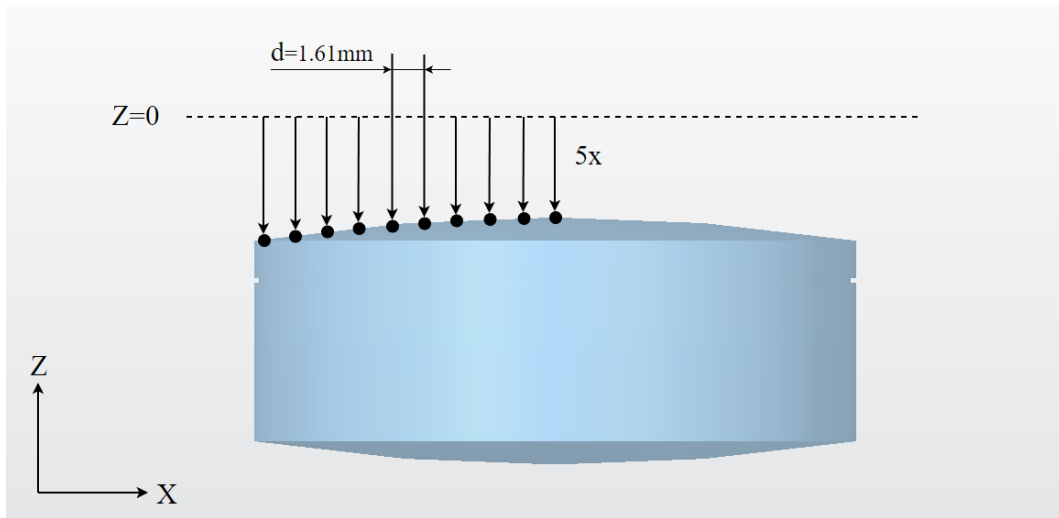

Figure 35: Representation of the probing points when recording a surface profile of an achromat

Based on the results of single-point and profile sampling, a decision was made about which of the two sensors was better suited for the application in the cleaning robot.

2.7.2 Load Cell Test

Since pressure resp. force measurement is an essential part of all three cleaning modes, the load cell was also subjected to two tests to determine the precision and linearity of the sensor.

Precision of the Load Cell

The first step was to investigate the behavior in continuous operation in order to identify possible trends and determine the precision. For this purpose, the cleaning head was first lowered to Z=-22 mm to build up pressure and then immediately raised again to unload the load cell. This procedure was carried out 200 times, taking a pause of 2.5 seconds after each cycle. Subsequently, the same test was repeated with a pause time of 5 s and 7.5 s, respectively. A visualization of the experiment can be seen in Figure 36 on page 77.
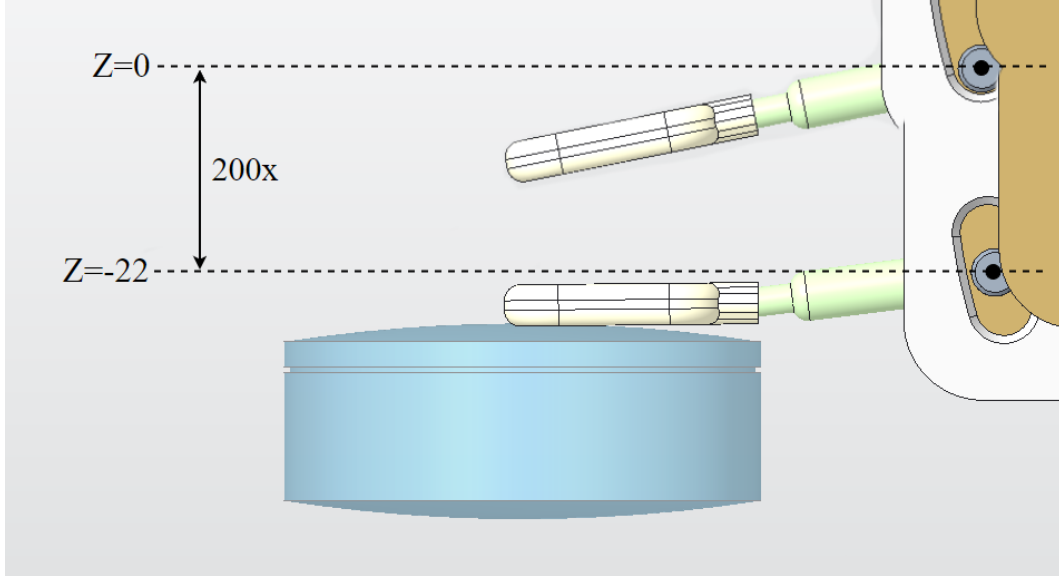
Figure 36: Method for determining the precision of the force sensor. The figure is also intended to illustrate that the pad adapts to the curved surface of the optics due to the flexibility of the shaft.

Load Cell Linearity

Another property of a load cell that is worth investigating is linearity. To determine this, the cleaning head was lowered in tenths of millimeter steps from Z=-17.0 mm to Z=-26 mm, and the pressure (resp. force) acting on the pad was measured and stored after each step. It was assumed that all elastic elements involved in the measurement, such as the compression spring, exhibit a constant *Hookian* behavior.

2.7.3 Determination of the Actual Rotation Speed

The rotation speed of the turntable can be controlled via the CNC controller, as already mentioned. Since the speed delivered to the motor shaft is translated via both, the planetary gear and the belt drive, the set speed does not match the actual rotation speed of the turntable. In addition, the CNC controller generates an unclean PWM signal, which further increases the deviation. For this reason, the actual rotation speed n_t was measured and compared to the set speed n_e. By linearizing the rotation speed curve determined this way, the coefficients p_1 and p_2 for the correction could be calculated and entered into the basic settings of the robot software. The relationship between the speeds can be described via the transformed linear equation (15).

$$n_e = \frac{n_t - p_2}{p_1} \tag{15}$$

To make the turntable finally reach the desired speed n_t, the corrected speed n_e must be sent to the controller.

For the measurement of the rotational speed, the line follower sensor board *KY-033* was used, which is marked with (1) in Figure 37. The line follower basically consists of an IR receiving and an IR transmitting diode and can distinguish between light and dark areas depending on the intensity of the reflected infrared light. If the received infrared light exceeds a certain threshold, the logic level at the output pin of the sensor changes.
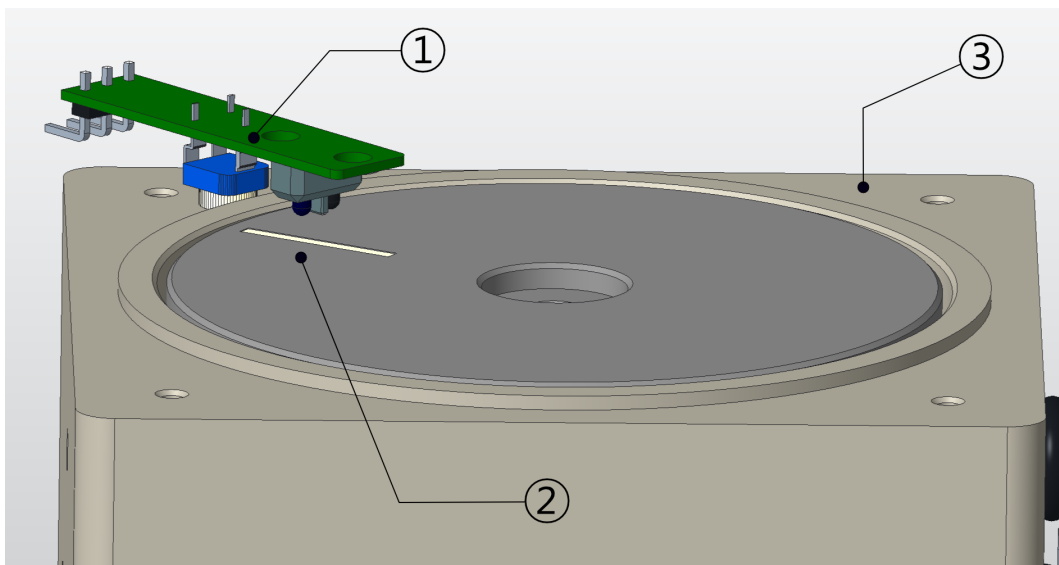

Figure 37: Rotational speed measurement by means of sensor board KY-033
(1) Sensor board with transmitting and receiving diode
(2) Turntable with white marker
(3) Gear block

Due to the rotation of the turntable, the level changes at regular intervals. The elapsed time between two level changes can be used to calculate the revolutions per minute. In order to achieve a more accurate result, the median of 20 time measurements was formed for each rotational speed. The acquisition was done with the help of the microcontroller board *Arduino UNO R3*.

Since the determination of the speed is based on a time measurement, the accuracy of the clock influences the measurement result. The used *Arduino* board has a 16 MHz ceramic resonator installed [57] which has a tolerance of $\pm\,0.3\,\%$ according to its data sheet [58]. The resulting measurement deviations of the considered speed range are less than one rpm and therefore influence the results only insignificantly.

2.7.4 Test Setup to Evaluate the Cleaning Success

For the evaluation of cleaning, the surfaces of two different optics were examined, which can be seen in Figure 38. It was tested how efficiently dust deposits, grease- and sweat-based fingerprints, and saliva droplets can be removed, since these types of soiling occur most often in the field.
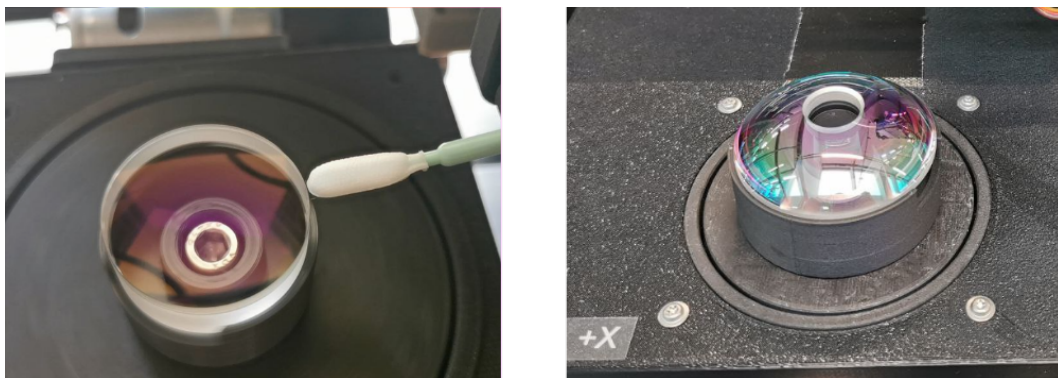

Figure 38: On the left, an achromat from an optical coherence tomograph (ophthalmology), and on the right, a spherical lens with a centering hole

Particulate Contaminants

Regarding the particulate contaminants, the cleaning success was quantified by counting the particles before and after cleaning and classifying them by size. The cleaning efficiency RE was then determined separately for each class of size. The procedure is inspired by the *Classification of Cleanability* described in the book „*Reinraumtechnik*" by Lothar Gail et al. [59] .

Formula (16) shows how to determine the cleaning efficiency for particles $\geq 10\mu m$. The variables n_{before} and n_{after} correspond to the number of particles before and after the cleaning process, respectively. The result of the calculation is expressed as a percentage.

$$RE_{\geq 10\mu m} = 100 \cdot \left(1 - \frac{n_{after,10\mu m}}{n_{before,10\mu m}} \right) \tag{16}$$

Figure 39 on page 80 shows that the images must be processed so that the size and number of particles can be determined by software. It is also necessary to adjust the scale of the image to the scale of the software.

In order to compare the mostly very differently shaped particles with respect to their size, the *Feret* diameter (equivalent diameter) was determined in each case.

All image processing and analyses were performed using the image processing software *ImageJ* (National Institutes of Health, Bethesda, USA).
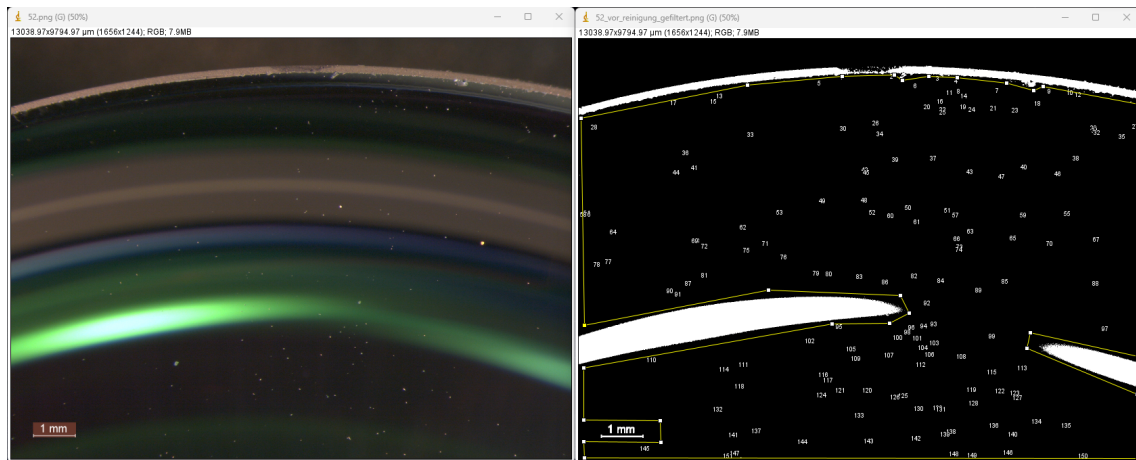
Figure 39: The left side shows the original image of a dirty optic. The right side shows the processed version, in which all detected particles are marked with an ID number.

Filmy Contamination

In contrast to particulate contamination, the procedure for quantifying NVRs is much more complex and, as mentioned in Chapter 1.5, requires highly accurate equipment for weight determination. In this work, cleaning results for filmy contaminants (fingerprints, saliva droplets) were determined by visual interpretation.

Measurement Setup

Figure 40 on page 81 shows the setup by which the surfaces of the optics were examined. The digital microscope *M80* and the image sensor *MC190 HD* (Leica, Wetzlar, Germany) were used in conjunction with the software *Leica Application Suite*.

To ensure that the same area of the surface was viewed before and after cleaning, the edge of the optics was marked with a permanent marker. The solvent used was mainly *Acetone* in various amounts.
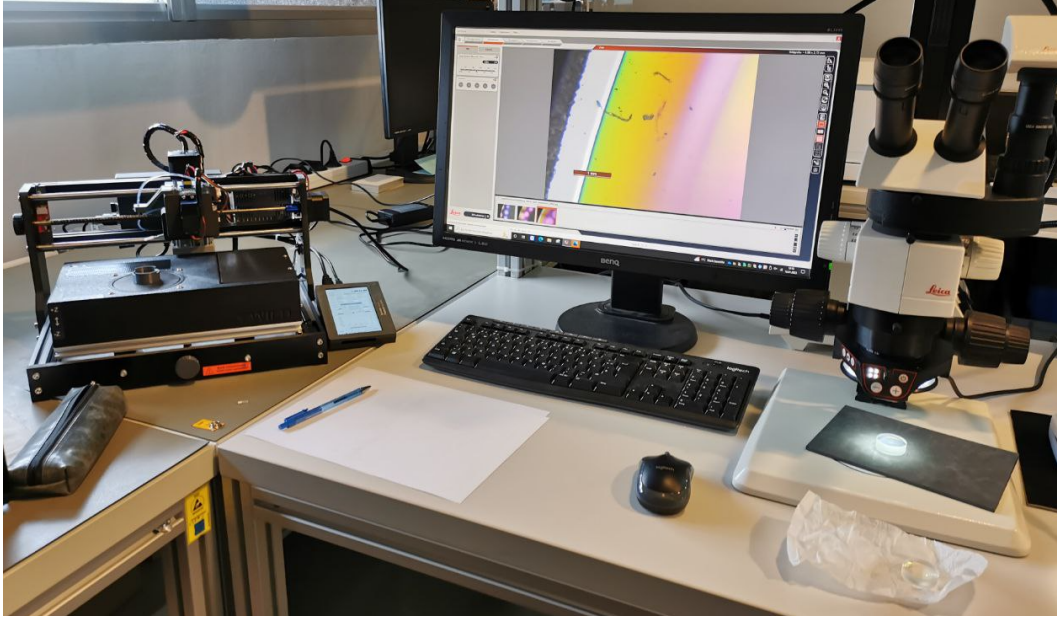
Figure 40: The left side of the image shows the cleaning robot, while the right side shows the digital microscope for inspecting the optical surfaces.

2.7.5 Evaluation and Presentation of Results

The mean values and standard deviations calculated from the measurement results were determined using the software *Matlab* (Mathworks Inc, Natick, USA). *Matlab* was also used to display the results in different plots.

3 Results

3.1 Profile Probing

3.1.1 Punctual Repeatability

Figure 41 shows the results of single point probing using the leveling sensor at three different points on the achromat. The results in Table 18 are based on 200 measured values each.
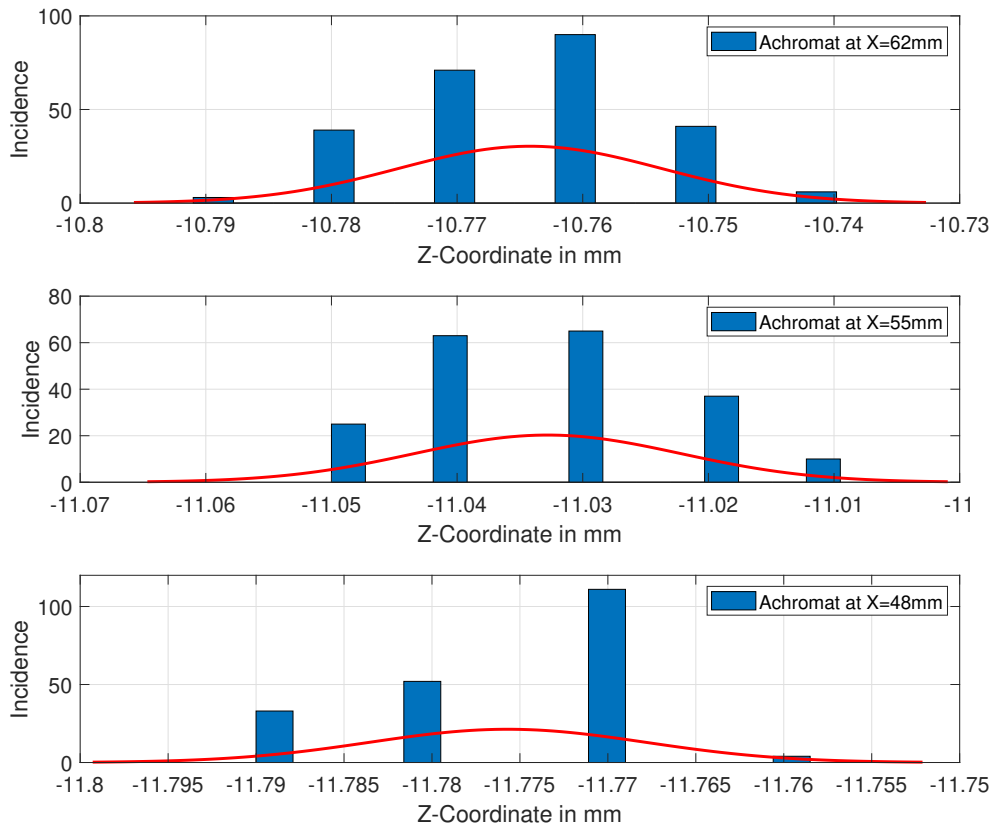
Figure 41: Histograms of single point probing at points X=62mm (top), X=55mm (middle) and X=48mm (bottom)

Table 18: Statistical parameters of the leveling sensor

Point	X position	Mean value μ	Standard deviation σ
1	62 mm	-10.7642 mm	10.5 μm
2	55 mm	-11.0328 mm	10.6 μm
3	48 mm	-11.7757 mm	7.9 μm

Corresponding to the histograms of the leveling sensor, the measured value distributions of the capacitive proximity switch are shown in Figure 42. The statistical characteristics in Table 19 show that the proximity switch has a nearly 5 times higher standard deviation compared to the leveling sensor.
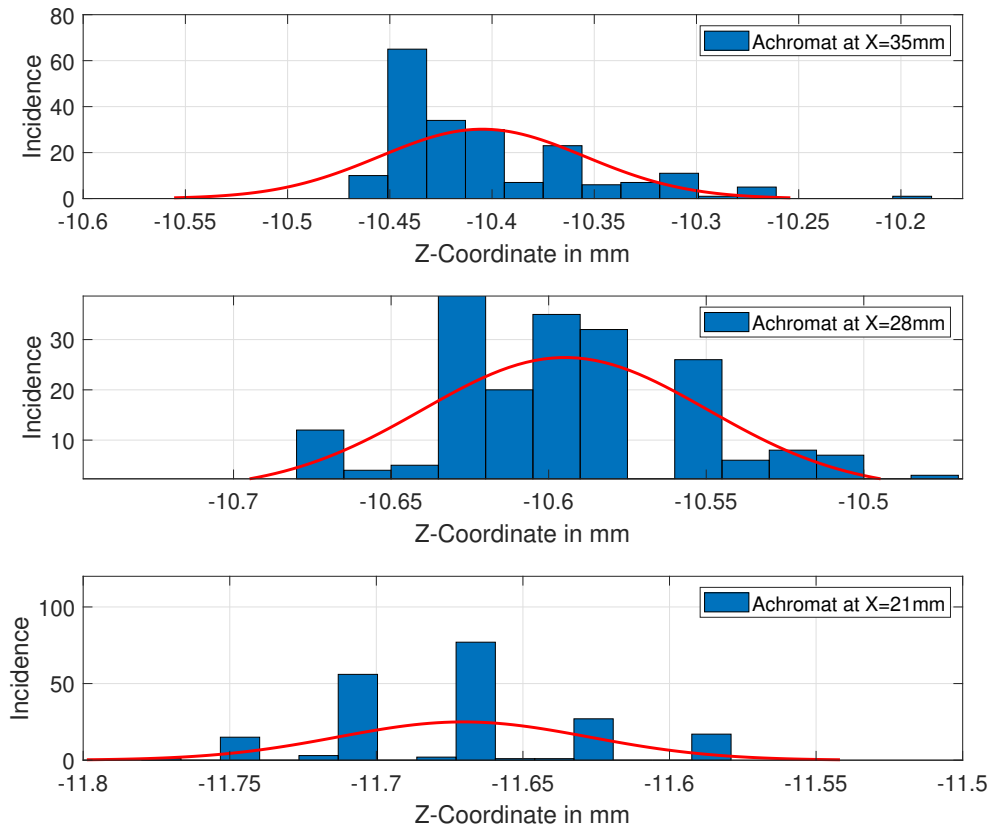
Figure 42: Results of single point probing by capacitive proximity switch at again three different surface points of the achromat

Table 19: Mean values and standard deviations of the capacitive proximity switch

Point	X position	Mean value μ	Standard deviation σ
1	35 mm	-10.4048 mm	50.2 μm
2	28 mm	-10.5948 mm	45.3 μm
3	21 mm	-11.6706 mm	42.8 μm

3.1.2 Repeatability of Profile Probing

Figure 43 shows the results of the profile scanning. The higher precision of the leveling sensor is also reflected in the recorded profiles. It is noticeable that on direct comparison the results differ greatly, see „Direct Comparison".
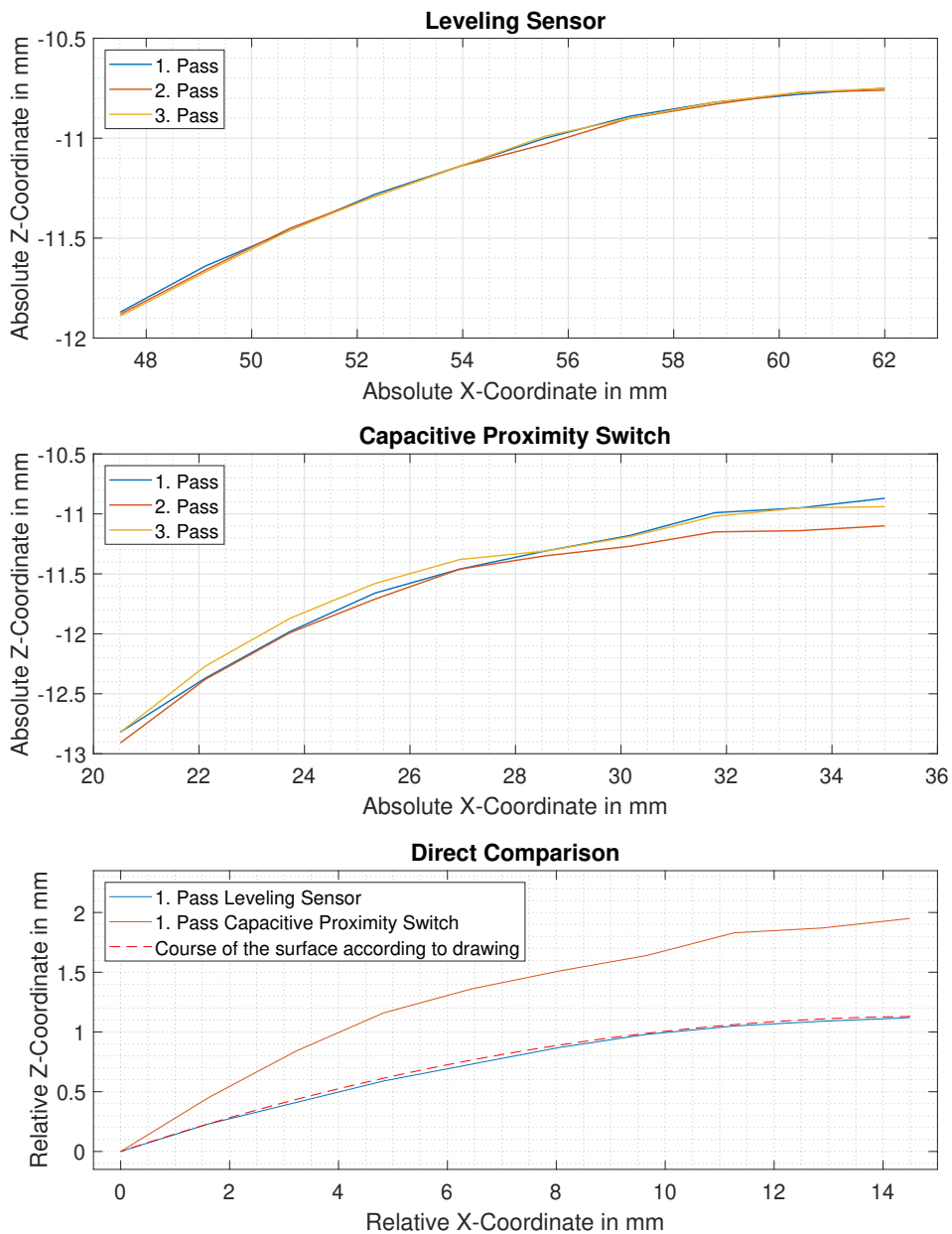
Figure 43: Results with multiple profile scans of the same achromat. When interpreting the diagrams, note that the X and Z axes have different scales.

3.2 Pressure Measurement

Precision of the Load Cell

The evaluations in Figure 44 show that the pause times between the individual measurements have an influence on the tendential course of the pressure value. The higher the pause, the less scatter can be observed, see Table 20.
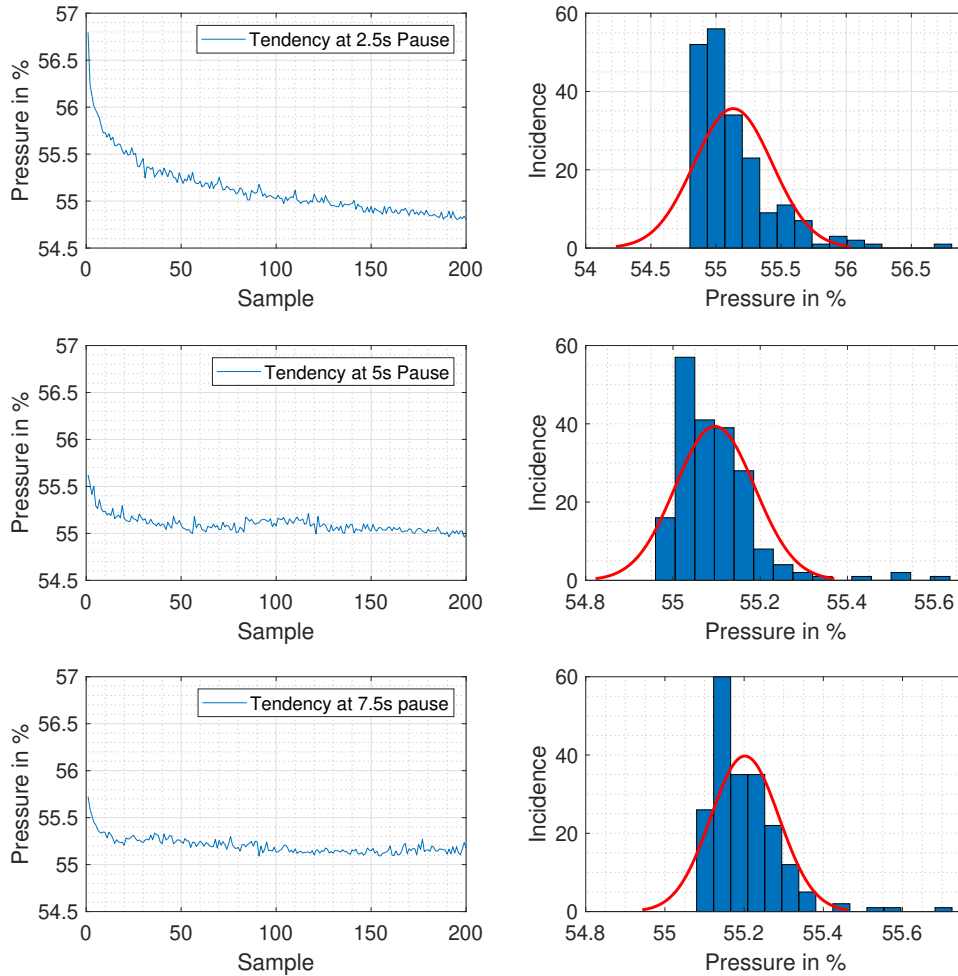
Figure 44: Precision of the load cell when the Z carrier is lowered to Z=-22mm

Table 20: Statistical evaluation of the measurement results of the load cell

Series	Pause	Mean value μ	Standard deviation σ
1	2.5 s	55.1323 %	0.3001 %
2	5.0 s	55.0962 %	0.0912 %
3	7.5 s	55.2018 %	0.0863 %

Linearity of the Load Cell

The diagram in Figure 45 compares the real pressure curve recorded by measurements with the ideal curve fitted by *Matlab*, which parameters can be found in Table 21. The real course is approximately linear and deviates from the ideal curve mainly at low loading of the load cell.
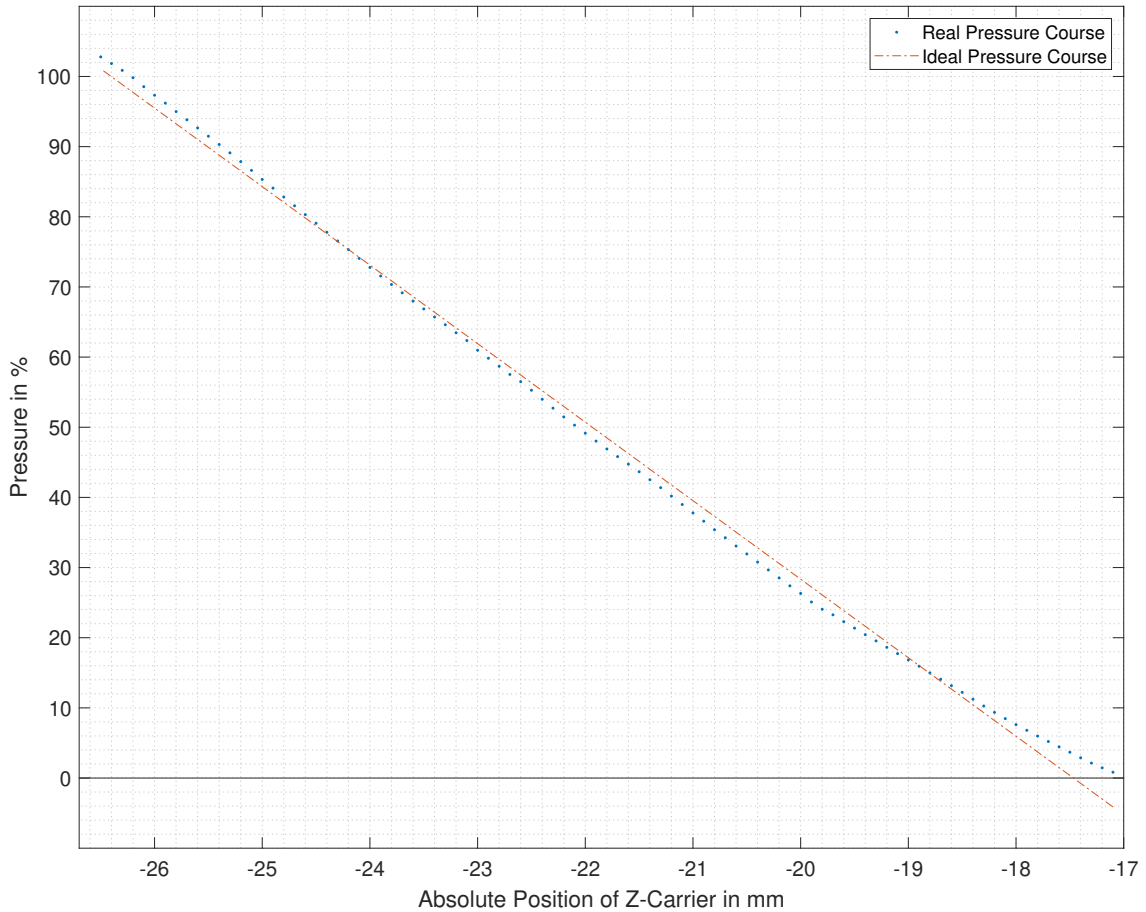
Figure 45: Pressure curve when lowering the Z-carrier from -17.0 mm to -26.5 mm in an interval of 0.1 mm. The fitted ideal curve follows the linear equation $y = k \cdot x + d$.

Table 21: Parameters of the fitted (ideal) curve

Parameter	Value
k	-11.1919
d	-195.4960

Pressure Curves of the Different Cleaning Modes

Figure 46 shows the results of the pressure measurement during a cleaning. The same achromat was used for all three modes. The blue courses represent the optimal progression with a correctly inserted cleaning rod or after optimization of the cleaning algorithms. Negative examples (lack of optimization, incorrectly inserted rod) are shown as orange curves.
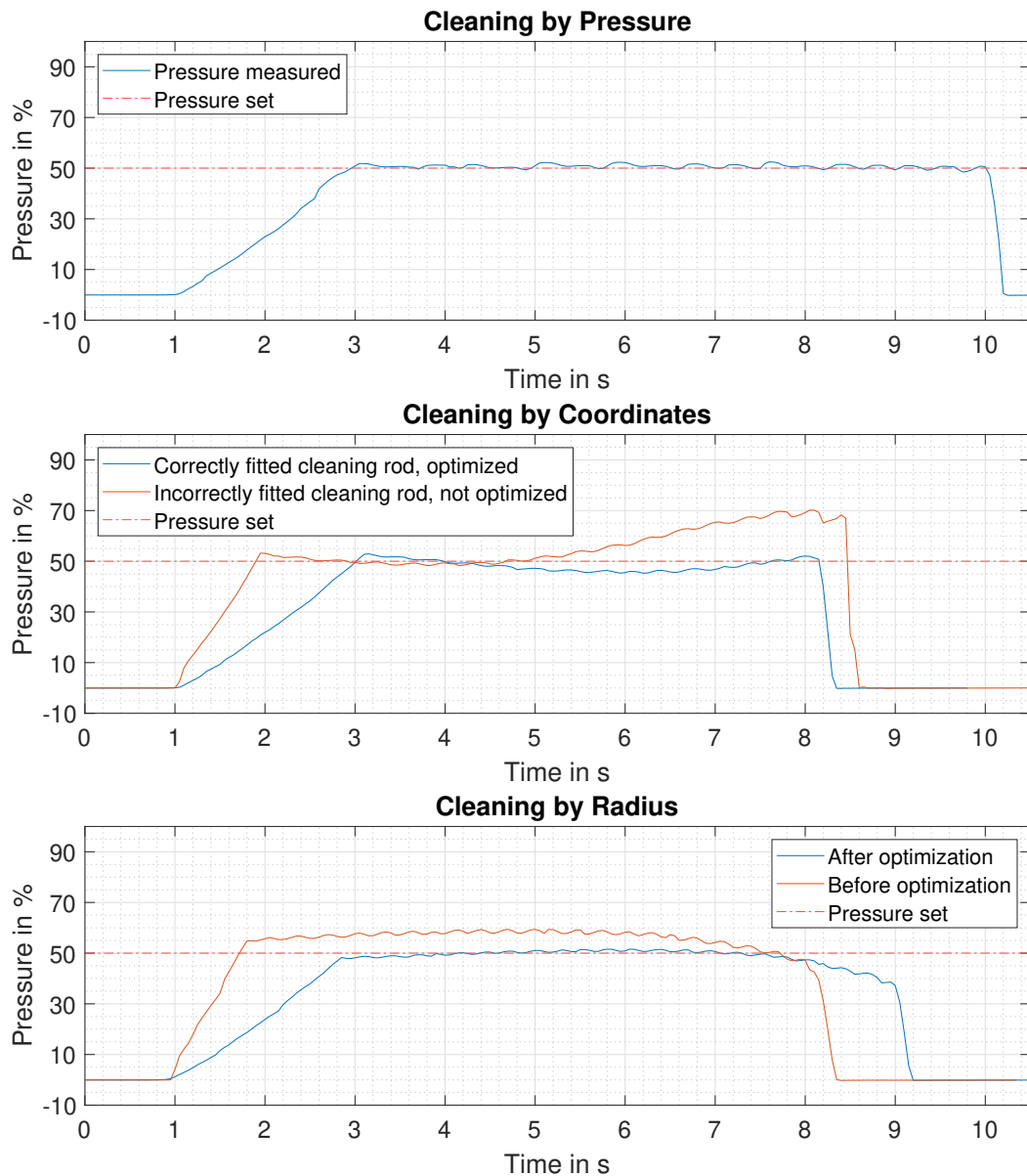
Figure 46: Comparison of the pressure curves with different cleaning modes. The pressure cleaning takes with more than 10 seconds clearly the longest.

3.3 Speed of the Turntable

3.3.1 PWM Signal

The signal curve shown in Figure 47 shows that the CNC controller does not provide a perfect PWM signal. The voltage rises to about 6.5 V even before the actual on-time of the signal, causing an increase in the average voltage $\overline{U_{PWM}}$. With a pulse width of t_{on}=137.6 μs, according to the calculation rule (3) on page 42, theoretically, an average voltage of $\overline{U_{PWM}} = 3.96$ V should be generated, but in fact this is 7.6 V.
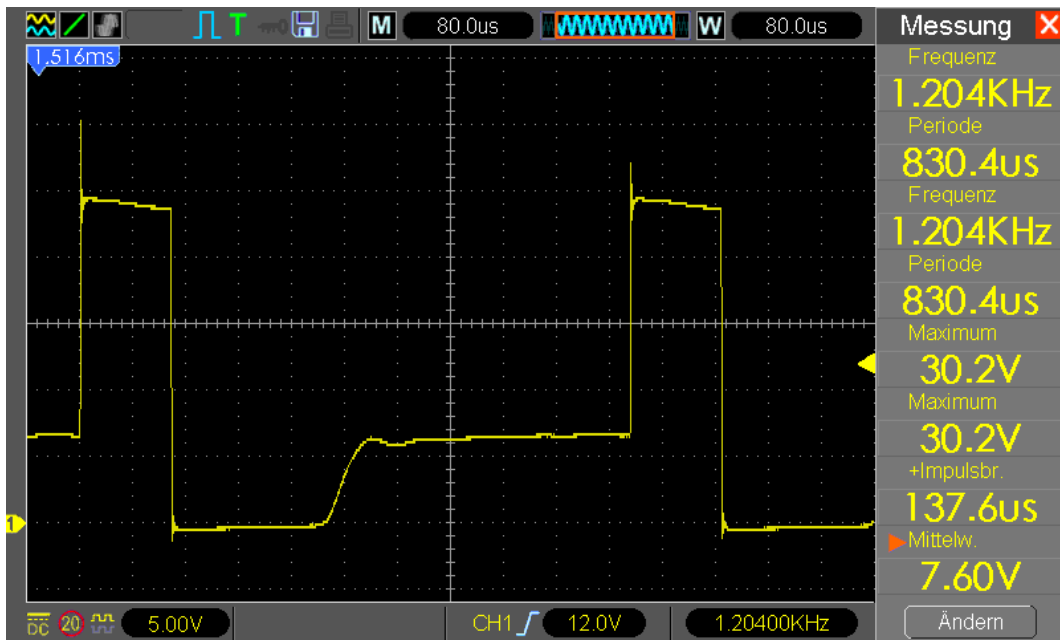
Figure 47: Real PWM signal generated by the CNC controller to drive the DC gearmotor

3.3.2 Linearity of the Rotational Speed

Figure 48 shows the relationship between set and measured speed. The orange, dash-dotted straight line corresponds to the ideal curve, which was created through linear regression.
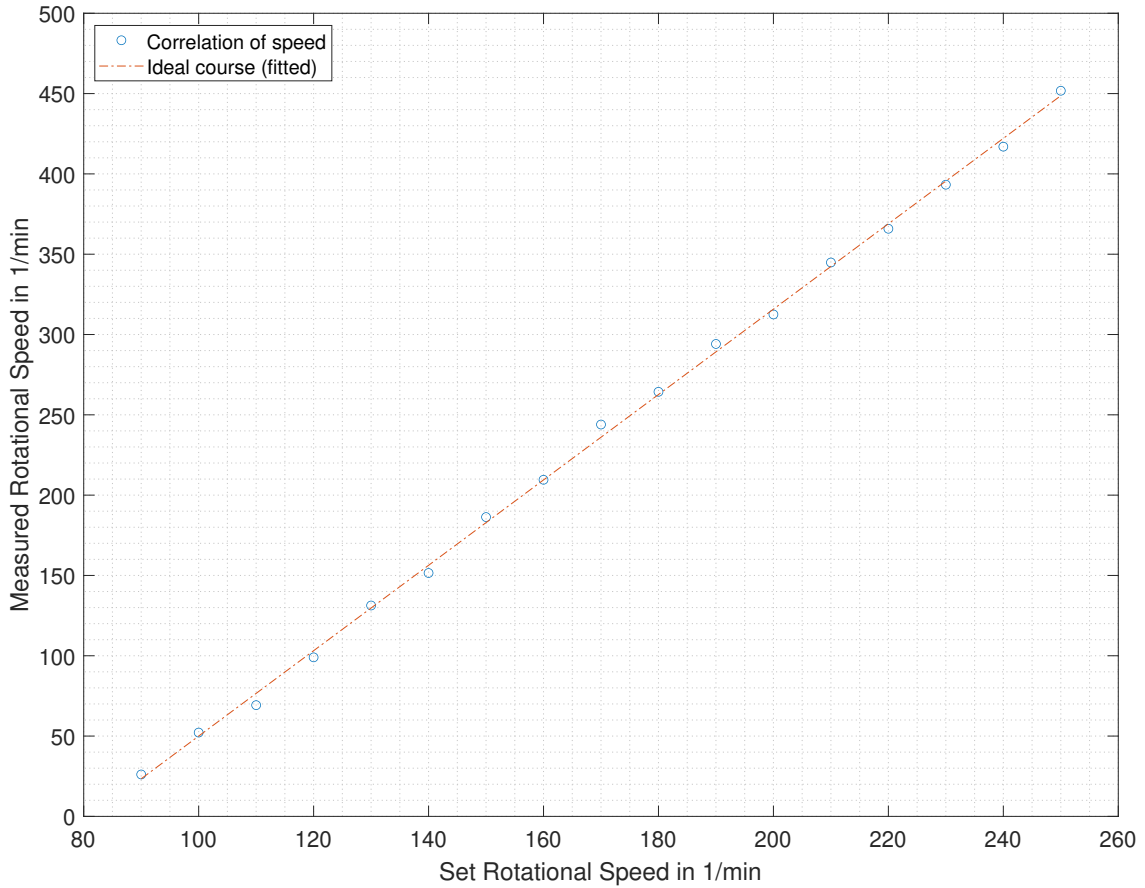
Figure 48: Results of the rotational speed measurement

Rotations below 25 min^{-1} could not be detected because at low speeds the average voltage of the PWM signal $\overline{U_{PWM}}$ is too low to overcome the breakaway torque of the DC gearmotor.

Table 22: Polynomial coefficients of linearization of 1st degree

Coefficient	Value
p_1	2.6581
p_2	-215.8110

The polynomial coefficients in Table 22 can be used to correct the speed that must be sent to the CNC controller to make the turntable rotate with the set speed.

3.4 Cleaning Results

3.4.1 Particulate Contamination

Figure 49 shows the spherical lens before and after cleaning by the robot. The appearance of the colors is due to the surface coating of the optics, in this case, an anti-reflective coating made for a wavelength of 1550 nm.
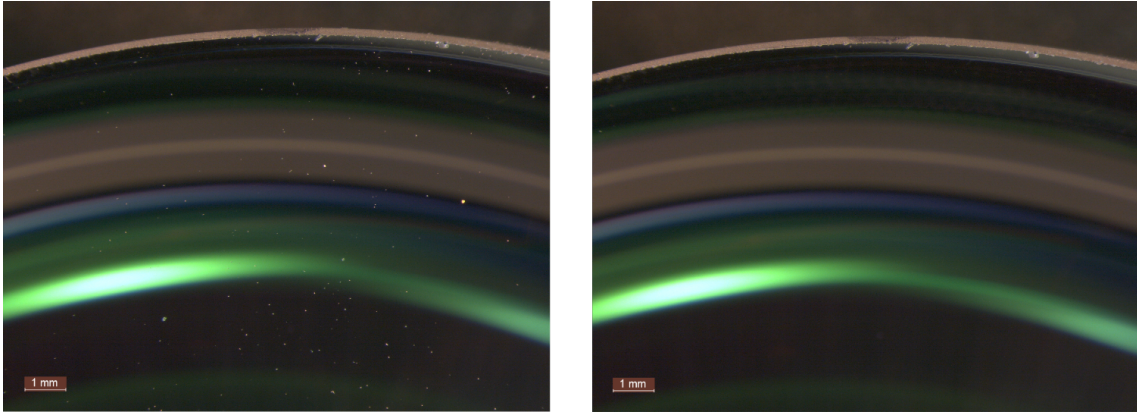
Figure 49: The left image shows the contaminated spherical lens directly after removal from the protective packaging. The recorded equivalent diameters (D_{eq}) of the particles are between 11.13 and 120.19 μm. On the right, the same lens after cleaning by robot. The cleaning was performed with a pressure of 50 %, a solvent volume of 50 μl and a rotational speed of 120 min^{-1}.

Table 23 summarizes the results of the counted particles as well as the calculated efficiency of the cleaning, sorted by occurring particle size.

Table 23: Cleaning results of the spherical lens

D_{eq} in μm	Particle concentration before cleaning	Particle concentration after cleaning	Cleaning efficiency in %
≥ 10	74	2	97.3
≥ 20	59	0	100
≥ 30	51	0	100
≥ 40	35	1	97.1
≥ 50	9	0	100
≥ 60	2	0	100
≥ 70	3	0	100
≥ 80	3	0	100

The pictures in Figure 50 show another before-and-after comparison of an optic contaminated by dust and lint. The purple, orange, and yellow colors are again due to the reflection of the surface coating. A closer look also reveals many gray spots that seem to cover the entire visible surface. These are due to the underlying foam base and should therefore not be interpreted as dirt.
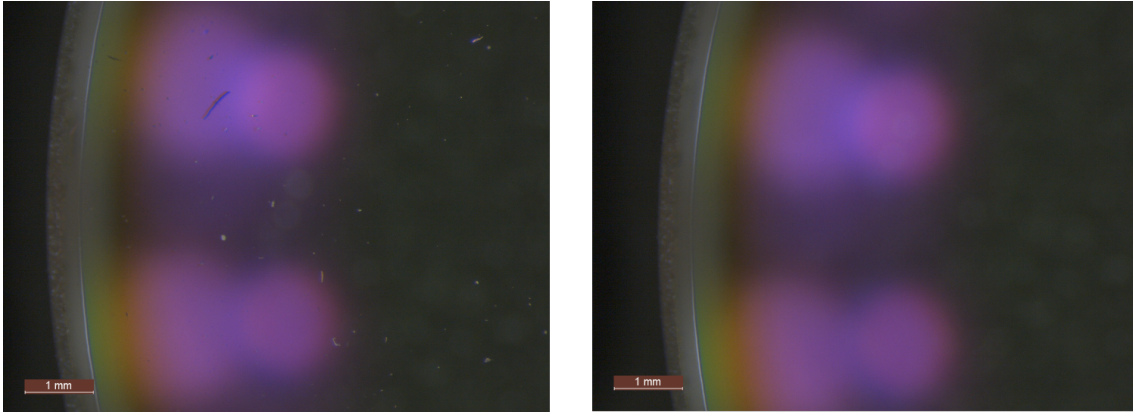
Figure 50: On the left the heavily soiled surface of the achromat and on the right the same surface after cleaning. The recorded equivalent diameters D_{eq} of the particles range from 15.75 to 540.15 μm. Cleaning was performed with 50 % pressure, 50 μl acetone and a rotational speed of 120 min^{-1}.

The results in Table 24 show that all particulate contaminants could be removed. It should be noted that particle diameters < 10 μm were not detected.

Table 24: Cleaning results of the achromat

D_{eq} in μm	Particle concentration before cleaning	Particle concentration after cleaning	Cleaning efficiency in %
≥ 10	61	0	100
≥ 20	43	0	100
≥ 30	19	0	100
≥ 40	3	0	100
≥ 50	4	0	100
≥ 60	7	0	100
≥ 70	3	0	100
≥ 80	9	0	100

3.4.2 Greasy Dirt Films

The comparisons in Figure 51 and 52 show the cleaning results when trying to remove a greasy fingerprint. The soiled area in this examples are very large, which is rarely the case in practice.
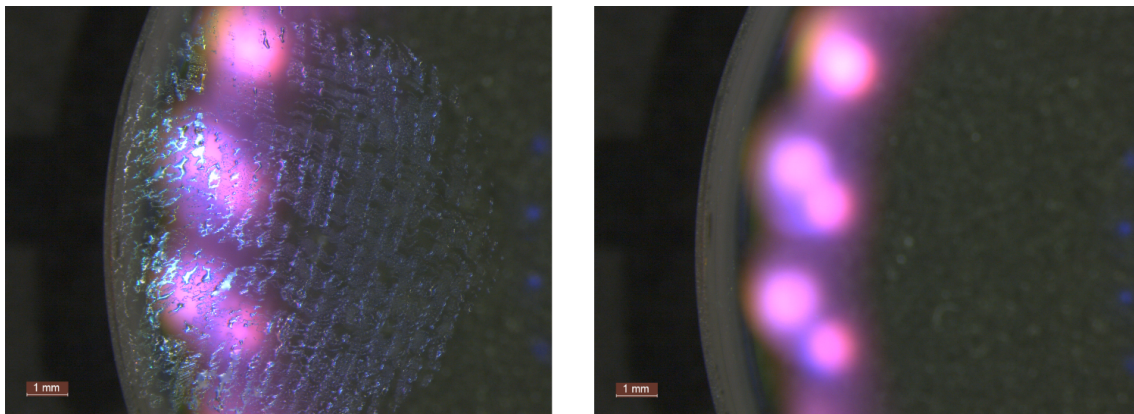
Figure 51: On the left one can see the achromat contaminated by a greasy fingerprint. On the right, the same achromat after cleaning. This result was obtained after a single run with 66 % pressure, 80 μl solvent and a rotational speed of 100 min^{-1}.
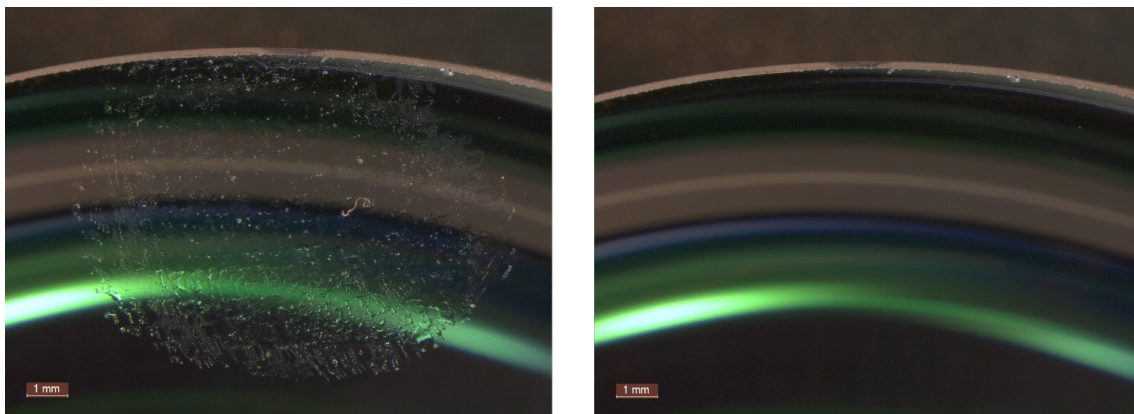
Figure 52: Left: Greasy fingerprint on the bottom of the spherical optics (flat surface); Right: Cleaning result after a single pass under a pressure of 40 %, a solvent volume of 60 μl, an adjustment angle of -12 $^\circ$ and a rotational speed of 100 min^{-1}.

3.4.3 Contamination Through Sweat-Based Fingerprints

The fingerprints in Figure 53 and 54, left image, were pressed onto the surface directly after removing the protective gloves (made of nitrile). In contrast to the fingerprints shown in Chapter 3.4.2, these are based on sweat. There are also sporadic particles visible which are assumed to be small salt crystals. In both cases, it can be seen that one cleaning cycle is not sufficient to completely remove the soiling.
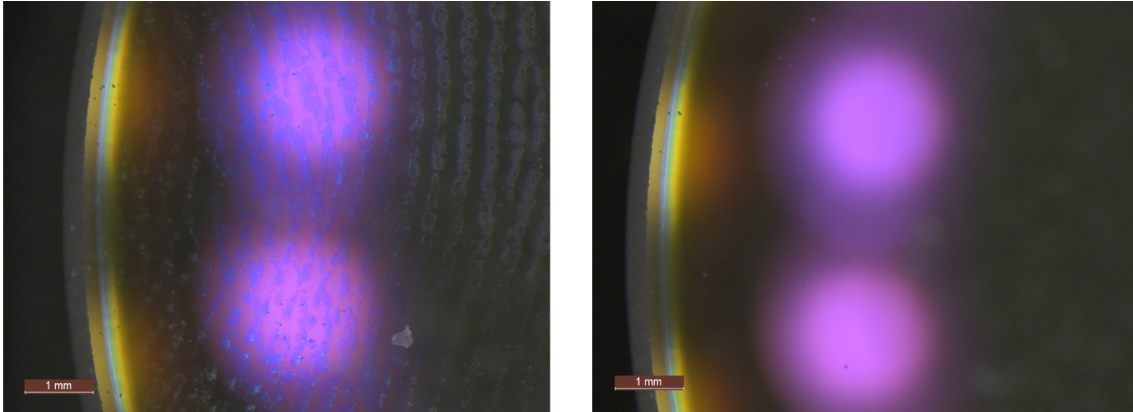
Figure 53: The left image shows a mixed contamination of particles, a sweat-based fingerprint and a skin flake. The right side shows the result after cleaning with 85 % pressure, 90 μl solvent and a rotational speed of 100 min^{-1}.
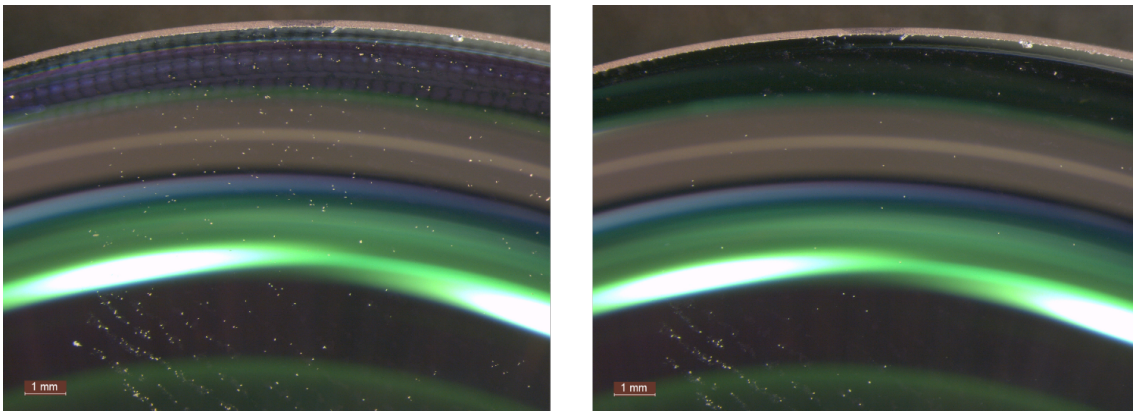
Figure 54: Another attempt to clean a dried sweat-based fingerprint - in this case on the spherical lens. The right photo shows the result after cleaning with 50 % pressure, 50 μl solvent and a rotational speed of 100 min^{-1}.

3.4.4 Contamination Due to Saliva Droplets

The photos in Figure 55 show contamination in form of saliva droplets in combination with particles. The concentric circles in the upper right photo occur when the rotation speed of the turntable is too high.
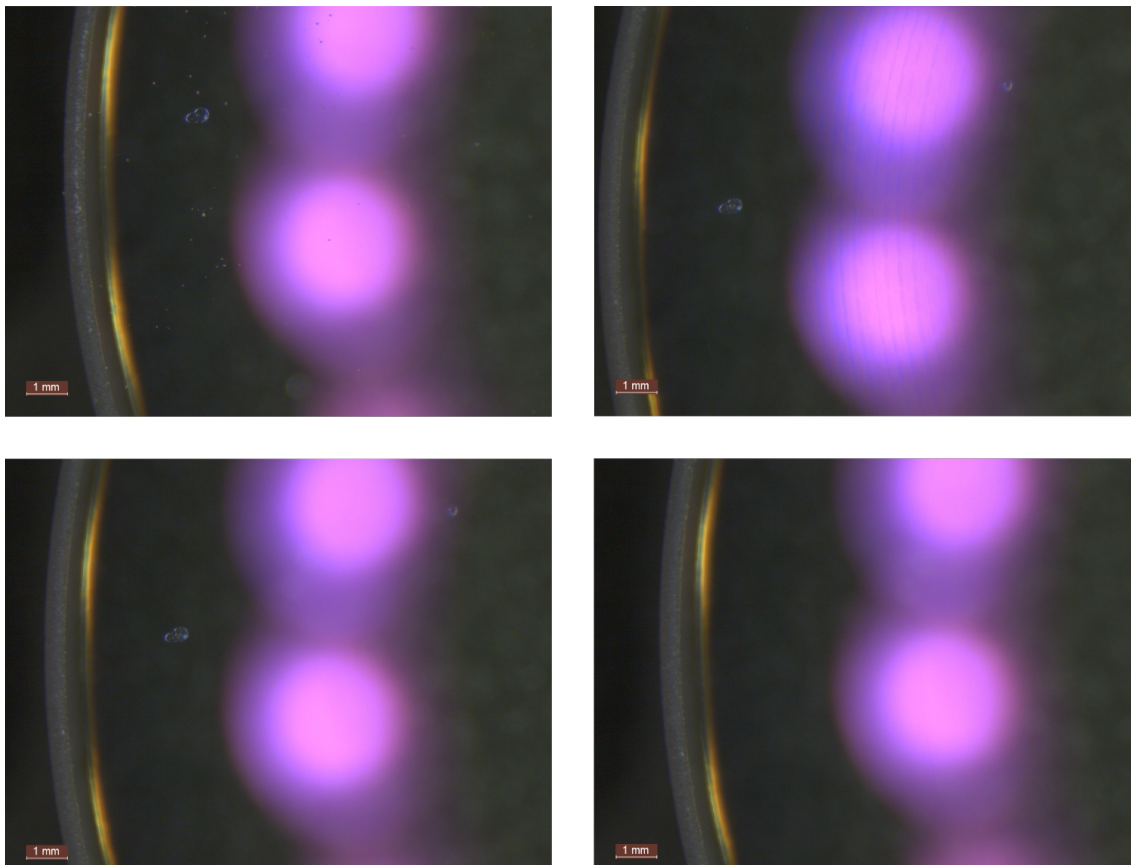
Figure 55: Attempt to clean an achromat contaminated by saliva droplets and particles. Upper left picture shows the initial situation. Right picture shows the result after the first cleaning attempt at 50 % pressure, 50 μl solvent and a rotational speed of 280 min^{-1}.

A closer look at Figure 55 shows that although all particles could be removed, the two saliva droplets are still present. A subsequent cleaning was also unsuccessful, as shown in the lower left image. The lower right image shows the cleaning result after five manual cleanings. In this case, instead of *Acetone*, breathing air fogged on the optics surface was used as „solvent".

3.4.5   Comparison Between Manual and Automatic Cleaning

The four images in Figure 56 are showing the direct comparison between manual and automated cleaning of the achromat. The upper before-and-after comparison is of automated cleaning using a robot, with the left image taken before cleaning and the right image taken after cleaning. The lower comparison shows the result of manual cleaning.
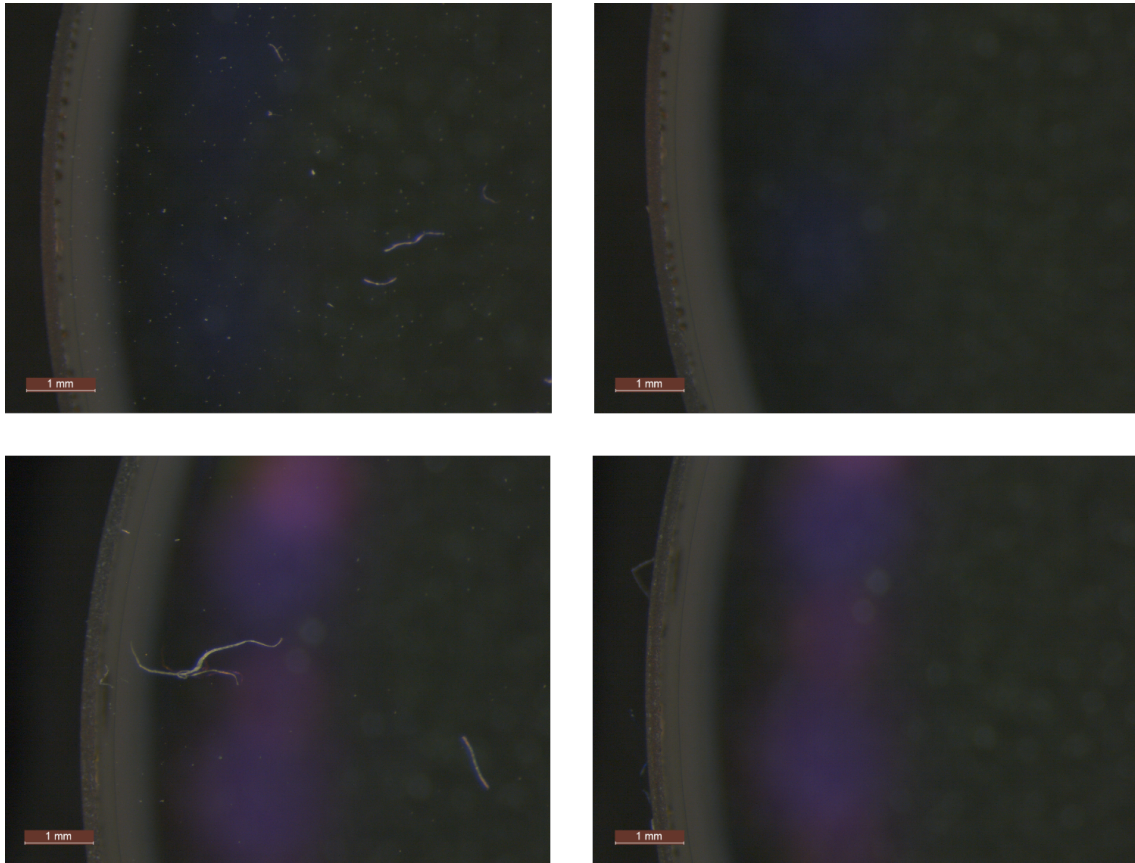
Figure 56: Direct comparison between manual (bottom) and automatic (top) cleaning. The result of automated cleaning was achieved with 50 % pressure, 50 μl solvent, and a rotational speed of 100 min^{-1}.

After both manual and automatic cleaning, no particulate residues are visually detectable. The light gray spots are again due to the foam base.

4 Discussion

4.1 CNC-Positioning System

The cleaning tests carried out have shown that the CNC positioning system used fulfills its purpose in the cleaning robot and that the positioning of the individual carriers is performed with sufficient accuracy. A small disadvantage results from the open control loop between the CNC controller and the stepper motors. Although the current position of the carriers is reported back to the central controller at 20 ms intervals, the coordinates do not necessarily correspond to the actual position. This is because the position feedback is not, as in professional CNC systems, realized by using *Encoders* sitting on the motor shafts, but is calculated by software. From a practical point of view, this only leads to a problem if the lead screws are unintentionally and unknowingly shifted by hand after the initialization process.

4.2 Controller Unit and Software

The single-board computer *Raspberry Pi 4*, which acts as the central controller, is powerful enough to run the robot software written in *Python*, which also includes the user interface, smoothly.

In principle, the peripherals connected to the pin header can also be controlled or read out without any problems. However, it could be observed that the external ADC *HX711* sometimes returns wrong pressure values. However, these are recognized and marked by the used *HX711* library. Thus, outliers can be filtered out and discarded by software without much effort. Since the sensor is read out at 20 Hz, the cleaning process remains unaffected.

The connected sensors and actuators occupy 17 of the 40 GPIO Pins. This means that the controller still offers sufficient potential for further development of the cleaning system in terms of hardware. For example, the turntable unit could be expanded to include an optical sensor that checks whether an optic has been inserted into the device before each cleaning. Another useful feature would be to add an air bubble detector to the robot to prevent dry cleaning.

4.3 Solvent Transport Unit

The solvent unit implemented as a syringe pump operates very reliably and, unlike the also considered *Peristaltic Pump*, requires less maintenance, since the tube is not consumable in this case. The combination of the 2 mm pitch trapezoidal lead screw and the 1/32 microstepping mode of the stepper motor allows a theoretical dispensing accuracy of 236.35 nl/mstep, which is more than adequate for a typical dispensing volume of 50 μl.

However, the transport system also has disadvantages. The following two points should therefore be taken into account: If, for example, no solvent transport takes place for several days, the solvent in the tube will slowly begin to evaporate. Therefore, it is advisable to close the nozzle airtight before a longer break (e.g. weekend) to prevent evaporation. From a safety point of view, the evaporated solvent does not pose a problem for the environment, since the quantities are in the nanoliter range and are released over a long period of time. Rather, the danger lies in the fact that after a longer standing time of the device, no solvent is dripped onto the polyester pad during the first cleaning cycles and the robot cleans the optics dry. The missing tube content can therefore be added manually via the software if necessary, see operating instructions Chapter A.

The system is also sensitive to air inclusions in the tube, which can occur especially when refilling the syringe. Air inclusions mean that the dispensing volume does not match the set values, therefore care must be taken to ensure that the tube system remains as free as possible from air bubbles.

4.4 Cleaning Head

4.4.1 Methods of Profile Sampling

When comparing the two tested sensors with regard to their measuring method, the capacitive proximity switch has the advantage that the distance is detected without contact. There is therefore no risk of damaging the coatings. In contrast, measurement by leveling sensor is based on surface contact.

It has been found that touching the surface is not a problem because the probe has a low dead weight and is made of plastic. Even after multiple scans of the same optic, no damage attributed to the probe could be detected.

4.4.2 Precision of Single Point Probing

The results in Table 18, page 82 and Table 19, page 83 show that when a single point is repeatedly sampled, both sensors provide usable results, but the level sensor is significantly more accurate.

The maximum standard deviation of the capacitive sensor is 50.2 μm, which would be sufficient for the present application. With the leveling sensor *BLTouch*, even standard deviations below 10 μm could be achieved. So in terms of precision, both sensors are suitable.

When interpreting the results, it should be noted that factors such as the resolution of the stepper motors or tolerances of the mechanical parts (e.g. the trapezoidal lead screw) also play a role. More precisely, the recorded measured values describe the precision of the sensor in interaction with the CNC positioning system.

4.4.3 Surface Profile Acquisition

The comparison of the recorded surface profiles in Figure 43 (page 84) confirms that more precise results can be obtained with the leveling sensor. A direct comparison of the two sensors also shows that the two profile curves created differ greatly from each other. If the actual dimensions of the optics are included, it becomes clear that the deviation is definitely due to the capacitive proximity switch.

A possible explanation for the non-constant switching distance of the proximity switch is that the generated electric field, on which the measurement is based [49], hits the surface of the optics at a different angle depending on the probing point and is thus damped to a different extent. In view of this circumstance and the already higher precision of the leveling sensor, the capacitive proximity switch is no longer an option.

4.4.4 Precision and Linearity of Pressure Measurement

The graphical evaluation of the measurement results in Figure 44 on page 85 revealed that the pressure decreases more or less depending on the pause time between the measurements. Especially with short pause times, a clear tendency can be seen. However, this behavior is not due to the load cell itself, as initially suspected. The reason is that the stiffness of the plastic shaft (cleaning rod), which is made of *Polypropylene*, is slightly reduced in the case of short repetitions. In the worst case (pause time = 2.5 s), the average deviation from the mean value of the pressure was 0.3%.

Since a cleaning process takes considerably longer than 2.5 s, see 46 on page 87, no significant influence on the pressure measurement and, in a broader sense, on the cleaning result, is to be expected.

As far as the linearity of the load cell is concerned, no major abnormalities are observable. The Figure 45, page 86 shows just minor deviations from the fitted ideal curve, and these are negligible for the current application. It can be assumed that all elements involved in the pressure measurement are operated in their elastic range, so subsequent linearization is not necessary.

4.4.5 Pressure Curves of Cleaning Modes

As can be seen in Figure 46 on page 87, the pressure curves (blue curves) of the three cleaning modes deviate slightly from each other. If we look at the maximum deviation from the setpoint, *Cleaning by Pressure* provides the best results. This can be explained by the fact that in this cleaning mode, the pressure on the surface is permanently regulated.

At the same time, however, it can be seen that the course has a slightly higher ripple compared to the *Cleaning by Profile* and *Cleaning by Radius* mode. A certain waviness of the signal can be observed in all pressure courses and is due to a „wobbly" movement of the optics, which occurs when the optics are inserted slightly tilted into the holder. In case of *Cleaning by Pressure*, an additional factor is that the regulation of the pressure also results in a slightly wavy course. The combination of both effects leads to a lightweight higher wave amplitude.

Regarding the *Cleaning by Profile* and *Cleaning by Radius* mode, different factors are crucial in order to achieve a pressure curve that is as constant as possible. The position of the cleaning rod has the greatest influence. If the notch of the shaft does not engage correctly in the holder, the resulting offset in the X and Z axes leads to an offset starting point and thus to an uneven pressure curve.

Apart from that, a too-rough step resolution as well as a too-high lowering speed cause an overshooting of the pressure value when lowering the cleaning head. In contrast to *Cleaning by Pressure*, an excessively high deviation of the pressure is not compensated during *Cleaning by Profile* and *Cleaning by Radius*. A fault resulting from this would subsequently extend over the entire profile. The algorithm of both cleaning modes has therefore been optimized to minimize overshooting.

Figure 46 on page 87 illustrates the situation just mentioned. If the cleaning rod is inserted incorrectly, the pressure curve deviates from the nominal value by up to 20 % (see orange curve at *Cleaning by Profile* resp. *by Coordinates*).

In summary, it can be said that the three modes do not differ significantly with regard to the pressure curves. The cleaning process is shorter for *Cleaning by Profile* and *Cleaning by Radius*, but *Cleaning by Pressure* has the advantage of being less sensitive to poorly inserted cleaning rods.

4.5   Rotary Table Unit

4.5.1   Force Transmission and Space Requirements

With regard to forces, the developed turntable unit meets the requirements. Even when the *Polyester Swab* is pressed onto the optics with 100 % of the possible pressure, the speed remains constant. This is due on the one hand to the powerful DC gear motor and on the other hand to the additional reduction by the belt gear. The compact design also allows the entire unit to be accommodated on the Y-carrier despite the limited space available.

4.5.2   Rotational Speed and Noise Level

The fact that the rotation speed of the turntable does not correspond to the speed sent to the CNC controller was to be expected due to the double reduction. In addition, the speed is additionally influenced by the unclean PWM signal that is generated by the CNC controller (see the voltage curve in Figure 47 on page 88). The comparison of measured and set speed in Figure 48 on page 89 shows that there is an almost linear relationship, which can be used to determine the speed to be sent to the CNC controller.

Improvements are needed with regard to noise development at speeds above 250 min^{-1}. This is caused by the double reduction ratio on the one hand and the poor quality of the bevel gears used to form the 90 ° gearbox on the other. It was found that the noise emission of the bevel gears is due to their poor concentricity.

4.6 Cleaning Efficiency

4.6.1 Particulate Contamination

Summarizing the results of the cleaning tests from Chapter 3.4.1, it can be seen that particulate contamination such as dust particles or lint can be removed very well by the robot. The cleaning efficiency is above 97 % in both cases, see Table 23 and 24 on page 90 and 91.

It should be noticed that only particles $\geq 10\ \mu m$ were considered. Regarding the number of smaller particles, no statement can be made. Due to the fact that optics are usually only inspected with the naked eye [11] and thus particles $\leq 10\ \mu m$ are not detected anyway [7], it can be concluded that the cleaning result is sufficient.

4.6.2 Filmy Contaminations

Greasy Fingerprints

A visual interpretation of the before and after images shows that the cleaning robot is able to completely remove greasy fingerprints. It should be noted that in the case of large-area, greasy contamination, the cleaning rod should be changed or rotated after each cleaning cycle, as otherwise the surface may become smeared during subsequent cleanings.

Sweat-Based Fingerprints

The cleaning tests showed that sweat-based fingerprints are very difficult to remove. At this point, it should be mentioned that this type of contamination cannot be easily cleaned even with the manual *Brush Technique*. The reason is that the *Acetone* used is not suitable for this type of contamination. The only effective „solvent" in this case was the breathing air fogged on the optic surface, which should be replaced with *Deionized Water* when the robot is in productive use.

Contamination Due to Saliva

This type of contamination represents the greatest challenge, both for cleaning by robot and for the manual *Brush Technique*. The reason is once again that saliva is difficult, or even impossible, to remove with the solvent used (*Acetone*). Again, in this case, *Deionized Water* should be used [11].

4.7 Conclusion

The aim of this master thesis was to develop a cleaning system that automates the previously manual cleaning of optical components using *Brush Technique*. The manual removal of contamination by employees is often performed with varying accuracy and the pressure applied to the optical surface varies from employee to employee. In some cases, excessive force or pressure can even lead to visually detectable, irreversible damage to the surface coating.

The semiautomatic cleaning robot developed regulates the pressure applied to the optics to be cleaned and thus keeps it constant. This prevents damage during the cleaning process. Three different cleaning modes were implemented to cover a broad range of different optics. No visually recognizable damage to the optics was detected after any of the subsequent cleaning tests.

The functional and mechanical requirements for the device specified in Chapter 1.7, could be completely fulfilled. The combination between CNC positioning system and leveling sensor allows profile sampling with a measurement uncertainty of maximum 10.6 μm, the pressure on the optics can theoretically be controlled down to 0.3 % and by means of implemented syringe pump the solvent to be applied can be dosed in μl steps. The robot basically functions as a stand-alone device, but can also be controlled via other network-compatible devices such as a notebook, PC or tablet, which can be particularly advantageous when creating and saving new optic profiles.

Through various tests, which were evaluated using visual interpretation and the *Classification of Cleanability*, it was determined that particulate soiling and greasy fingerprints can be removed almost completely with the help of the cleaning robot using *Acetone*. Sweat-based fingerprints and saliva droplets, on the other hand, still pose a challenge to the cleaning system. By expanding the transport unit to include additional solvents, it would also be possible to remove this type of contamination in the future.

Based on a direct comparison between manual and automated cleaning, it was shown that with the use of the cleaning robot at least equally good cleaning results can be achieved.

References

[1] A. Thoß, D. Eidemüller, *et al.*, "Biomedizinische Optik und Augenoptik: Photonik in den Lebenswissenschaften," in *Clusterreport Optik & Photonik*, p. 96, Wirtschaftsförderung Brandenburg, September 2018.

[2] Wild Gruppe, "Medizinische Lasertechnik," October 2018. `https://www.wild.at/wp-content/uploads/2018/10/WILD-Gruppe_Market-Focus_Medizinische-Lasertechnik_web.pdf`.

[3] Wild Gruppe, "Lasertechnik: Laseranwendungen für höchste Ansprüche," November 2020. `https://www.wild.at/wp-content/uploads/2020/11/trm-broschuere.pdf`.

[4] Wild Gruppe, "Testen, testen, testen.," September 2020. `https://www.wild.at/news/pcr-test-blutgasanalyse-ivd/`, visited on: 20.01.2023.

[5] J.-Y. Plesseria, M. Henrist, *et al.*, "A New Guideline on Contamination Control for Space Optical Instruments," vol. 467, pp. 129 – 134, January 2001.

[6] A. Polinski, "Optiken richtig reinigen: Ein Leitfaden zur Handhabung und Reinigung von Optiken," February 2018. `https://www.asphericon.com/blog/detail/optiken-richtig-reinigen`, visited on: 13.10.2022.

[7] I. F. Stowers and H. G. Patton, "Cleaning Optical Surfaces," in *Optical Coatings: Applications and Utilization II* (G. W. DeBell and D. H. Harrison, eds.), vol. 0140, pp. 16 – 31, International Society for Optics and Photonics, SPIE, September 1978.

[8] R. Trierweiler, *Staub: Natürliche Quellen und Mengen*. Essentials, Springer Fachmedien Wiesbaden, 2020.

[9] I. Fernandes, "Staub ist nicht gleich Staub," March 2020. `https://www.planet-wissen.de/gesellschaft/sauberkeit/staub_feine_partikel_mit_grosser_wirkung/index.html`, visited on: 14.10.2022.

[10] M. Zölffel, "The Clean Microscope," Septmeber 2008. `https://hcbi.fas.harvard.edu/files/hcbidoug/files/50-10025_the_clean_microscope_e.pdf`.

[11] R. Schalck, *The Proper Care of Optics: Cleaning, Handling, Storage, and Shipping*. SPIE Digital Library, SPIE Press, 2013.

[12] P. Weinzerl, "Arbeitsanweisung AA-0003: Montage und Prüfung von Optik-Baugruppen," April 2021. (unveröffentlicht).

[13] Spetec, "Reinraumtechnik: Portable Reinraumtechnik," December 2021. `https://www.spetec.de/downloads/Reinraumtechnik_Prospekt.pdf`.

[14] Edmund Optics, "Reinigung von Optiken: Tipps für eine sachgemäße Pflege," `https://www.edmundoptics.de/knowledge-center/application-notes/optics/cleaning-optics/`, visited on: 17.10.2022.

[15] R. Paschotta, "Cleaning of Optics," `https://www.rp-photonics.com/cleaning_of_optics.html`, visited on: 18.10.2022.

[16] Floriane Teofanescu, "Cleaning Optics: Choosing the Best Method," `https://www.photonics.com/Articles/Cleaning_Optics_Choosing_the_Best_Method/a32199`, visited on: 17.10.2022.

[17] G. Guéhenneux *et al.*, "Impact of outgassing organic contamination on laser-induced damage threshold of optics: effect of laser conditioning," in *Laser-Induced Damage in Optical Materials: 2005* (G. J. Exarhos, A. H. Guenther, *et al.*, eds.), vol. 5991, p. 59910F, International Society for Optics and Photonics, SPIE, 2006.

[18] D. Hamilton and J. Hamilton, "Optics restoration - First Contact Liquid Polymer Restores Sensitive Optical Surfaces to >As New< Condition," pp. 32 – 34, February 2012.

[19] E. Kubacki, "The dirt on cleaning optics," *Photonics spectra*, vol. 40, pp. 56 – 60, March 2006.

[20] Newport, "Technical Note: How to Clean Optics," `https://www.newport.com/n/how-to-clean-optics`, visited on: 17.10.2022.

[21] Sunex, "Cleaning Procedure for Optics," `https://sunex.com/2020/01/31/cleaning-procedure-for-optics/`, visited on: 21.10.2022.

[22] R. Rottenfusser, E. E. Wilson, *et al.*, "Microscope Cleaning and Maintenance," `https://zeiss-campus.magnet.fsu.edu/print/basics/care-print.html`, visited on: 19.10.2022.

[23] I. Cordero, "How to care for and clean optical surfaces," *Community Eye Health Journal*, vol. 23, December 2010.

[24] J. Millington, "*How to Clean Microscope Optics*," `https://opti-tech.ca/how-to-clean-microscope-optics/`, visited on: 18.10.2022.

[25] P. Jackson and J. Hamilton, "Cleaning and Protecting Large Mirrors Using a Polymer Solution," April 2008. `https://www.mobilityengineeringtech.com/component/content/article/adt/pub/briefs/photonics/4809`, visited on: 18.10.2022.

[26] E. S. Bailey, N. Confer, *et al.*, "Increased Laser Damage Threshold by Protecting and Cleaning Optics Using First Contact Polymer Stripcoatings: Preliminary Data," *Laser-Induced Damage in Optical Materials*, vol. 7132, 2008.

[27] F. Fuchs, "19 - Ultrasonic cleaning and washing of surfaces," in *Power Ultrasonics*, pp. 577–609, Elsevier Ltd, 2015.

[28] L. Azar, "Cavitation in Ultrasonic Cleaning and Cell Disruption," *Controlled Environments*, pp. 14–17, February 2009.

[29] J. L. Lizon and S. Deiries, "Cleaning of extremely sensitive optical surfaces," in *Advances in Optical and Mechanical Technologies for Telescopes and Instrumentation*, vol. 9151, pp. 1793–1800, SPIE, 2014.

[30] R. Kohli, "Chapter 1 - Sources and Generation of Surface Contaminants and Their Impact," in *Developments in Surface Contamination and Cleaning* (R. Kohli and K. Mittal, eds.), pp. 1–49, Oxford: William Andrew Publishing, 2015.

[31] Mettler Toledo, "Test auf nicht flüchtige Rückstände: Gravimetrische Bestimmung des NVR-Gehalts," `https://www.mt.com/at/de/home/applications/Laboratory_weighing/non-volatile-residue-test-gravimetric-determination.html`, visited on: 14.01.2022.

[32] ISO 14644-9:2022, "Cleanrooms and associated controlled environments — Part 9: Assessment of surface cleanliness for particle concentration," Norm, International Organization for Standardization, Geneva, CH, November 2022.

[33] PhysicsOpenLab, "Light Scattering," July 2019. `https://physicsopenlab.org/2019/07/10/light-scattering/`, visited on: 15.01.2023.

[34] D. Katsir, "Stray Light Reduction in Industrial Optics," March 2021. `https://acktar.com/stray-light-reduction/`, visited on: 03.11.2022.

[35] M. Damm, "Entwicklung eines automatisierten Messplatzes zur Bestimmung ultrakurzpuls-laserinduzierter Zerstörschwellen optischer Komponenten," Master's thesis, Friedrich-Schiller-Universität Jena, May 2009.

[36] Edmund Optics, "Hintergrundinformationen zu optischen Spezifikationen: Laserzerstörschwelle," `https://www.edmundoptics.de/knowledge-center/application-notes/optics/understanding-optical-specifications/`, visited on: 03.11.2022.

[37] Markforged, "Onyx Chemical Resistivity," Datasheet, May 2018. `https://static.markforged.com/downloads/ChemicalResistivitySlick.pdf`.

[38] Raspberry Pi, "Datasheet: Raspberry Pi 4 Model B," Datasheet, June 2019. `https://datasheets.raspberrypi.com/rpi4/raspberry-pi-4-datasheet.pdf`, Release 1.

[39] M. Natali, "Ansteuerung unterschiedlicher Sensoren und Aktoren über einen Microcontroller," Seminararbeit, September 2022. (unveröffentlicht).

[40] SaintSmart, *Benutzerhandbuch: SainSmart Genmitsu Controller Board*, June 2020. `http://s3.amazonaws.com/s3.image.smart/download/101-60-284/Controller_Board_Benutzerhandbuch-German-V1.0-20200612.pdf`.

[41] SaintSmart, "GRBL Controller Board for Genmtisu CNC Router 3018, 3018-PRO, 1810-RPO," `https://www.sainsmart.com/collections/genmitsu-cnc-replacement-upgrade-parts/products/controller-board-for-genmtisu-cnc-router-3018-3018-pro-1810-rpo`, visited on: 22.01.2023.

[42] Handson Technology, "Data Specs: 17HS4401S Stepper Motor," Datasheet, June 2017. `https://www.handsontec.com/dataspecs/17HS4401S.pdf`.

[43] T. Friebel *et al.*, "Grbl Wiki," October 2021. `https://github.com/gnea/grbl/wiki`, visited on: 22.01.2023, Revision 26.

[44] RS Pro, "Datasheet: 12 V dc, 1000 gcm, Brushed DC Geared Motor, Output Speed 1318 rpm," Datasheet, March 2020. `https://docs.rs-online.com/d935/A700000007082005.pdf`.

[45] K. Tkotz *et al.*, *Fachkunde Elektrotechnik*. Haan-Gruiten: Verlag Europa-Lehrmittel, 23 ed., 2002.

[46] M. Fatma and M. Hamid, "PWM speed control of dc permanent magnet motor using a PIC18F4550 microcontroller," *IOP Conference Series: Materials Science and Engineering*, vol. 602, p. 012017, September 2019.

[47] AVIA Semiconductor, "HX711: 24-Bit Analog-to-Digital Converter (ADC) for Weigh Scales," Datasheet, June 2009. `https://cdn.sparkfun.com/datasheets/Sensors/ForceFlex/hx711_english.pdf`.

[48] SPT, "SPT4412LV-210," Datasheet, June 2021. `http://www.spt-servo.com/Product/1568293017.html`, visited on: 29.11.2022.

[49] G. Häberle *et al.*, *Tabellenbuch Mechatronik: Tabellen, Formeln, Normenanwendung*. Haan, Deutschland: Europa-Lehrmittel, 4 ed., January 2006.

[50] Antclabs, "BLTouch: Auto Bed Leveling Sensor for 3D Printers," `https://www.antclabs.com/bltouch-v3`, visited on: 04.12.2022.

[51] Texas Instruments, "DRV8825 Stepper Motor Controller IC," Datasheet, July 2014. `https://www.ti.com/lit/ds/symlink/drv8825.pdf`, Revision F.

[52] Elecrow, "RC050 5 inch HDMI 800 x 480 Capacitive Touch LCD Display," `https://www.elecrow.com/wiki/index.php?title=RC050_5_inch_HDMI_800_x_480_Capacitive_Touch_LCD_Display_for_Raspberry_Pi/_PC/_SONY_PS4`, visited on: 06.12.2022.

[53] J. Calvert, A. Scheller, *et al.*, "Raspberry Pi Documentation: The raspi-config Tool," April 2022. `https://www.raspberrypi.com/documentation/computers/configuration.html`, visited on: 22.01.2023.

[54] K. Huang, "Robotics and Embedded Systems: Interrupts vs. Polling," Technische Universität München, October 2015. `http://archive.www6.in.tum.de/www6/pub/Main/TeachingWs2015HSCDLegoCar/4.3-IO-Interrupts.pdf`.

[55] Python Software Foundation, "*Thread-based parallelism: Lock Objects*," `https://docs.python.org/3/library/threading.html?highlight=locks#lock-objects`, visited on: 23.01.2023.

[56] Sphinx developers, "SPHINX Python Documentation Generator." `https://www.sphinx-doc.org/en/master/index.html`, visited on: 09.01.2023.

[57] Arduino, "Arduino (TM) UNO Rev3," Schematic. `https://www.arduino.cc/en/uploads/Main/Arduino_Uno_Rev3-schematic.pdf`.

[58] Murata, "Ceramic Resonators (CERALOCK)," Datasheet, March 2021. https://www.mouser.at/datasheet/2/281/p16e-522700.pdf.

[59] L. Gail and U. Gommel, *Reinraumtechnik*. VDI-Buch, Berlin, Heidelberg: Springer Berlin / Heidelberg, 4 ed., 2018.

A Operating Instructions

Grundlegendes

Aufbau der Benutzeroberfläche

Die grafische Benutzeroberfläche gliedert sich ein einen statischen Kopf- und Fußbereich sowie einem dynamischen Mittelbereich, dessen Inhalt auf vier Registerkarten aufgeteilt ist.
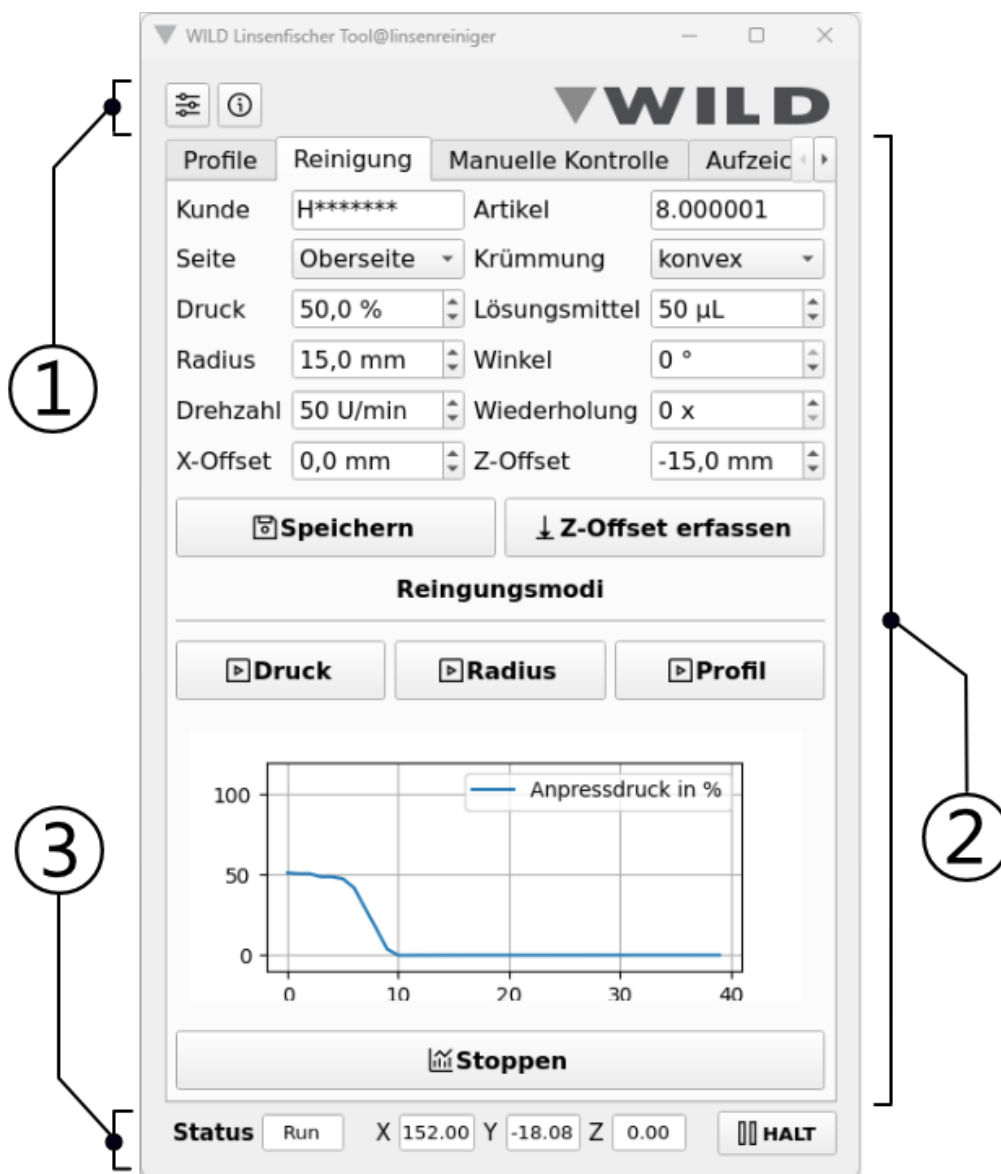
Figure 57: Grundlegender Aufbau der Benutzeroberfläche, (1) Kopfbereich, (2) Mittelbereich und (3) Fußbereich

Kopfbereich

Der Kopfbereich beinhaltet allgemeine Information über Softwareversion und Einstellungen, welche über die Schaltflächen $\boxed{\text{Einstellungen}}$ (Schieberegler Symbol) und $\boxed{\text{i}}$ abrufbar sind.

Mittelbereich

Über den Mittelbereich lässt sich der Roboter bedienen. Die Software startet in der Registerkarte *Profile*. Die Funktionalität dieser und aller weiteren Registerkarten wird in Kapitel A näher erläutert.

Fußbereich

Der Fußbereich gibt Auskunft über den aktuellen Status des Gerätes und die gegenwärtige Absolutposition von X-, Y- und Z-Schlitten. Mit dem Button $\boxed{\text{Halt}}$ lassen sich im Bedarfsfall Bewegungen des Gerätes ohne Positionsverlust pausieren.

In- und Außerbetriebnahme

Für die Inbetriebnahme des Roboters sind folgende Schritte durchzuführen:

1. Das Gerät mit dem Netzteil verbinden, über den Netzschalter (roter Kippschalter auf der rechten Seite) einschalten und den Boot-Vorgang abwarten.

2. Über die Desktop-Verknüpfung $\boxed{\text{START}}$ die Software des Roboters starten. Während dem Start wird die Hardware initialisiert.

3. Der Roboter ist bereit, sobald der Status im Fußbereich von $\boxed{\text{Run}}$ auf $\boxed{\text{Idle}}$ wechselt.

Wird das Gerät nicht mehr benötigt kann es auf zwei verschiedene Arten ausgeschaltet werden:

1. In der Benutzeroberfläche in den Reiter *Manuelle Kontrolle* wechseln und dort im Abschnitt *Makros* auf $\boxed{\text{Ausschalten}}$ klicken.

2. Die Software mit Klick auf die Schaltfläche $\boxed{\text{X}}$ in der Titelleiste des Softwarefensters beenden. Anschließend kann die zentrale Steuerung manuell über $\boxed{\text{Start}}$ > $\boxed{\text{Abmelden}}$ > $\boxed{\text{Herunterfahren}}$ beendet werden.

Um Beschädigungen der SD-Karte zu vermeiden, darf der Netzschalter erst betätigt werden, wenn die Steuerung vollständig heruntergefahren ist. Dafür muss mindestens fünf Sekunden gewartet werden.

Funktionen

Anlegen eines neuen Optikprofils

Für ein optimales Reinigungsergebnis müssen zuerst die Reinigungsparameter ermittelt werden. Diese unterscheiden sich von Optik zu Optik und sind zuvor anhand von Reinigungsversuchen zu ermitteln. Der Software bietet folgende Einstellungsmöglichkeiten:

Table 25: In der Software einstellbare Reinigungsparameter

Parameter	Einheit	Kurzbeschreibung
Druck	%	Maximaler Druck, mit welchem das Polyester-Pad auf die Oberfläche der Optik drückt; ein Wert von 100 % entspricht einem Druck von 1.45 $\frac{N}{cm^2}$
Lösungsmittel	nl	Menge an Lösungsmittel welches auf das Polyester-Pad aufgebracht wird
Radius	mm	Radius der eingelegten Optik
Winkel	°	Winkel des Reinigungskopfes (muss nur bei konkav-gekrümmten Oberflächen verstellt werden, der Einstellbereich liegt zwischen 0 und -20 °)
Drehzahl	$\frac{1}{min}$	Drehzahl mit welcher die Drehtellereinheit rotiert; die Mindestdrehzahl liegt bei 40 $\frac{1}{min}$
Wiederholungen	x	Anzahl der Wiederholungen (sollte grundsätzlich bei '0x' belassen und nur bei hartnäckigen Verschmutzungen erhöht werden)
X-Offset	mm	Gibt den Abstand zwischen optischer Achse und Reinigungsstartpunkt in X-Richtung an; wird nur bei speziellen Optiken benötigt
Z-Offset	mm	Gibt den Abstand zwischen Z=0 und Reinigungsstartpunkt in Z-Richtung an

Für spezielle Optiken, z.B. Linsen mit Zentrierbohrungen, ist es unter Umständen notwendig die X-Koordinate des Reinigungsstartpunktes zu versetzten. Das lässt sich durch Erhöhung des X-Offsets erreichen. Der Z-Offset hingegen legt fest, wie weit der Roboter den Reinigungskopf im Eilvorgang senkt, bevor er sich in kleinen Schritten an die Oberfläche heran tastest.

Je höher der Z-Offset ist, desto schneller ist der initiale Absenkvorgang. Der Wert lässt sich auch automatisch ermitteln, indem der Button ⎡Z-Offset erfassen⎤ im Reiter *Reinigung* gedrückt wird. X- und Z-Offset können unabhängig voneinander eingestellt werden.
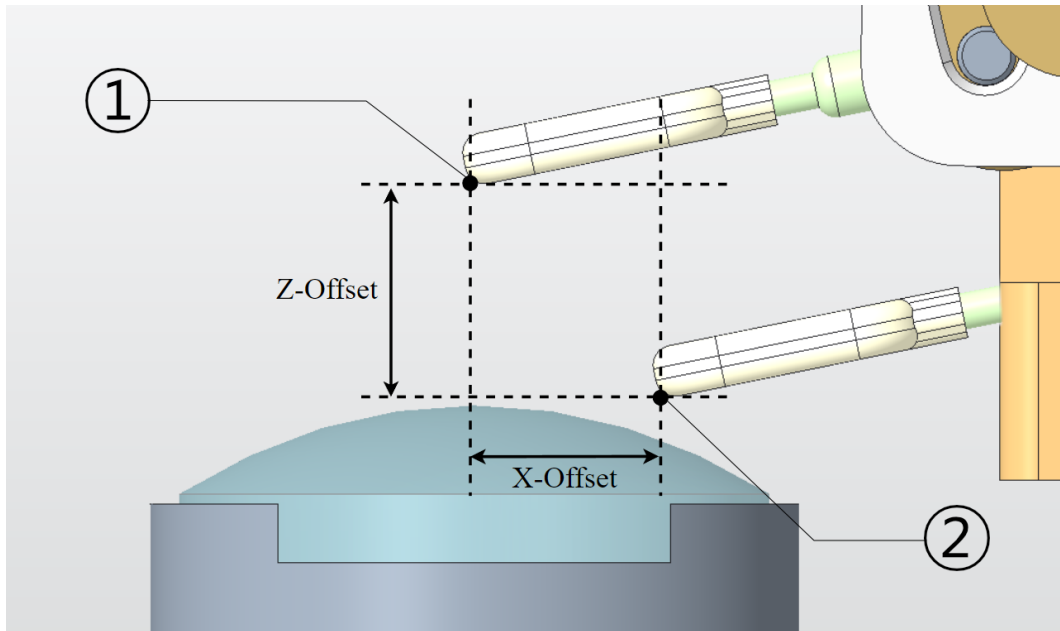
Figure 58: Bedeutung der beiden Parameter X- und Z-Offset. (1) Startpunkt der Reinigung, (2) In X- und Z-Richtung versetzter Startpunkt

Das Profil einer Optik besteht neben den Reinigungsparametern auch aus einem allgemeinen Teil, dessen Information die Reinigung nicht direkt beeinflussen. Tabelle 26 fasst diese kurz zusammen.

Table 26: Allgemeine Eigenschaften eines Optikprofils.

Feld	Kurzbeschreibung
Kunde	Diese Eigenschaft hat keinen Einfluss auf die Reinigung. Sie ist als zusätzliche Information zu sehen und hilft bei der Auswahl des Profils im Profilbrowser.
Artikelnummer	Firmeninterne Artikelnummer welche zur eindeutigen Identifikation eines Profils im Profilbrowser dient
Seite	Mit dieser Eigenschaft wird zwischen `'Oberseite'` und `'Unterseite'` der Optik unterschieden.
Krümmung	Als Krümmung kann wahlweise zwischen `'konvex'`, `'konkav'` und `'planar'` gewählt werden. Diese Einstellung wird nur bei der Druckreinigung berücksichtigt.

Sind Reinigungsparameter und allgemeine Angaben getätigt, kann das Profil über den Button Speichern der Profildatenbank hinzugefügt werden. Dabei wird eine Profil-Datei im Ordner

```
'home\wild\Python\linsenfischer\profile\'
```

abgelegt. Sind Änderungen des Optikprofils nötig, so können diese auch direkt in den Profildateien durchgeführt werden.

Erstellung eines Optikprofils

Optional ist es möglich, ein XZ-Oberflächenprofil der Optik zu erstellen. Das XZ-Oberflächenprofil bietet eine weitere Möglichkeit der Reinigung und basiert im Gegensatz zur Druckreinigung nicht auf der Ausregelung des Drucks. Bei dieser Methode werden die erfassten Koordinaten verwendet, um das Polyester-Pad entlang der Oberfläche zu bewegen. Ein Oberflächenprofil muss nur einmal erfasst werden und kann anschließend über das Optikprofil mitgespeichert werden.

Table 27: Einstellungsmöglichkeiten bei der Erfassung eines Oberflächenprofils.

Feld	Einheit	Kurzbeschreibung
Samples	x	Gibt an, wie viele Punkte entlang des angegebenen Radius abgetastet werden; Die Auflösung lässt sich verfeinern, indem die Anzahl der Samples erhöht wird.
Radius	mm	Radius der eingelegten Optik; Ein Sicherheitsfaktor von 1 mm wird automatisch durch die Software abgezogen.
X-Offset	mm	Gibt den Abstand zwischen optischer Achse und Reinigungsstartpunkt in X-Richtung an; Wird nur bei speziellen Optiken benötigt.
Z-Offset	mm	Gibt den Abstand zwischen Z=0 und Reinigungsstartpunkt in Z-Richtung an

Je mehr Samples eingestellt werden, desto länger dauert der Abtastvorgang. Der Fortschritt ist in dem *Ladebalken* im unteren Abschnitt des Fensters ersichtlich. Die Ergebnisse werden anschließend in einem Diagramm visualisiert.

Abtastvorgang

1. In den Reiter *Aufzeichnung* wechseln und die Parameter ändern.

2. Abtastung mit Klick auf | Koordinaten aufzeichnen | starten, der Roboter wechselt in die Beladeposition.

3. Optik einlegen und die Aufforderung mit | OK | bestätigen. Die Aufzeichnung startet, indem der Roboter in die Abtastposition fährt. Den anschließenden Abtastprozess abwarten.

4. Nach erfolgreicher Profilaufnahme, wechselt der Roboter wieder in die Beladeposition. Optik wieder entnehmen und das Popup mit | OK | schließen.

Durchführung einer Reinigung

Grundsätzlich stehen drei verschiedene Reinigungsmodi zur Auswahl, die Druck-, die Profil- und die Radiusreinigung. Die letzten beiden lassen sich nur durchführen, wenn zuvor ein Oberflächenprofil mit mindestens drei Abtastpunkten erstellt und gespeichert wurde.

Druckreinigung

1. Im Reiter *Profile* das gewünschte Profil suchen und markieren. Mit dem Button | Profil laden | lässt sich die Auswahl öffnen. Das Programm wechselt automatisch in den Reiter *Reinigung*.

2. Bei Bedarf die Reinigungsparameter anpassen.

3. Mit Klick auf | Druckverlauf anzeigen | lässt sich das Live-Diagramm aktivieren (optional).

4. Reinigung mit Klick auf | Druckreinigung | starten, der Roboter nimmt die Beladeposition ein.

5. Linse einlegen und in der Software mit | OK | bestätigen. Abwarten, bis die Reinigung durchgeführt wurde und der Roboter wieder in die Beladeposition wechselt.

6. Die Optik entnehmen und das Popup wieder mit | OK | bestätigen.

Profil- und Radiusreinigung

Der Ablauf von Profil- und Radiusreinigung unterscheidet sich nur unwesentlich von der Druckreinigung. Der einzige Unterschied liegt in Punkt 4, bei welchem in diesem Fall der Button | Profilreinigung | bzw. | Radiusreinigung | zu wählen ist.

Manuelle Kontrolle des Roboters

Über den Reiter *Manuelle Kontrolle* ist es möglich die einzelnen Hardwareeinheiten des Roboters manuell zu steuern. Das betrifft das CNC-Positionierungssystem, die Winkelverstellung des Reinigungskopfes, den Drehteller sowie die Spritzenpumpe. Außerdem sind im Abschnitt *Makros* weitere nützliche Funktion zu finden.
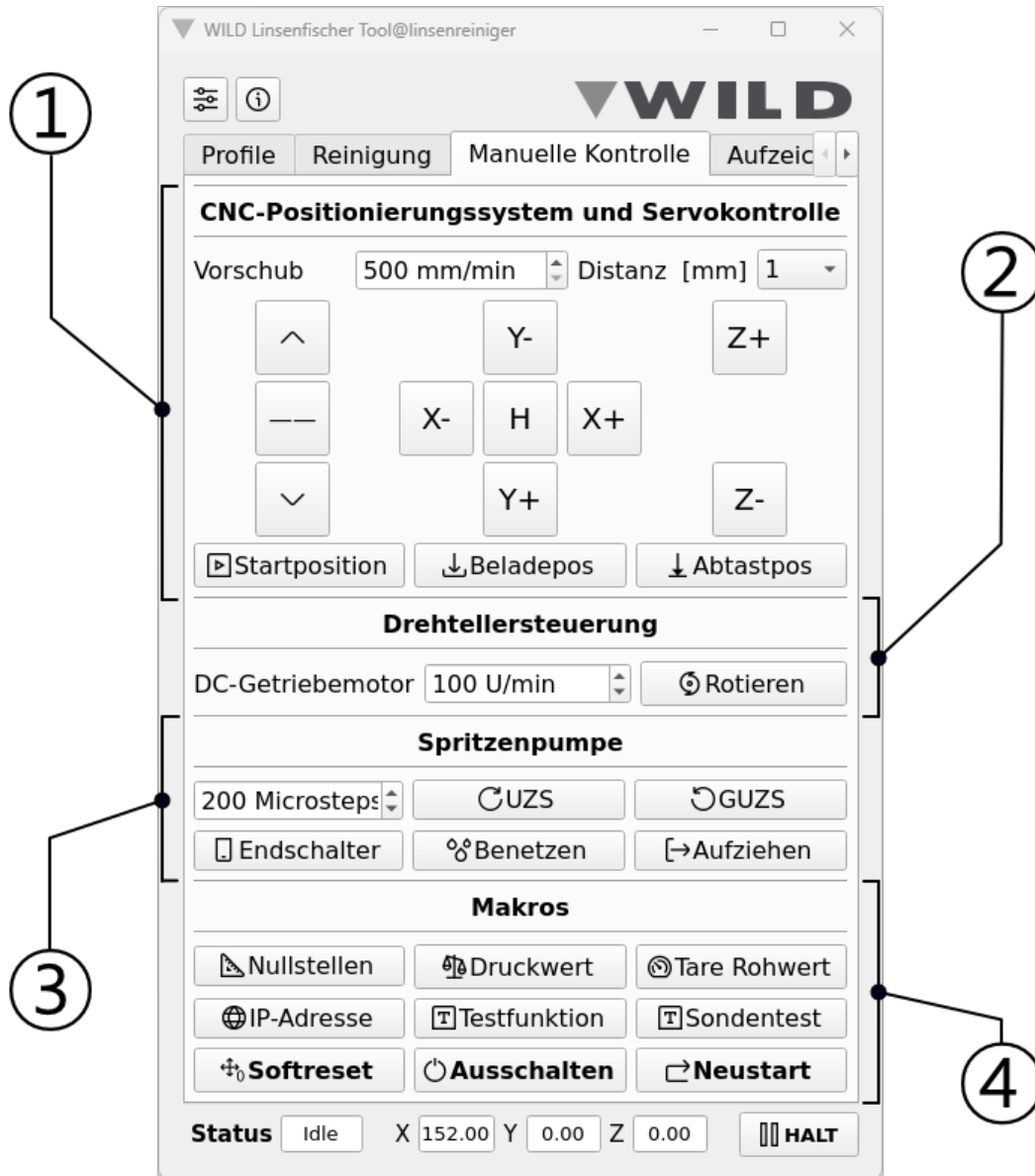

Figure 59: Grafische Oberfläche des Reiters *Manuelle Kontrolle*
(1) CNC-Positionierungssystem und Servokontrolle
(2) Steuerung des Drehtellermotors
(3) Manuelle Kontrolle der Spritzenpumpe
(4) Weitere Funktionen

CNC-Positionierungssystem und Servokontrolle

In diesem Abschnitt lassen sich X-, Y- und Z-Schlitten unter Angabe von Distanz und des Vorschub manuell verstellen. Ein manuelles Verfahren der Schlitten ist für gewöhnlich nur im Fehlerfall notwendig.

$\boxed{\pm\text{X, Y, Z}}$	Positioniert die Schlitten entlang der der jeweiligen Achse
$\boxed{\text{H}}$	Fährt die Schlitten in den Maschinennullpunkt
$\boxed{\text{Startpos}}$	Fährt den Roboter in die Reinigungsposition
$\boxed{\text{Beladepos}}$	Fährt den Roboter in die Be- und Entladeposition
$\boxed{\text{Abtastpos}}$	Fährt den Roboter in die Abtastposition
$\boxed{\wedge}$	Verstellt den Reinigungskopf um 2° nach oben
$\boxed{\text{- -}}$	Grundposition des Reinigungskopfes
$\boxed{\vee}$	Verstellt den Reinigungskopf um 2° nach unten

Drehtellersteuerung

In diesem Bereich ist es möglich den Drehteller mit unterschiedlichen Geschwindigkeiten rotieren zu lassen. Die Drehzahl lässt sich mittels Spin-Box $\boxed{\text{DC-Getriebemotor}}$ einstellen. Eine Drehzahländerung wird erst übernommen, wenn der Motor aus- und wieder eingeschaltet wird. Ein- und Ausschalten geschieht über den Toggle-Button $\boxed{\text{Rotieren}}$ bzw. $\boxed{\text{Aus}}$.

Spritzenpumpe

Im Abschnitt *Spritzenpumpe* lässt sich die Lösungsmittelfördereinheit manuell steuern. Dazu stehen fünf Funktionen zur Verfügung:

$\boxed{\text{UZS}}$	Dreht den Pumpenmotor um die eingestellte Schrittzahl im Uhrzeigersinn
$\boxed{\text{GUZS}}$	Dreht den Pumpenmotor um die eingestellte Schrittzahl gegen den Uhrzeigersinn
$\boxed{\text{Benetzen}}$	Benetzt das Polyester-Pad mit Lösungsmittel
$\boxed{\text{Aufziehen}}$	Zieht die Spritze auf
$\boxed{\text{Endschalter}}$	Gibt den Status des Endschalters der Spritzenpumpe aus

Makros

Der Abschnitt *Makros* beinhaltet eine Sammlung an funktionalen und informativen Funktionen. Rückgabewerte werden über ein Popup eingeblendet.

Nullstellen	Setzt den aktuellen Wert des Kraftsensors auf Null
Druckwert	Gibt den aktuellen Druckwert in % aus
Benetzen	Gibt den Tare-Rohwert aus
IP-Adresse	Zeigt die aktuelle IP-Adresse und den Hostnamen an
Testfunktion	Reservierter Button zum Debuggen der Software
Sonde	Toggle-Button der die Sonde aus- bzw einfährt
Softreset	Setzt den CNC-Controller zurück, z.B. bei Schrittverlusten notwendig
Ausschalten	Beendet die Software und fährt die zentrale Steuerung herunter
Neustart	Beendet die Software und startet die zentrale Steuerung neu

Anzeige & Änderung der Basiseinstellungen

Damit Änderungen grundlegender Einstellungen nicht direkt im Quellcode durchgeführt werden müssen, gibt es eine Konfigurationsdatei, welche alle Grundeinstellungen des Reinigungsroboters enthält. Die dort festgelegten Werte lassen sich zwar in der GUI über die Schaltfläche Einstellungen anzeigen, aber aus Sicherheitsgründen nicht ändern. Eine Änderung ist ausschließlich in der Konfigurationsdatei selbst durchführbar, welche unter folgendem Pfad zu finden ist:

```
'\home\wild\Python\linsenfischer\einstellungen\einstellungen.cfg'
```

Jede Änderung ist mit Bedacht durchzuführen, da sie das Verhalten des Roboters beeinflusst bzw. dessen Funktion beeinträchtigen kann. Eine Änderung darf nur durch geschultes Personal durchgeführt werden, da sonst unter Umständen eine Beschädigungen der Hardware droht.

Instandhaltung

Tausch des Reinigungsstäbchens

Die eingesetzten Reinigungsstäbchen (Polyester-Pads) müssen von Zeit zu Zeit getauscht werden. Das Intervall hängt vom Verschmutzungsgrad und dem Kontaminationstyp der zu reinigenden Optiken ab und ist deshalb nicht fix vorgegeben. Als Richtlinie können die empirisch ermittelten Werte in Tabelle 28 herangezogen werden.

Table 28: Maximale Anzahl empfohlener Reinigungsdurchgänge je Padseite.

Typ / Grad	lose Partikel	haftende Partikel	Schmutzfilme
niedrig	15	10	5
mittel	12	5	3
hoch	8	5	2

Der Wechsel erfolgt indem das alte Stäbchen aus der Aufnahme gezogen wird. Beim Einsetzten des neuen Stäbchens ist darauf zu achten, dass die Kerbe des grünen Kunststoffschafts am Passstift einrastet. Die richtige Position des Reinigungsstäbchens ist essentiell für den Reinigungsprozess.
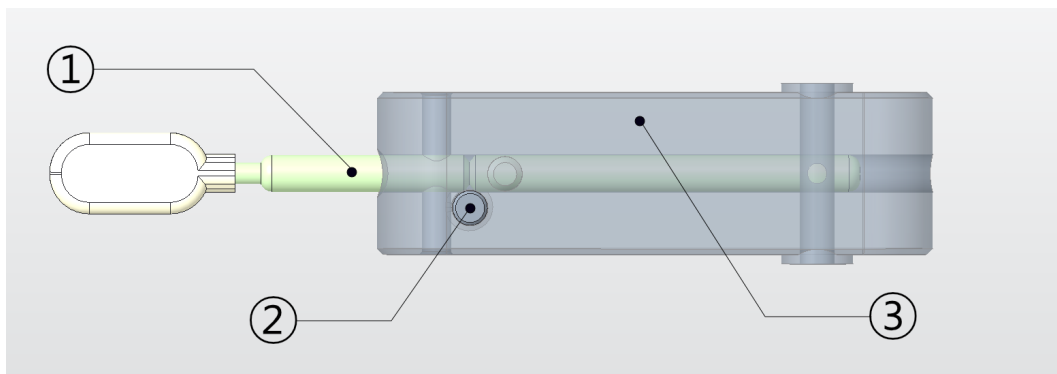

Figure 60: Darstellung des Kerbe-Stift Klicksystems
(1) Schaft mit Kerbe
(2) Passstift
(3) Aufnahme für Reinigungsstäbchen

Als Reinigungsstäbchen eignen sich ausschließlich die *Polyester-Tupfer* TX761K des Herstellers Texwipe. Es ist zu beachten, dass die Stäbchen vor dem Einsetzen auf eine Schaftlänge von ca. 24 mm gekürzt werden müssen.

Befüllen der Lösungsmittelspritze

Der Roboter prüft vor jeder Reinigung, ob sich noch genug Lösungsmittel in der Spritze befindet. Ist der Inhalt aufgebraucht, wird der Anwender über ein Popup darüber informiert.
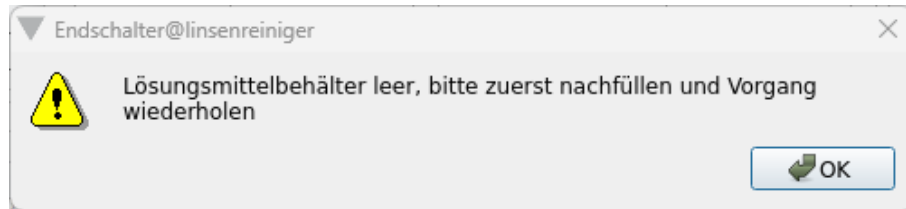
Figure 61: Popup bei leerem Lösungsmittelbehälter

Ein erneutes Auffüllen der Lösungsmittelspritze lässt sich auf zwei unterschiedliche Arten durchführen. Bei beiden Varianten ist zwingend darauf zu achten, dass eine persönliche Schutzausrüstung (Schutzbrille etc.) getragen wird, da ein ungeschütztes Hantieren mit Lösungsmitteln gesundheitliche Schäden zur Folge haben kann.

Variante 1

1. Die beiden Schrauben auf der Oberseite des Y-Schlittens lösen und den Wartungsdeckel öffnen, um zur Spritzenpumpe zu gelangen.

2. Die Spritze aus der Pumpe entnehmen und vollständig aufziehen, um das restliche Lösungsmittel aus dem Schlauch zu entfernen. Das ist notwendig, da sonst das Lösungsmittel beim Abstecken der Spritze aus dem Schlauch rinnt.

3. Spritze vom Schlauchsystem abstecken und einen Hilfsbehälter mit genügend Lösungsmittel befüllen.

4. Die Spritzenspitze in den Lösungsmittelbehälter eintauchen und vollständig (bis auf die 12 ml Markierung) aufziehen. Etwaige Lufteinschlüsse vorsichtig herausdrücken.

5. Spritze wieder mit dem Schlauchsystem verbinden und ca. 2 ml per Hand herausdrücken, um den Schlauch wieder zu befüllen.

6. In der Roboter-Software, in den Reiter *Manuelle Kontrolle* wechseln und dort im Abschnitt *Spritzenpumpe* den Button $\boxed{\text{Aufziehen}}$ betätigen.

7. Anschließend kann die auf ca. 10 ml aufgezogene Spritze wieder eingelegt werden. Den Wartungsdeckel wieder schließen und verschrauben.

Die zweite Variante ist wesentlich einfacher, birgt aber die Gefahr, dass während dem Aufziehen der Spritze, Luft in das Schlauchsystem gelangt. Ist dies der Fall, muss die eingeschlossen Luft über Variante 1 wieder entfernt werden.

Variante 2

1. Einen temporären Behälter vorbereiten und mit ausreichend Lösungsmittel befüllen.

2. Die Gewindeschraube am Düsenhalter lösen und die Düse vorsichtig aus der Halterung ziehen.

3. Anschließend die Düse tief genug in den mit Lösungsmittel gefüllten Behälter tauchen.

4. In der Roboter-Software, in den Reiter *Manuelle Kontrolle* wechseln und dort im Abschnitt *Spritzenpumpe* den Button $\boxed{\text{Aufziehen}}$ anklicken. Dabei darauf achten, dass beim Aufziehen keine Luft mit eingesaugt wird.

5. Düse aus dem Lösungsmittelbehälter entfernen und wieder am Düsenhalter festschrauben.

Fehlerbehebung

CNC-Controller reagiert nicht mehr

Sollte der CNC-Controller, oder das Programm nicht mehr reagieren, muss der Roboter neugestartet werden. Dazu folgende Schritte durchführen:

1. X- und Y-Schlitten über die Rändelschrauben auf den Maschinennullpunkt zurück bewegen.

2. Im Reiter *Manuelle Kontrolle*, Abschnitt *Makros* den Button $\boxed{\text{Neustarten}}$ betätigen.

3. Reagiert auch die Software nicht mehr, kann die zentrale Steuerung manuell über $\boxed{\text{Start}}$ > $\boxed{\text{Abmelden}}$ > $\boxed{\text{Neustarten}}$ neugestartet werden.

Tare-Wert außerhalb der Toleranz

Ist das Polyester-Pad während der Initialisierung des Kraftsensors belastet, wird eine Fehlermeldung ausgegeben. Zur Behebung sind folgende Schritte durchzuführen:

1. X- und Y-Schlitten über die Rändelschrauben soweit verstellen, dass das Polyester-Pad entlastet ist.

2. In den Reiter *Manuelle Kontrolle* wechseln und dort im Abschnitt *Makros* den Button $\boxed{\text{Nullstellen}}$ betätigen.

3. War die Nullstellung erfolgreich, Popup mit Klick auf $\boxed{\text{OK}}$ bestätigen.

4. Zur Kontrolle über den Button $\boxed{\text{Druckwert}}$ den aktuellen Druckwert auslesen. Nach erfolgreicher Nullstellung wird ein Druckwert um `'0%'` ausgegeben.

Vorgehen bei Schrittverlusten

Wird eine der Spindeln nach Initialisierung des Gerätes beabsichtigt oder auch unbeabsichtigt per Hand verdreht, geht die Position der Schrittmotoren verloren. Ein anschließendes Verfahren der Schlitten kann zur Beschädigung der Hardware führen, da die, in der CNC-Steuerung hinterlegte Position nicht mehr mit den tatsächlichen Koordinaten übereinstimmt. In dieser Situation sind folgende Punkte durchzuführen:

1. X- und Y-Schlitten über die Rändelschrauben per Hand auf den Maschinennullpunkt zurückbewegen.

2. Im Reiter *Manuelle Kontrolle* im Abschnitt *Makros* den Button $\boxed{\text{Soft-Reset}}$ betätigen.

Alarm-Status beheben

Befindet sich der Roboter nach dem Einschalten im Status `'Alarm'`, deutet das auf eine fehlgeschlagene Referenzfahrt hin. Zur Behebung des Problems, ist vor dem Start der Software zu überprüfen, dass keiner der drei Schlitten einen Endschalter betätigt.

Ein weiteres Indiz für eine fehlgeschlagene Referenzfahrt ist, dass sich die Schlitten über den Reiter *Manuelle Kontrolle* nicht verschieben lassen.

B Parts Lists

Table 29: Listing of all mechanical and electrical purchased parts

Component	Manufacturer	Description	Pcs.
Geared motor	RS Pro	12 V (DC), 1000 g·cm, 1318 min^{-1}	1
CNC mill	Saint Smart	Genmitsu 3018-PRO	1
Servo motor	SPT	SPT4412LV, 6V, 12 kg.cm	1
Anti-Backlash Nut	POLISI3D	T8x2mm	1
Controller	Raspberry PI	Raspberry PI 4 8 GB	1
Limit switch	WJMY	3-pole, 19.3x14.4x2.7 cm	4
Silicone tube	Antrella	Inner-Ø 1.6 mm, Outer-Ø 3 mm	1
ADC	Angeek	HX711 breakout board, 24 Bit	1
Load cell	Sourcing Map	200 g, 4.7x1.2x0.63 cm	1
Bevel gear	RS Pro	POM, 1:1, 20 teeth, bore 6 mm	2
Trapezoidal leadscrew	Sienoc	T8 2 mm pitch, 100 mm, with copper nut	1
Driver board	DollaTek	Expansion board, 42x42x15 mm	1
Stepper driver	AZDelivery	DVR8825	1
Stepper motor	Usongshine	NEMA17, 1.5 A, 1.8 °	1
Display	Elecrow	5" capacitive touch display, 800x480 px, HDMI	1
DC-DC	Yizhet	LM2596, 3.0-40 V to 1.5-35 V	1
Leveling sensor	Antclabs	BLTouch, Smart V3.1	1
USB cable	Goobay	Micro-USB to USB-A, 0.6 m	1
HDMI cable	Goobay	HDMI to micro HDMI, 0.5 m	1
USB cable	Delock	Mini-USB to USB-A, 0.5 m	1
Syringe	Norm-Ject	Luer exzentric, 10/12 ml	1
Dispense needle	Gonano	Luer-Lock, Inner-Ø 1.37 mm	2
USB-C plug	JSER	USB 3.1, black case	1

Table 30: Listing of all mechanical manufactured parts

Component	Filename	Material	Pcs.
Z-Schlitten	z_schlitten_v2.prt	Onyx	1
Befestigung Z-Schlitten	befestigung.prt	PLA	1
Rändelschraube	raendelschraube.prt	PLA	2
Steuerungsgehäuse	halterung_rpi4.prt	PLA	1
Steuerungsgehäuse Deckel	halterung_rpi4_deckel.prt	PLA	1
Adapter	adapter.prt	Onyx	1
Kopf	kopf_v2.prt	Onyx	1
Aufnahme	pad_halter.prt	Onyx	1
Halterung für Feder	federhalter.prt	Onyx	1
Halterung Düse	duesen_halter.prt	PLA	1
Endschalteradapter X	adapter_endschalter_x.prt	Onyx	1
Endschalteradapter Y	adapter_endschalter_y.prt	Onyx	1
Endschalteradapter Z	adapter_endschalter_z_v2.prt	Onyx	1
Displaygehäuse Basis	display_gehaeuse_unten.prt	PLA	1
Displaygehäuse Deckel	display_gehaeuse_oben.prt	PLA	1
Displaygehäuse Deckel	display_gehaeuse_oben.prt	PLA	1
Displayhalterung	display_halter.prt	ABS	1
Deckel Y-Schlitten	haube_deckel.prt	Onyx	1
Drehteller Getriebeblock	karussell_getriebeblock.prt	Onyx	1
Drehteller	drehteller.prt	Onyx	1
Halterung DC-Motor	halterung_dcmotoerv2.prt	Onyx	1
Synchronscheibe T40	gt2_t40.prt	PLA	1
Befestigungswinkel Drehteller	karussell_winkel_rechts.prt	PLA	3
Befestigungsschiene Drehteller	karussell_winkel_links.prt	PLA	1
Befestigungswinkel Abdeckung	gehaeuse_winkel_schmal.prt	PLA	1
Befestigungswinkel Abdeckung	gehaeuse_winkel_schmal.prt	PLA	1
Spritzenpumpe Basis	boden.prt	PLA	1
Kolbenschieber	kolbenschieber.prt	PLA	1
Welle 6 mm	-	NiRoSta	1

Table 31: Listing of all installed standard parts except screws, nuts and pins

Component	Manufacturer	Description	Pcs.
Ball bearing	SKF	6207-Z/C3, Inner-Ø 35 mm, Outer-Ø 72 mm, Width 17 mm	1
Ball bearing	GRW Germany	SS696 2Z, Inner-Ø 6 mm, Outer-Ø 15 mm, Width 5 mm	3
Linear bearing	Sourcing Map	LM8UU, Inner-Ø 8 mm, Outer-Ø 15 mm, Length 17 mm	3
Linear bearing	Sourcing Map	LM10UU, Inner-Ø 10 mm, Outer-Ø 19 mm, Length 29 mm	4
Slide bearing	Iglidur	GFM-0506-06, Inner-Ø 5 mm, Outer-Ø 6 mm, Length 5 mm	1
Slide bearing	Iglidur	GFM-0405-06, Inner-Ø 4 mm, Outer-Ø 5 mm, Length 6 mm	1
Slide bearing	Iglidur	GSM-0405-04, Inner-Ø 4 mm, Outer-Ø 5 mm, Length 4 mm	1
Synchronous pulley	SeeRaph	GT2, 16 teeth, 6 mm bore, aluminium	1
Timing belt	Turmberg3D	GT2, 320 mm Length, 6 mm Width	1
Thread insert	Bossard	outer thread M5, inner thread M3, Length 4 mm	7
Lock washer	Bossard	BN 810 for 6 mm shaft	1

C Equipment and Software Used

Table 32: Measuring devices used for the development of the robot

Device	Manufacturer	Model	Serial number
Multimeter	Fluke	175 True RMS	54520442
Oscilloscope	Voltcraft	DSO1062D	T 1G/012 009902
Digital force gauge	Alluris	FMI-100B5	05688
Microscope	Leica	M80	-
Digital camera	Leica	MC190 HD	1120133289

Table 33: Software used for the development of the robot

Name	Manufacturer	Category	Version
Creo	PTC	CAD	7.0.0.0
Matlab	MathWorks	Mathematics	R2020a
Affinity Photo	Serif	Image processing	1.10.6.1655
Visual Studio Code	Microsoft	IDE	1.74.2
Thonny	Raspberry Pi	Software development	3.3.14
GIT	-	Software development	2.39.0
MobaXterm	Mobatek	Terminal, X11	22.1
ImageJ	National Institute of Health	Image processing	1.53t
Leica Application Suite	Leica Microsystems	Image processing	4.13.0
Arduino IDE	Arduino	Software development	2.0.3
Qt-Designer	Qt Company	GUI design	5.11.1
Sphinx	-	Software development	5.3.0
Python Interpreter	Python Software Fd.	Software development	3.9.2

D Correspondences

... / [Kontakt Webseite asphericon] // Verschmutzungsgrad von Optiken

Stefan Klinzing <s.klinzing@asphericon.com>   6. Januar 2023 um 11:16
An: manuel.natali@gmail.com

Hallo Herr Natali,
vielen Dank für Ihre Nachricht!

Ich habe Ihre Frage bzgl. "Verschmutzungsgrad von Optiken" mit unserer Qualitätssicherung besprochen und kann Ihnen nun Folgendes mitteilen:
"... speziell für Optiken gibt es eine solche Norm nicht, wohl aber die allgemeine DIN EN ISO 14644-9, die sich mit Verschmutzungen durch Partikel beschäftigt, in diese auch Optiken fallen. Auch die VDA 19 sei hier genannt. Was filmische Verunreinigungen anbelangt, existieren derzeit noch keine allgemeinen Normen."

Ich hoffe, diese Informationen helfen Ihnen weiter und wünsche Ihnen viel Erfolg für Ihre Diplomarbeit.

Freundliche Grüße

--

Stefan Klinzing
Vertrieb / Sales
E-Mail: s.klinzing@asphericon.com